Visible Light Wireless Communications and Its Fundamental Study

2005

Toshihiko Komine

Contents

List of Figures

List of Tables

Abstract

In 1990's, white LEDs (Light Emitting Diodes) have been invented for various uses and subsequently investigated. Compared with conventional lighting devices, the white LED has lower power consumption, lower voltage, longer lifetime, smaller size, faster response, and cooler operation. The white LED will eventually replace incandescent or fluorescent lights in offices and homes.

In this dissertation, an indoor visible light wireless communication system utilizing white LED lighting equipment is proposed. In this system, these devices are used not only for illuminating rooms but also for a wireless optical communication system. This dual function of LED, for lighting and communication, is creating many new and interesting applications. The function is based on the fast switching of LEDs and the modulation of the visible light waves for free-space communications. The system has large power compared with infrared wireless communication system. Based on lighting engineering, their communication performances are evaluated.

Then, various new communication schemes in indoor visible light environment are proposed and discussed. A diversity technique is proposed so that shadowing problem may be alleviated. Moreover, to overcome the intersymbol interference caused by optical path difference between lighting equipments, an adaptive equalizer is proposed and discussed. The effectual interval of training sequence for channel estimation alleviates the influence of shadowing.

Finally, an integrated system of visible light wireless communication and power line communication for improvement of convenience and user friendliness is proposed. This system can also be considered as a very economical integration between power line communication and wireless communication. In this system, there is no necessity to lay a new communication cable in a ceiling. And, by screwing the electric bulb into a socket, the data transmission becomes possible.

From these proposals, it is found that the idea of the proposed systems is very promising for future high speed wireless networks and the visible light wireless communication can be one choice for an indoor optical wireless data transmission system.

Chapter 1

General Introduction

Visible light wireless communication is the communication technology using "Visible Light"; the visible light everywhere around our daily life. We are heavily relying on our eyes to gather almost all information for our day-to-day activities. Visible light has an impact on virtually every phase of human experience, since we perceive the world largely through vision. Evolution of human being, human life, observation of natural phenomena such as rainbows and sunsets, and recognition of objects about us—all involve the visible light. Therefore "Visibility" is one of the most important things for human being, and many devices are developed to assist our "Visibility". For instance, there are many devices including the lightings in our offices, home, the lightings on roads, commercial displays, small lamps on electronic home appliances including TVs, etc. Recently, the visible light wireless communication, which adds the secondary function of data transmission to these infrastructure devices, has been receiving increasing attention in consumer communication.

1.1 Historical Overview of Visible Light Wireless Communication

One of the first visible light wireless communication systems was reported by Alexander Graham Bell. In 1880, he transmitted the wireless telephone message on his newly invented "photophone" [1.1]. The device allowed for the transmission of sound on a beam of visible sunlight. Bell's photophone worked by projecting voice through an instrument toward a mirror. Vibrations in the voice caused similar vibrations in the mirror. Bell directed sunlight into the mirror, which captured and projected the mirror's vibrations. The vibrations were transformed back into sound by a sensitive selenium crystal (Fig. 1.1). Although communication over several hundreds of meters was proved, the evolution of visible light wireless communication had to wait until more appropriate devices had been developed. Meanwhile, primitive signaling systems with flashing lamps, based on Morse

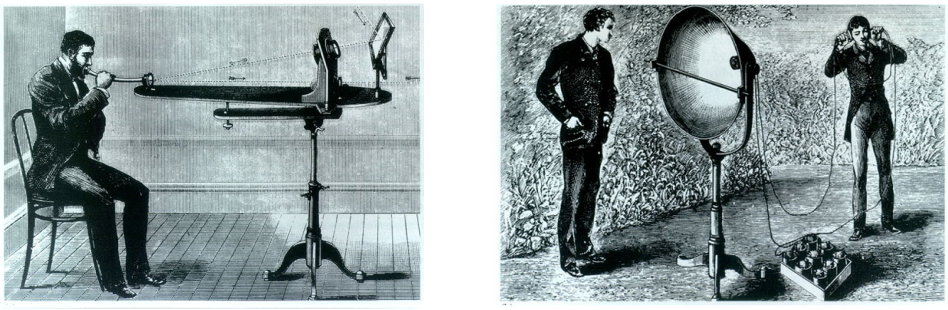

(a) Transmitter. (b) Receiver.

Figure 1.1: Photophone. (Lucent Technologies, Bell Labs Innovations)

transmission with the human eye as the detector, were widely used, e.g. for exchanging messages between ships.

In 1990's, white LEDs (Light Emitting Diodes) have been invented for various uses and subsequently investigated. However, it was impossible to obtain white LED until 1990's due to the lack of highly efficient blue and green LED. InGaN-based highly efficient blue LED and GaP-based green LED have now become commercially available. Using these LEDs, it is possible to fabricate white LEDs by mixing the three primary colors (red, green, and blue). Compared with conventional lighting devices, the white LED has lower power consumption, lower voltage, longer lifetime, smaller size, faster response, and cooler operation. As a result of these developments, much of the growth for LEDs will be concentrated in three main areas: The first is in automotive applications and traffic control devices such as head lights, tail lights, road lightings, and traffic signals. The second is in variable message signs such as the one located at Times Square of New York which displays commodities, news and other information. The third concentration would be in standard lighting sources such as architectural lighting, aerospace and automotive interior lighting, exit signs and emergency lighting, flashlights, and so on.

In 1999 to 2001, traffic information systems using modulated LED traffic signal have been proposed [1.2–1.4]. In these systems, the function is based on the fast switching of LEDs and the modulation of the visible light waves for outdoor free space communication. In 2000's, visible light wireless communication utilizing white LED lightings for indoor wireless networks have been proposed by a group including the author [1.5–1.9]. Owing to the function of lighting, the system has large power in comparison with indoor wireless LAN (Local Area Network) systems including infrared, and wide radiation pattern at transmitter. As just described, the peculiar characteristics and the problems in visible light wireless communication have been discussed. By these proposals, the possibility of broad-

band communication for consumer and the expectation to pervasive computing have been suggested. Visible light wireless communication has been consequently brought to public attention.

1.2 Difference between Visible Light Wireless Communication and Other Wireless Communications

In indoor wireless communication, optical radiation offers several significant advantages over radio. Optical emitters and detectors capable of high speed operation are available at low cost. The optical spectral region offers a virtually unlimited band width that is unregulated worldwide. It may not provide the biological damages to humans by the electromagnetic. Since no malfunction such as aircraft equipment and medical instruments is anticipated, it enables the optical wireless communication in airports and hospitals where radio wireless communication cannot be used according to electromagnetic wave interference. Infrared and visible light are close together in wavelength, and they exhibit qualitatively similar behavior. Both are absorbed by dark objects, diffusely reflected by light colored objects, and directionally reflected from shiny surfaces. Both types of light penetrate through glass, but not through walls ore other opaque barriers, so that optical transmissions are confined to the room in which they originate. This signal confinement makes it easy to secure transmissions against casual eavesdropping, and it prevents interference between links operating in different rooms. Thus, optical wireless LAN's can potentially achieve a very high aggregate capacity, and their design may be simplified, since transmissions in different rooms need not be coordinated. When an optical link employs intensity modulation with direct detection (IM/DD), the short carrier wavelength and large area, square law detector lead to efficient spatial diversity that prevents multipath fading. By contrast, radio links are typically subject to large fluctuations in received signal magnitude and phase. Freedom form multipath fading greatly simplifies the design of optical links [1.10].

The optical medium is not without drawbacks, however. Because optical cannot penetrate walls, communication from one room to another requires the installation of infrared access points that are interconnected via a wired backbone. In many indoor environments there exists intense ambient noise, arising from sunlight, incandescent lighting and fluorescent lighting, which induce noise in an optical receiver.

Infrared wireless communication has an eye safety problem in conjunction with the possible dangerous high energy density due to its invisibility. Therefore, the higher data rate transmission is not easy through infrared wireless communication. As compared to infrared wireless communication, the visible light wireless communication is suitable to human eyes in terms of "Visibility". The system

Table 1.1: Comparison between radio, infrared, and visible light system for indoor wireless communication.

Property of Medium	Radio	Infrared (IM/DD)	Visible Light (IM/DD)
Bandwidth Regulated	Yes	No	No
Transmission Power Limitation	Radio Law	Eye Safety	Illuminance, Luminance
Transmission Power	Low	High	Very High
Multipath Fading	Yes	No	No
Multipath Distortion	Yes	Yes	Yes
Passes Through Walls	Yes	No	No
Security	Low	High	Very High
Device	Complexity	Simplicity	Simplicity
Source of Dominant Error	Other Users	Background Light	Background Light
Input $X(t)$ Represents	Amplitude	Power	Power
SNR Proportional to	$\int \lvert X(t)\rvert^2 dt$	$\int \lvert X(t)\rvert^2 dt$	$\int \lvert X(t)\rvert^2 dt$
Average Power Proportional to	$\int \lvert X(t)\rvert^2 dt$	$\int \lvert X(t)\rvert dt$	$\int \lvert X(t)\rvert dt$

employs visible LED, which can be transmitted by a few watts, a relatively high energy for the use of lighting. This means that the visible light communication is capable to transmit data by the higher data rate. And visible light communication has infrastructure. Many devices are developed to assist our "Visibility". There are many devices including the lightings in our offices, home, the lightings on roads, traffic signals, commercial displays, small lamps on electronic home appliances including TVs, etc. Therefore, in visible light wireless communication, these devices can use as assist of visibility and communication device. Moreover, because of the visibility, user can recognize lighting area as communication service area. Thus, visible light communication is very suitable to the environment which requires human interface.

The characteristics of radio, infrared, visible light indoor wireless links are compared in Table 1.1.

1.3 Conventional Optical Wireless Communication Systems

There is a growing interest in indoor wireless networks as a consequence of the large-scale utilization of personal computers and mobile communicators. In this applications, an optical wireless communication system is a candidate for the media of wireless networks. Infrared is preferred as wavelength in these applications, originally. This is because essentially a large total transmission bandwidth is possible, facilitating fast transmission systems due to the very high frequency involved in optical carrier. Moreover, because of the short wavelength, optical radiation is confined within a room since the radiation is either reflected or absorbed by the

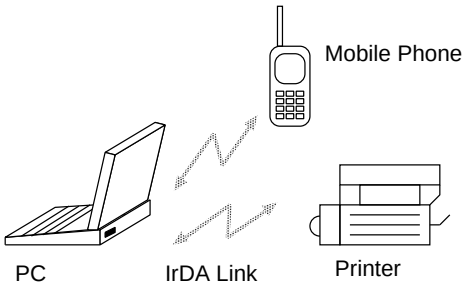

Figure 1.2: An example of an IrDA.

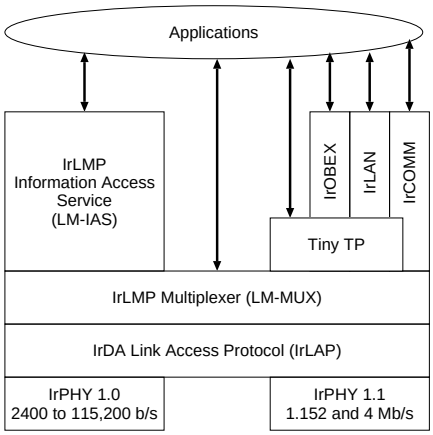

Figure 1.3: The IrDA protocol stack.

walls. Therefore cell planning in networks is simple.

1.3.1 IrDA links

The infrared data association (IrDA) was established in 1993 as a collaboration between major industrial organizations in order to establish an open standard for infrared data communication [1.11–1.16]. The resulting IrDA protocol was aimed to provide a simple, low-cost, reliable means of infrared communication between devices such as portable computers, desktop computers, printers, other peripherals, and LANs using directed point-to-point connectivity. Figure 1.2 illustrates an example image of an IrDA link with which PC peripherals are connected to a PC. IrDA links can currently provide a baud rate up to 115.2 kbit/s, or 16 Mbit/s with a high-speed extension, using half-duplex point-to-point connectivity. The IrDA protocol stack is shown in Fig. 1.3. The IrDA protocol stack consists of three mandatory layers: the physical (IrPHY) layer, the IrLAP layer, and the IrDA Link Management Protocol (IrLMP) layer.

The IrDA physical layer provides half-duplex point-to-point communication through the infrared medium and provides services to the upper IrLAP layer. The infrared medium interface specification requires a maximum link distance of at least 1 m and a half angle range of 15 to 30 degrees. This configuration is shown in Fig. 1.4. infrared transmitters have to conform to eye safety limitations on power output [1.17]. The maximum output intensity is specified at 500 mW/sr. Typical output power of transmitters is in tens of milliwatts range. In an IrDA link, nearly visible light (850 to 950 nm) is used. Version 1.0 of the physical layer provided a data rate of up to 115.2 kbit/s using a connection to the standard universal asynchronous receiver transceiver (UART) of the IrDA device. The hardware typically consists of an infrared transceiver module containing infrared LED with output driver and

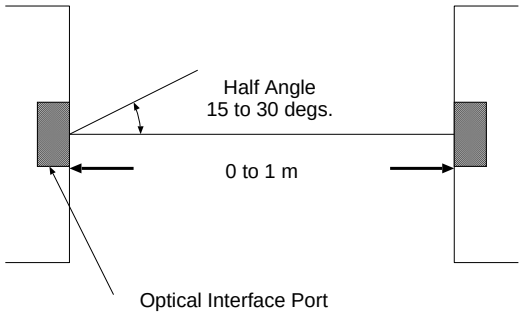

Figure 1.4: IrDA optical geometry.

Table 1.2: Signaling rate and pulse duration specifications of IrDA 1.4.

Signaling Rate	Modulation	Pulse Duration Minimum	Pulse Duration Nominal	Pulse Duration Maximum
2.4 kbit/s	RZI	1.41 ms	78.13 ms	88.55 ms
9.6 kbit/s	RZI	1.41 ms	19.53 ms	22.13 ms
19.2 kbit/s	RZI	1.41 ms	9.77 ms	11.07 ms
38.4 kbit/s	RZI	1.41 ms	4.88 ms	5.96 ms
57.6 kbit/s	RZI	1.41 ms	3.26 ms	4.34 ms
115.2 kbit/s	RZI	1.41 ms	1.63 ms	2.23 ms
0.576 Mbit/s	RZI	295.2 ns	434.0 ns	520.8 ns
1.152 Mbit/s	RZI	147.6 ns	217.0 ns	260.4 ns
4.0 Mbit/s				
(single pulse)	4PPM	115.0 ns	125.0 ns	135.0 ns
(double pulse)	4PPM	240.0 ns	250.0 ns	260.0 ns
16.0 Mbit/s	HHH(1,13)[1]	38.3 ns	41.7 ns	45.0 ns

infrared detector and receiver, and encoding/decoding circuitry. This can be as a plug-in adapter to the portable computers. The modulation scheme is return-to-zero (RZ) with a 3/16 bit time pulse duration. Version 1.1 extends the specification to support data rates of 1.152 Mbit/s and 4 Mbit/s. The 1.152 Mbit/s system uses return-to-zero (RZ) modulation scheme as in version 1.0 of the specification, but 4 Mbit/s system requires additional hardware for a 4-pulse position modulation (PPM) scheme and phase-locked loop (PLL) detection. Version 1.4 of IrDA standard will be published in 2001. This version supports data rates of 16 Mbit/s with low duty cycle, rate 2/3, and (d, k) = (1, 13) run-length limited (RLL) code [1.18]. The modulation scheme in version 1.4 is summarized in Table 1.2.

[1]HHH(1.13) modulation is a newly coding which is utilized low duty cycle, rate 2/3, and (d, k) = (1, 13) run-length limited (RLL) code.

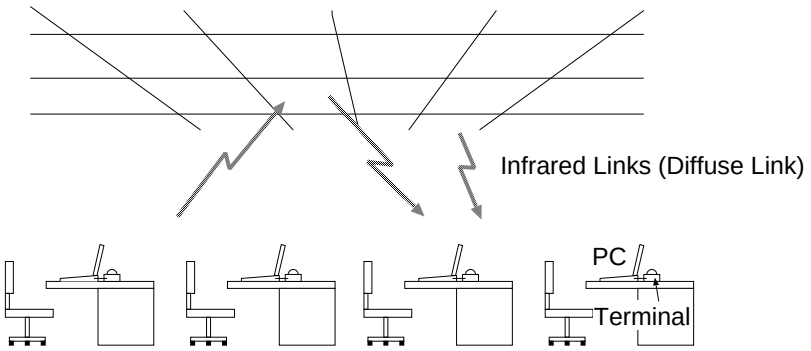

Figure 1.5: An example of an IEEE 802.11 network with infrared transmission.

1.3.2 Physical layer for IEEE 802.11

IEEE 802.11 standard for wireless LANs defines a specification for an infrared physical layer [1.19, 1.20]. In the United States, the executive committee of the IEEE 802 project created the IEEE 802.11 group to work on the specification of a wireless LAN for different technologies, including radio and infrared. The standard was approved in June 1997. An essential characteristic of the IEEE 802.11 specification is that there is a single medium access control (MAC) sub-layer common to all physical (PHY) layers. This feature will allow easier interoperability among the many physical layers that are expected to be defined in the future, driven by the fast technological progress in this field. There are presently three different PHY layers in the standard: infrared, frequency hopping spread-spectrum (FHSS), and direct sequence spread-spectrum (DSSS). Infrared and radio can be considered complementary technologies for the support of wireless LANs. Infrared technology is well suited for low-cost low-range applications, such as ad hoc networks. In this layers of the IEEE 802.11 standard, nearly visible light (850 to 950 nm) is used. Figure 1.5 illustrates an example image of an IEEE 802.11 network with infrared transmission.

The infrared PHY layer supports two data rates: 1 and 2 Mbit/s. The specification of two data rates is aimed at following:

- A smooth migration to higher data rates
- Asymmetric operation of the basic service set (BSS)

PPM scheme is utilized in the IEEE 802.11 standard, basically. There is a different PPM scheme for each data rate: 16-PPM for 1 Mbit/s and 4-PPM for 2 Mbit/s. The purpose of this feature is to ensure that the basic pulse is the same at both data rates, which minimizes the additional complexity introduced by the 2 Mbit/s data rate. The emitter and receiver circuits can be almost identical (in particular, the same front-end can be used at both data rates), and the most significant enhancements

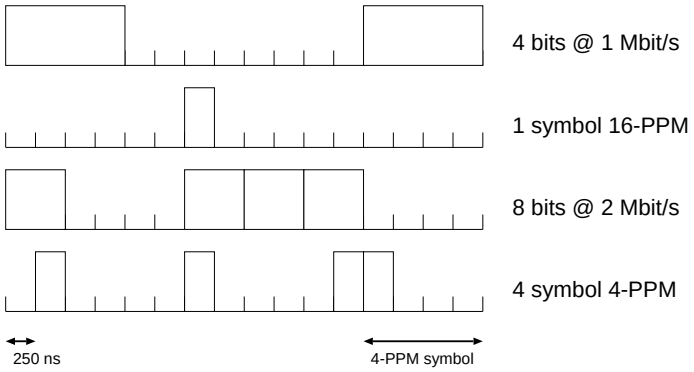

Figure 1.6: PPM signals at 1 and 2 Mbit/s.

are required on the synchronization circuits. The PPM signals at 1 and 2 Mbit/s are represented in Fig. 1.6. The duration of each pulse is 250 ns, and the peak optical power is 2 W. Therefore, the average optical power is 250 mW at 2 Mbit/s and 125 mW at 1 Mbit/s.

1.4 Purpose and Position of This Study

Trends in the telecommunications and computer industries suggest that the network of the future will consist of a high capacity backbone network with short-range communication links providing network access to portable communicators and portable computers. In this vision of the future, mobile users will access to similar grade high-speed network services available to wired terminals. For this purpose, some parts of communication links need to be constructed wireless.

During the last decade, therefore, the wireless communication technology has grown rapidly [1.21–1.25].The technology base for implementing this concept does not yet exist, however. Radio technology, although well-suited for moderate-speed applications such as voice, may not be sufficient to support many high-speed applications. To illustrate the potential capacity requirements of a wireless network, consider the needs of a portable high-quality digital display. To reduce its size, weight, battery-power consumption, and cost, it may be advantageous to make it simple as possible, having little on-board computational power, and relegating intensive signal-processing tasks such as video decompression to the transmitter platform. To accomplish this, however, it will require mid-range or short-range wireless communication links with extremely high capacity. In an extreme case, for example, uncompressed high-definition video can require a data rate of 1 Gbit/s or more. More realistically, data rates over 100 Mbit/s may be adequate for practical applications.

Moreover, radio wave transmission technology suffers from electro-magnetic

interference (EMI) problems as the radio spectrum gets increasingly crowded. Now that personal communicators and wireless computer networks are evolving rapidly, the available spectrum is considered to be a scarce resource. Simultaneously, there is an increase in the interference level caused by switched power supplies and other high-frequency equipment. Particularly in hospitals and industrial environments, the applicability of radio systems is already seriously limited by these problems. Extensive frequency allocation regulations can only partly solve them. Although eventually EMI aspects will become an integral part of every system design, future applications require the exploration of new wavelength ranges.

An optical wireless communication system is an attractive alternative to radio, primarily because of a virtually unlimited, unregulated bandwidth [1.26–1.28]. The optical spectrum is a universally available resource without frequency and wavelength regulations. An optical wireless communication system has the advantage of requiring low-cost and low-power consumption components, also [1.29]. Moreover, for indoor applications, optical radiation is confined within a room since the radiation is either reflected or absorbed by the walls because of its short wavelength. Therefore cell planning in networks is simple and easy. In the near future, optical wireless communication system will be an attractive candidate for wireless access network.

As earlier mentioned, visible light wireless communication will be a powerful candidate for future indoor high speed optical wireless communication systems, such as more than hundreds Mbit/s transmission speed, to support real multimedia transmissions. In this dissertation, indoor visible light wireless communication systems utilizing white LED lightings will be proposed, and the peculiar characteristics and the problems will be discussed. Moreover, some adaptation schemes will be proposed in visible light wireless environment. Through this dissertation, the potentiality of visible light wireless communication technology for the future indoor wireless system will be shown.

The relationship between the previous researches of visible light wireless communication system and this dissertation is summarized in Fig. 1.7.

1.4.1 Outline of the Dissertation

This dissertation is organized as follows. Chapter 1 which is the present chapter has introduced the overview of visible light wireless communication systems and described the motivations of this research. In chapter 2, basic knowledge for indoor optical wireless communication systems has introduced. Some numerical analyses and computer simulations are introduced. In the following chapter 3, basic white LED characteristics by measurements has shown. In chapter 4, indoor visible light data transmission system with white LED lighting equipment is proposed and discussed. Based on lighting engineering, their communication performance is

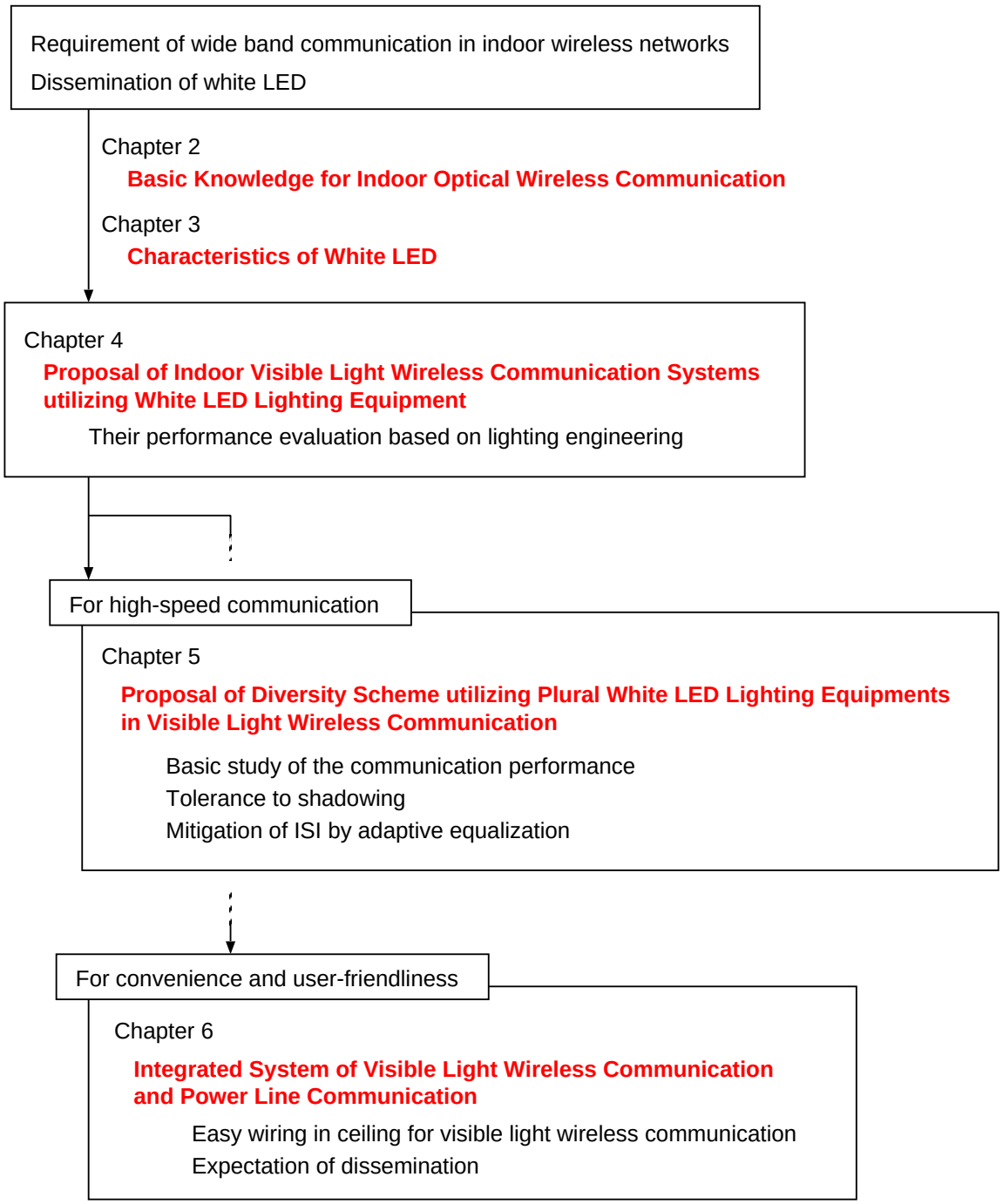

Figure 1.7: Outline of the dissertation.

evaluated. In chapter 5, various new schemes in indoor visible light environment are proposed and discussed. In this chapter, diversity technique is proposed so that shadowing problem may be alleviated and the availability of the system is shown. Moreover, to overcome the intersymbol interference caused by optical path difference between lighting equipments, adaptive equalizer is proposed and discussed. In chapter 6, integrated system of visible light wireless communication and power line communication for improvement of convenience and user friendliness is proposed. Finally, this dissertation is concluded in chapter 7 and future issues are described.

1.5 References

[1.1] A. G. Bell, "On the Production and Reproduction of Sound By Light," American Journal of Sciences, Third Series, vol. XX, no. 118, pp. 305–324, 1880.

[1.2] G. Pang, T. Kwan, H. Liu, Chi-Ho. Chan, "Optical Wireless based on High Brightness Visible LEDs," IEEE Conference of Industry Applications, vol. 3, pp. 1693–1699, 1999.

[1.3] G. Pang, T. Kwan, Chi-Ho. Chan, "LED Wireless," IEEE Industry Applications Magazine, vol. 8, issue 1, pp. 21–28, 2002.

[1.4] M. Akanegawa, Y. Tanaka, M. Nakagawa, "Basic Study on Traffic Information System using LED Traffic Lights," IEEE Transactions on Intelligent Transportation Systems, vol. 2, issue 4, pp. 197–203, 2001.

[1.5] Y. Tanaka, S. Haruyama, M. Nakagawa, "Wireless Optical Transmissions with White Colored LED for Wireless Home Links," IEEE International Symposium on Personal, Indoor and Mobile Radio Communications, vol. 2, pp. 1325–1329, 2000.

[1.6] T. Komine, Y. Tanaka, S. Haruyama, M. Nakagawa, "Basic Study on Visible-Light Communication using Light Emitting Diode Illumination," International Symposium on Microwave and Optical Technology, pp. 45–48, 2001.

[1.7] Y. Tanaka, T. Komine, S. Haruyama, M. Nakagawa, "A Basic study of optical OFDM system for Indoor Visible Communication utilizing Plural White LEDs as Lighting," International Symposium on Microwave and Optical Technology, pp. 303–306, 2001.

[1.8] T. Komine, M. Nakagawa, "Integrated System of White LED Visible-Light Communication and Power-Line Communication," IEEE Transactions on Consumer Electronics, vol. 49, no. 1, pp. 71–79, 2003.

[1.9] Y. Tanaka, T. Komine, S. Haruyama, M. Nakagawa, "Indoor Visible Light Data Transmission System utilizing White LED Lights," IEICE Transactions on Communications, vol. E86–B, no. 8, pp. 2440–2454, 2003.

[1.10] J. M. Kahn, J. R. Barry, "Wireless Infrared Communications," Proceedings of the IEEE, vol. 85, no. 2, pp. 265–298, 1997.

[1.11] P. Barker, A. C. Boucouvalas, "Performance modeling of the IrDA protocol for infrared wireless communications," IEEE Communications Magazine, vol. 36, no. 12, pp. 113–117, 1998.

[1.12] Infrared Data Association, Walnut Creek, CA, "Infrared Data Association Serial Infrared Link Access Protocol (IrLAP), version 1.1," 1996.

[1.13] Infrared Data Association, Walnut Creek, CA, "Infrared Data Association Link Management Protocol (IrLMP), version 1.1," 1996.

[1.14] Infrared Data Association, Walnut Creek, CA, "Infrared Data Association Link Access Protocol Specification for 16 Mb/s Addition (VFIR), Errata to IrLAP version 1.1," 1999.

[1.15] Infrared Data Association, Walnut Creek, CA, "Infrared Data Association Serial Infrared Physical Layer Link Specification for 16 Mb/s Addition (VFIR), Errata to IrPHY version 1.3," 1999.

[1.16] Infrared Data Association, "`http://www.irda.org/`".

[1.17] International Electrotechnical Commission, Geneva, Switzerland, "IEC 60825-1: Safety of Laser Products," 1998.

[1.18] Infrared Data Association, Walnut Creek, CA, "Infrared Data Association Serial Infrared Physical Layer Specification, version 1.4," 2001.

[1.19] IEEE 802 LAN/MAN Standards Committee, "`http://www.ieee802.org/`".

[1.20] R. T. Valadas, A. R. Tavares, A. M. de Oliveira Duarte, "The infrared physical layer of the IEEE 802.11 standard for wireless local area networks," IEEE Communications Magazine, vol. 36, no. 12, pp. 107–112, 1998.

[1.21] J. E. Padgett, C. G. Günther, T. Hattori, "Overview of wireless personal communications," IEEE Communications Magazine, vol. 33, no. 1, pp. 28–41, 1995.

[1.22] D. C. Cox, "Wireless personal communications : What is it?," IEEE Personal Communications Magazine, vol. 2, no. 2, pp. 20–35, 1995.

[1.23] R. Pandya, "Emerging mobile and personal communication systems," IEEE Communications Magazine, vol. 33, no. 6, pp. 44–52, 1995.

[1.24] R. O. LaMaire, A. Krishna, P. Bhagwat, J. Panian, "Wireless LANs and mobile networking : Standards and future directions," IEEE Communications Magazine, vol. 34, no. 8, pp. 86–94, 1996.

[1.25] K. Pahlavan, A. Zahedi, P. Krishnamurthy, "Wideband local access : Wireless lan and wireless atm," IEEE Communications Magazine, vol. 35, no. 11, pp. 34–40, 1997.

[1.26] J. R. Barry, "Wireless Infrared Communications," Kluwer Academic Press, Boston, MA, 1994.

[1.27] D. J. T. Heatley, D. R. Wisely, I. Neild, P. Cochrane, "Optical wireless: The story so far," IEEE Communications Magazine, vol. 36, no. 12, pp. 72–82, 1998.

[1.28] R. Otte, L. P. de Jong, A. H. M. van Roermund, "Low-power Wireless Infrared Communications," Kluwer Academic Publishers, The Netherlands, 1999.

[1.29] A. M. Steel, R. N. Stavinou, D. C. O'Brien, D. J. Edwards, "Indoor optical wireless systems – a review," Optical and Quantum Electronics, vol. 29, no. 3, pp. 348–378, 1997.

Chapter 2

Basic Knowledge for Indoor Optical Wireless Communication

2.1 Intensity Modulation and Direct Detection Channels

Modulation techniques for radio wireless systems include amplitude, phase, and frequency modulation (AM, PM, and FM), as well as some generalizations of these techniques. Radio receivers employ one or more antennas, each followed by a heterodyne of homodyne down-converter, which is comprised of a local oscillator and a mixer. Efficient operation of this mixer relies upon the fact that it receives both the carrier and the local oscillator in a common electromagnetic mode. The down-converter output is an electrical signal whose voltage is linear in the amplitude of the received carrier electric field.

In a low-cost optical wireless system, it is extremely difficult to collect appreciable signal power in a single electromagnetic mode. This spatially incoherent reception makes it difficult to construct an efficient heterodyne or homodyne down-converter for AM, PM, and FM, or to detect AM or PM by any other means. For optical wireless links, the most viable modulation is intensity modulation, in which the desired waveform is modulated onto the instantaneous power of the carrier. The most practical down-conversion technique is direct detection, in which a photo detector produces a current proportional to the received instantaneous power, i.e., proportional to the square of the received electric field.

The modeling of optical wireless channels with IM/DD is illustrated in Fig. 2.1. The transmitted waveform $X(t)$ is the instantaneous optical power of the lightwave emitter. The received waveform $Y(t)$ is the instantaneous current in the receiving photo detector, which is proportional to the integral over the photo detector surface of the total instantaneous optical power at each location. The received electric field generally displays spatial variation of magnitude and phase, so that a multipath fading would be experienced if the detector were smaller that a wavelength. Fortunately, typical detector areas are millions of square wavelength, leading to spatial diversity that prevents a multipath fading. Thus when the detector is moved by a distance of the order of a wavelength, no change in the channel is observed. As the transmitted optical power $X(t)$ propagates along various paths

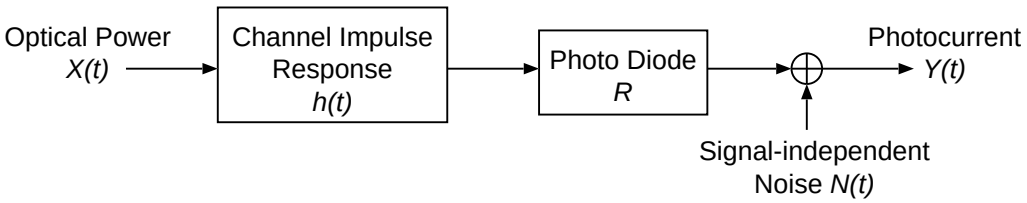

Figure 2.1: Modeling link as a baseband filter, time-invariant system having impulse response $h(t)$, with signal-independent, additive noise $N(t)$. The photodetector has responsivity R.

of different lengths, optical wireless channels are still subject to multipath distortion. The channel can be modeled as a baseband linear system, with instantaneous input power $X(t)$, output current $Y(t)$, and an impulse response $h(t)$, as shown in Fig. 2.1. Alternately, the channel can be described in terms of the frequency response [2.1]

$$H(f) = \int_{-\infty}^{\infty} h(t) e^{-j2\pi f t} dt, \tag{2.1}$$

where is the Fourier transform of $h(t)$. It is usually appropriate to model the channel "$h(t) \Leftrightarrow H(f)$" as fixed, since it usually changes only when the transmitter, receiver, or objects in the room are moved by tens of centimeters. The linear relationship between $X(t)$ and $Y(t)$ is a consequence of the fact that the received signal consists of many electromagnetic modes. By contrast, we note that when IM/DD is employed in dispersive single-mode optical fiber, the relationship between $X(t)$ and $Y(t)$ is sometimes nonlinear.

In many applications, optical wireless links are operated in the presence of intense infrared and visible background light. While received background light can be minimized by optical filtering, it still adds shot noise, which is usually the limiting noise source in a well-designed receiver. The desired signals contain a time-varying shot-noise process which has an average rate of 10^4 of 10^5 photons/bit. In the channel model, however, intense ambient light striking the detector leads to a steady shot noise having a rate of order of 10^7 to 10^8 photons/bit, even if a receiver employs a narrow-band optical filter. However, we neglect the shot noise caused by signals and model the ambient-induced shot noise as a Gaussian process. When little of no ambient light is present, the dominant noise source is receiver pre-amplifier noise, which is also signal-independent and Gaussian (though often non-white). Thus we usually model the noise $N(t)$ as Gaussian and signal-independent. This stands in contrast to the signal-independent, Poisson noise considered in photon-counting channel models. Fluorescent lamps emit infrared that is modulated in nearly periodic fashion; when present, this adds a cyclostationary component to $N(t)$ [2.2, 2.3].

The baseband channel model is summarized by

$$Y(t) = RX(t) \otimes h(t) + N(t), \tag{2.2}$$

where the "$\otimes$" symbol denotes convolution and R is the detector responsivity (A/W). While Eq. (2.2) is simply a conventional linear filter channel with additive noise, optical

wireless systems differ from conventional electrical or radio systems in several respects. Because the channel input $X(t)$ represents instantaneous optical power, the channel input is non-negative:

$$X(t) \geq 0, \tag{2.3}$$

and the average transmitted optical power P_t is given by

$$P_t = \lim_{T\to\infty} \frac{1}{2T} \int_{-T}^{T} X(t)dt, \tag{2.4}$$

rather than the usual time-average of $|X(t)|^2$, which is appropriate when $X(t)$ represents amplitude. The average received optical power is given by

$$P_r = H(0)P_t, \tag{2.5}$$

where the channel DC gain is $H(0) = \int_{-\infty}^{\infty} h(t)dt$. The performance of a wireless optical link at bit rate R_b is related to the received electrical SNR

$$SNR = \frac{R^2P^2}{R_bN_0} = \frac{R^2H^2(0)R_t^2}{R_bN_0}, \tag{2.6}$$

assuming that $N(t)$ is dominated by a Gaussian component having double-sided power-spectral density N_0. From Eq. (2.6), we see that the SNR depends on the square of the received optical average power, implying that IM/DD optical wireless links must transmit at a relatively high power and can tolerate only a limited path loss. This stands in contrast to the case of radio wave channels, where the SNR is proportional to the first power of the received average power.

2.2 Channel Direct Current Gains

The frequency responses of optical channels are relatively flat near direct current (DC), so for most purposes, the signal most important quantity characterizing a channel is the DC gain $H(0)$, which relates the transmitted and received average powers via Eq. (2.5). In this subsection we compute the DC gains of line of sight (LOS) link.

In LOS links, the DC gain can be computed fairly accurately by considering only the LOS propagation path. We consider the link geometry shown in Fig. 2.2. Suppose the transmitter emits an axially symmetric radiation pattern described by the radiant intensity (W/sr) $P_tR_0(\phi)$. Here, $R_0(\phi)$ is normalized so that $2\pi \int_0^{\pi} R_0(\phi) \sin\phi d\phi = 1$. At the receiver, located at distance d and angle ϕ with respect to the transmitter, the irradiance (W/cm^2) is $I_s(d,\phi) = P_tR_0(\phi)/d^2$. The received power is

$$P_r = \begin{cases} I_s(d,\phi)AT_s(\psi)g(\psi)\cos\psi, & 0 \leq \psi \leq \Psi_c \\ 0, & \psi > \Psi_c. \end{cases} \tag{2.7}$$

where $T_s(\psi)$ is the signal transmission of the filter, $g(\psi)$ is the concentrator gain and Ψ_c is the concentrator FOV (semiangle). $T_s(\psi)$ may represent an average over the filter transmission at different wavelengths (if the source spectrum is not narrow) and/or angles of incidence

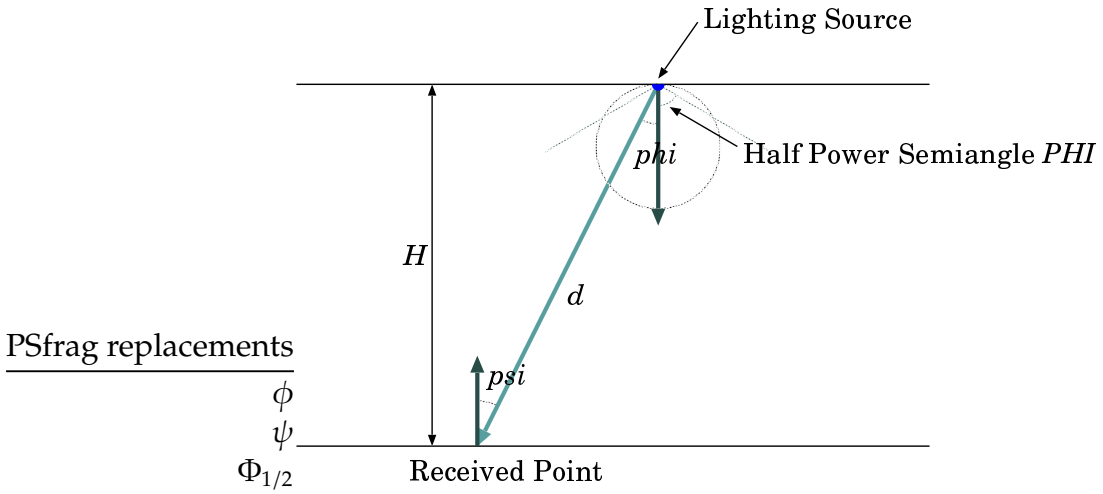

Figure 2.2: Calculation for channel DC gain.

upon the filter (if different rays strike the filter at different angles of incidence). In this dissertation, for simplicity, we assume $T_s(\psi) = 1$ and $g(\psi) = 1$. We obtain the channel DC gain:

$$H(0) = \begin{cases} \frac{A}{d^2} R_0(\phi) T_s(\psi) g(\psi) cos\psi, & 0 \le \psi \le \Psi_c \\ 0, & \psi > \Psi_c. \end{cases} \tag{2.8}$$

which we observe is proportional to d^{-2}. From Eq. (2.11), we observe that if d and $R_0(\phi)$ are fixed, the most effective means to increase $H(0)$ are to increase the detector area A.

The emission from a variety of practical LOS transmitters can be modeled reasonably using a generalized Lambertian radiant intensity [2.4]

$$R_0(\phi) = \frac{m+1}{2\pi} \cos^m(\phi). \tag{2.9}$$

The order m is related to Ψ_c, the transmitter semiagnel at half power, by

$$m = -\frac{\ln 2}{\ln(\cos \Phi_{1/2})}. \tag{2.10}$$

The channel DC gain is given by

$$H(0) = \begin{cases} \frac{(m+1)A}{2\pi d^2} \cos^m \phi T_s(\psi) g(\psi) cos\psi, & 0 \le \psi \le \Psi_c \\ 0, & \psi > \Psi_c. \end{cases} \tag{2.11}$$

2.3 Electrical SNR and BER

In this section we compute the electrical SNR at receiver and BER. Each sample of the receiver output contains a Gaussian noise having a total variance (A^2) that is the sum of contributions from shot and thermal noises

$$\sigma_{total} = \sigma_{shot} + \sigma_{thermal}. \tag{2.12}$$

The electrical SNR is expressed as

$$SNR = \frac{(RP_r)^2}{\sigma^2_{total}}, \tag{2.13}$$

where received optical power is given by

$$Pr = H(0)P_t. \tag{2.14}$$

And the BER is given by

$$OOK : BER = Q(\sqrt{SNR}), \tag{2.15}$$

$$L - PPM : BER = Q(\sqrt{\frac{1}{2}L\log_2 L}\sqrt{SNR}), \tag{2.16}$$

where

$$Q(x) = \frac{1}{\sqrt{(2\pi)}}\int_x^\infty e^{-y^2/2}dy. \tag{2.17}$$

For example, to achieve BER = 10^{-6} it requires SNR = 13.6 dB in OOK and 2-PPM. The shot noise variance is given by

$$\sigma_{shot} = 2qRP_rB + 2qI_{bg}I_2B, \tag{2.18}$$

where q is the electronic charge, B is equivalent noise bandwidth, I_{bg} is background current. I_2, noise bandwidth factor, is set to 0.562. At OOK, noise bandwidth B is equivalent to data rate R_b. And at 2-PPM, B is equivalent to $2R_b$.

Among pre-amplifier designs, the transimpedance type is best suited to most optical link applications, because its achieves a large dynamic range and a wide bandwidth without the need for equalization [2.5]. Under typical conditions, lower noise is achieved if the front-end device is a field-effect transistor (FET), rather than a bipolar-junction transistor (BJT) [2.5, 2.6]. If power consumption is constrained, however, a BJT may achieve superior results. We follow the analysis of Smith and Personick in computing the receiver noise [2.5, 2.7]. We assume the use of p-i-n photodetectors in conjunction with FET-base transimpedance pre-amplifiers. We neglect FET gate leakage and 1/f noise. The thermal noise variance is given by

$$\sigma_{thermal} = \frac{4kT_k}{R_F}I_2B + \frac{16\pi^2kT_k\Gamma}{g_m}(C_d + C_g)^2I_3B^3. \tag{2.19}$$

The first term represents thermal noise from the feedback resistor; k is Boltzmann's constant, T_k is absolute temperature, and R_F is the feedback resistance. In the second term, which

describes thermal noise from the FET channel resistance, Γ is the FET channel noise factor, g_m is the FET transconductance, C_d is the capacitance of a detector, C_g is the FET gate capacitance, and $I_3 = 0.0868$.

In order to determine explicitly how the two noise terms in Eq. (2.19) depend on the received size, we assume that the photodetector has a fixed capacitance per unit area η, i.e., $C_d = \eta A$, where A is the detector area. For simplicity, we assume that $c_g \ll C_d$. we assume that the transimpedance amplifier has a limited open-loop voltage gain G. in order to minimize the noise, it is desirable to maximize R_F, but if the pre-amplifier is to achieve a 3-dB cutoff frequency equal to B, then we must impose the condition $R_F = G/(2\pi BC_d)$. Then Eq. (2.19) becomes

$$\sigma_{thermal} = \frac{8\pi kT_k}{G}\eta A I_2 B^2 + \frac{16\pi^2 kT_k\Gamma}{g_m}\eta^2 A^2 I_3 B^3, \tag{2.20}$$

We choose the following parameter values [2.8]: $T_k = 298$ K, $G = 10$, $g_m = 30$ mS, $\Gamma = 1.5$, and $\eta = 112$ pF/cm^2.

2.4 References

[2.1] J. M. Kahn, J. R. Barry, "Wireless Infrared Communications," Proceedings of the IEEE, vol. 85, no. 2, pp. 265–298, 1997.

[2.2] A. J. C. Moreira, R. T. Valadas, A. M. de Oliveira Duarte, "Optical interference produced by artificial light," Wireless Networks, vol. 3, no. 2, pp. 131–140, 1997.

[2.3] A. J. C. Moreira, R. T. Valadas, A. M. de Oliveira Duarte, "Characterization and modelling of artificial light interference in optical wireless communication systems," IEEE International Symposium on Personal, Indoor and Mobile Radio Communications, pp. 326–331, 1995.

[2.4] F. R. Gfeller, U. Bapst, "Wireless in-house data communication via diffuse infrared radiation," Proceedings of the IEEE, vol. 67, no. 11, pp. 1474–1486, 1979.

[2.5] S. D. Personick, "Receiver design for digital fiber optic communications system, I and II," Bell System Technical Journal, vol. 52, no. 6, pp. 843–886, 1973.

[2.6] T. D. Nguyen, M. S. report, University of California Berkeley, 1995.

[2.7] R. G. Smith, S. D. Personick, "Receiver design for optical fiber communication systems," in Semiconductor Devices for Optical Communication, New York: Springer -Verlag, 1980.

[2.8] R. Djahani, J. M. Kahn, "Analysis of Infrared Wireless Links Employing Multibeam Transmitters and Imaging Diversity Receivers," IEEE Transactions on Communications, vol. 48, no. 12, pp. 2077–2088, 2000.

Chapter 3

Characteristics of White LED

LED has lower power consumption, lower voltage, longer lifetime, smaller size, faster response, and cooler operation, compared with conventional lighting devices. LED is used in full color displays, traffic signals, and many other means of illumination. Now, white LED is considered as a strong candidate for the future lighting technology [3.1, 3.2]. Compared with conventional lighting methods, white LED has lower power consumption, lower voltage, longer lifetime, smaller size, and cooler operation. The Ministry of Economy, Trade and Industry of Japan estimates, if LED replaces half of all incandescent and fluorescent lamps currently in use, Japan could save equivalent output of six mid-size power plants, and reduce the production of greenhouse gases. A national program underway in Japan has already suggested that white LED deserves to be considered as a general lighting technology of the 21st century owing to electric power energy consumption.

White LED is currently achieved by using two different methods. The first is by combining a blue 450 nm - 470 nm GaN (Gallium Nitride) LED with YAG (Yttrium Aluminum Garnet) phosphor. The blue wavelength excites the phosphor causing it to glow white. The second method is to combine red, green, and blue LEDs in the proper proportion to achieve a white color. The former is presently the most dominant and efficient technique used. Recently, new white LEDs have become available by combining a UV (Ultra Violet) LED, 380 nm, with phosphor. In addition, by combining different phosphor types with a UV LED, other colors such as purple, orange, pink etc. can be achieved.

Generally, modulation bandwidths of white LED in typical low cost device as lighting source range from 10 kHz to tens of MHz. With the explosion of interest in visible light wireless communication using white LED, it is quite likely that white LED has wide modulation bandwidth like infrared LED for communication purpose. Recently, RC-LED (Resonant Cavity LED) have been developed. Their structures are epitaxially grown by MBE on double polished n+ GaAs substrates and emit through the substrate, which is nominally transparent at these wavelength. The active layers in the cavity are 3 or 4 strained $In_xGa_{1-x}As$ (x~0.17) Quantum Wells (QWs) clad by GaAs barrier layers. The bottom mirror is a multiple quarter-wave stack of GaAs/AlAs layers, known as a Distributed Bragg Reflector (DBR). The cavity is completed by the deposition of a metal mirror on the upper surface of the multilayer structure. A key property of RC-LED of application is the ability to determine the emission angular beam profile by designing the emission wavelength of the QWs inside the cavity to be approximately 10-20 nm shorter than the

resonance wavelength of the cavity. Moreover the modulation bandwidth of RC-LED are achieved to approximately 500 MHz [3.3–3.5]. In [3.6], a waveform compensation by pre-emphasis circuit in electrical stage has been reported. The modulation bandwidth of output waveform from RC-LED has been enlarged from 73 MHz to 223 MHz.

In this section, we measure the basic white LED (GaN LED with YAG phosphor) characteristics, analyze the experimental parameters. As common white LED, we use the Luxeon V Portable LXHL-LW6C (LUMILEDS) on the market. And the results of numerical analysis are approximated by using the experimental parameters.

3.1 Basic Properties of LED Light

We will explain the basic properties of LED light. LED light has two basic properties, a luminous intensity and a transmitted optical power. Luminous intensity is the unit that indicates the energy flux per a solid angle, and it is related to illuminance at an illuminated surface. At this time, the energy flux is normalized with visibility. The luminous intensity is used for expressing the brightness of an LED. On the other hand, the transmitted optical power indicates the total energy radiated from an LED, and as is a parameter from the point of view of optical communication.

The luminous intensity is given as:

$$I = \frac{d\Xi}{d\Omega}, \tag{3.1}$$

where Ξ is the luminous flux, which can be given from the energy flux Ξ_e as:

$$\Xi = K_m \int_{380}^{780} V(\lambda)\Xi_e(\lambda)d\lambda, \tag{3.2}$$

where $V(\lambda)$ is the spectral luminous efficiency as shown in Fig. 3.1, K_m is the maximum visibility, and the maximum visibility is approximately 683 lm/W at $\lambda = 555$ nm.

The integral of the energy flux Ξ_e in all directions is the transmitted optical power P_t, given as:

$$P_t = \iint_{\Lambda_{min}}^{\Lambda_{max}} \Xi_e \, d\theta \, d\lambda, \tag{3.3}$$

where Λ_{min} and Λ_{max} are determined by the sensitivity curve of the photodiode.

3.2 Radiation Pattern

We employ a power meter (ADVANTEST: Q8230 and Q82313). And we correct the optical sensor area to 0.1 cm^2. The measuring method is shown in Fig. 3.2. The input voltage of LED and input current are 6.42 V and 700 mA, respectively. And we set the junction temperature at 25 deg. C.

Figure 3.3 presents measured radiation pattern and the approximated Lambertian radiation pattern. The measured white LED of the half power semiangle is 60.0 deg.. We can know that the assumption of Lambertian radiation is correct, approximately.

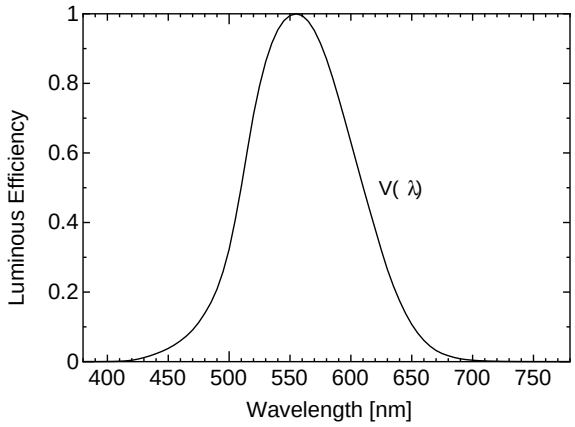

Figure 3.1: Spectral luminous efficiency functions as defined by the CIE.

Figure 3.2: Measuring method of radiation pattern.

3.3 Luminous Intensity and Optical Output Power

In this section, we analyze the luminous intensity and optical output from measured values. The measuring method is shown in Fig. 3.4. First, we measure the illuminance by illuminance meter in a direction toward the optical axis at 10 cm intervals. The illuminance meter is vertically set up in an optical axis. Here we set the current of electricity at 700 mA, and the junction temperature at 25 deg. C.

The illuminance expresses the brightness of an illuminated surface. The LED has a luminous intensity $I(0)$ on optical axis and an Lambertian distribution is assumed as its light distribution. The radiant intensity depends on the angle of irradiance. Therefore, the luminous intensity in angle ϕ is given by

$$I(\phi) = I(0)\cos^m(\phi). \tag{3.4}$$

The m is the order of Lambertian emission, which is given by the semiangle at half power of an LED $\Phi_{1/2}$ as

$$m = \frac{-\ln 2}{\ln(\cos \Phi_{1/2})}. \tag{3.5}$$

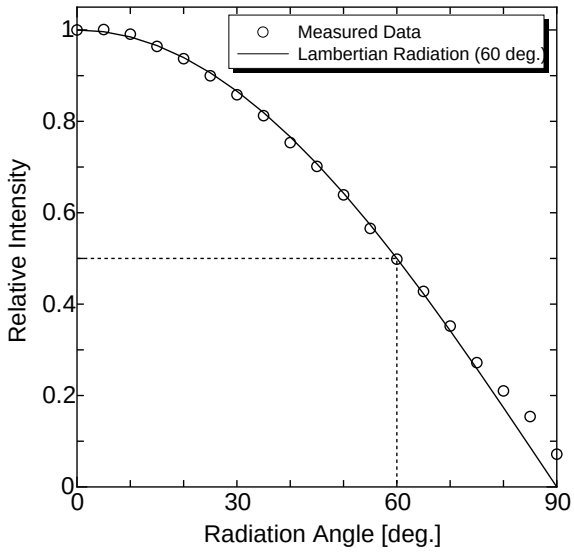

Figure 3.3: Radiation pattern.

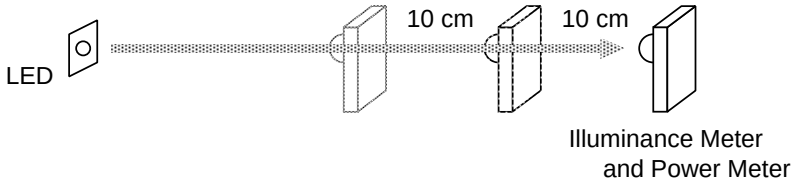

Figure 3.4: Measuring method of optical output power and luminous intensity.

A horizontal illuminance E is given by

$$E = \frac{I(\phi)}{d^2}\cos(\psi), \tag{3.6}$$

where ϕ is the angle of irradiance, ψ is the angle of incidence, and d is the distance between an LED and a detector's surface. In this section, owing to the measurement on optical axis, ϕ is 0 deg.. Since the illuminance meter is vertically set up in the optical axis, ψ is 0 deg.. Therefore, a horizontal illuminance on an optical axis $E_{optical\ axis}$ is given by

$$E_{optical\ axis} = \frac{I(0)}{d^2}. \tag{3.7}$$

From this equation, we calculate the luminous intensity.

Figure 3.5 shows measured illuminance and calculated luminous intensity on optical axis. From this figure, when the distance between light source and receivers is near, we can know that the luminous intensity is not constant. This is because the equation is true

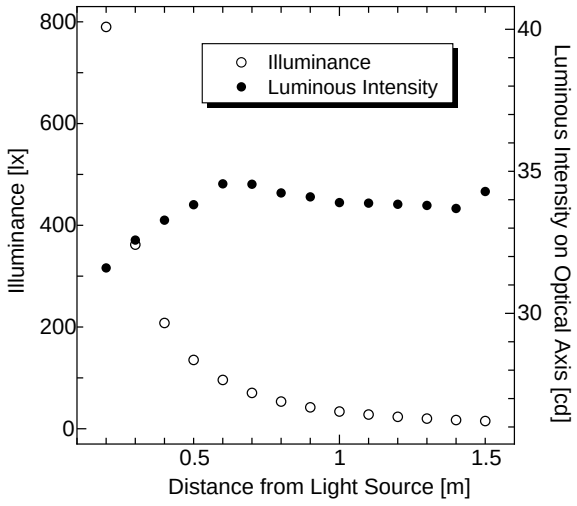

Figure 3.5: Luminous intensity.

when the light source is point source. So, when the distance is near, the light source can not assume as point source. Therefore accurate value is not calculated.

Generally, the photometry bound distance r_p is given by

$$r_p = h_r \sqrt{\frac{1-\sigma}{\sigma}}, \tag{3.8}$$

where, h_r is radius of light source, σ is acceptable error range. When the radius of light source is 0.003 m, and we set the acceptable error range at 1e-4, the photometry bound distance is about 0.30 m. So, we calculate the luminous intensity as average on 0.5 to 1.2 m. Therefore, the calculated luminous intensity is 34.11 cd.

In the similar way, we calculate an optical output power by received power. we measure the received power by power meter in a direction toward the optical axis at 10 cm intervals, similarly. The power meter is vertically set up in an optical axis. In an optical link, the received power P_r on directed path is given as:

$$P_r = \begin{cases} P_t \cdot \dfrac{(m+1)A}{2\pi d^2} \cos^m(\phi) T_s(\psi) g(\psi) \cos(\psi), & 0 \le \psi \le \Psi_c, \\ 0, & \psi > \Psi_c, \end{cases} \tag{3.9}$$

where P_t is optical output power, A is the physical area of a detector in a photodiode, $T_s(\psi)$ is the signal transmission of the filter, and $g(\psi)$ is the concentrator gain. In this case, the parameters are ϕ=0, ψ=0, $T_s(\psi)$=1, $G(\psi)$=1. And the order m is related to Ψ_c, the transmitter semiagnel at half power, by $m = -\ln 2/\ln(\cos\Phi_{1/2})$. Since the semiangle at half power is 60.0 deg. from section 3.2, m=1. Therefore, the received power on the optical axis is given by

$$P_{r\ optical\ axis} = P_t \cdot \frac{(m+1)A}{2\pi d^2}, \tag{3.10}$$

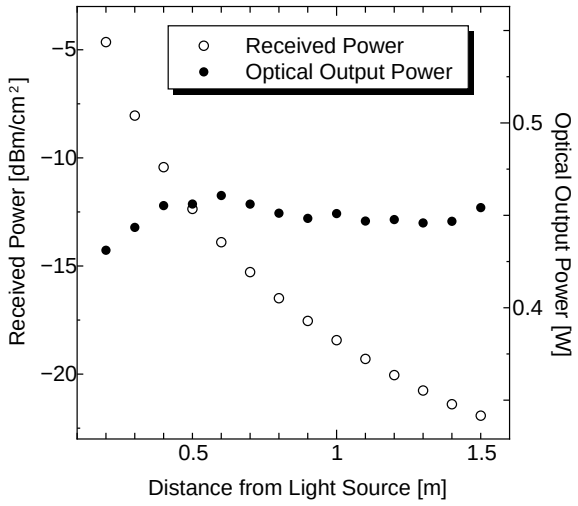

Figure 3.6: Optical output power.

Table 3.1: Results of measurements.

Semiangle of Half Power [deg.]	60.0
Luminous Intensity [cd]	34.11
Optical Output Power [W]	0.452
E/O Conversion Efficiency	0.101
Total Luminous Flux [lm]	107.16

Note: Input current of electricity is 700 mA, junction temperature is 25 deg. C.

From this equation, we calculate the optical output.

Figure 3.6 shows the received power and the optical output power. we calculated the optical output power as average on 0.5 to 1.2 m, similarly. It is found from the result that the calculated optical output power is 0.452 W.

3.4 Total Luminous Flux

Total luminous flux Ξ is related to irradiance ϕ and κ, by

$$\Xi = \int_{\kappa=0}^{2\pi} \int_{\phi=0}^{\pi} I(\phi, \kappa) \sin\phi d\phi d\kappa. \tag{3.11}$$

The radiation pattern of LED is rotation symmetry on optical axis. Then Eq. (3.11) becomes

$$\Xi_{LED} = 2\pi \int_{\phi=0}^{\pi} I(\phi) \sin\phi d\phi, \tag{3.12}$$

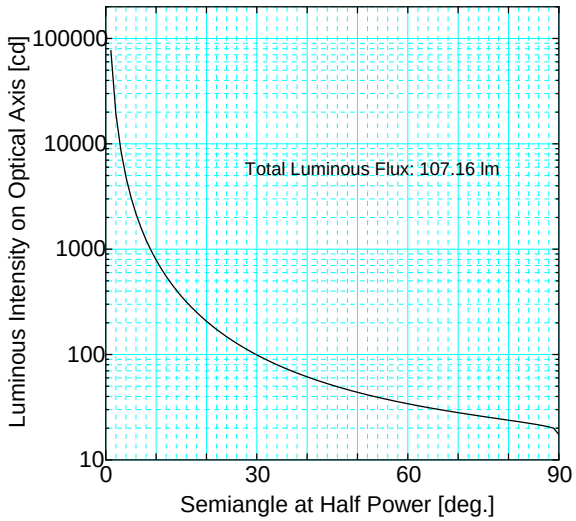

Figure 3.7: Semiangle at half power and luminous intensity on optical axis.

Table 3.2: Semiangle at half power and luminous intensity on optical axis.

Semiangle at Half Power [deg.]	Luminous Intensity on Optical Axis [cd]
10.0	789.30
20.0	207.11
30.0	99.24
40.0	61.41
50.0	43.81
60.0	34.11
70.0	28.07
80.0	23.81

$$\Xi_{LED} = 2\pi \int_{\phi=0}^{\pi} I(0) \cos^m \phi \sin \phi d\phi. \tag{3.13}$$

From Eq. (3.13), we can calculate the total luminous flux with luminous intensity and semiangle of half power. Therefore, we can calculate that the total luminous flux is 107.16 lm. Table 3.1 summarizes the results of the calculated parameters.

Next we discuss the luminous intensity of measured white LED, when semiangle of half power is changed by lens. Using Eq. (3.13), we show the relation between semiangle of half power and luminous intensity on optical axis at fixed total luminous flux in Fig. 3.7 and Table 3.2. These parameters are used in the following chapters.

3.5 References

[3.1] S. Nakamura, "Present performance of InGaN based blue / green / yellow LEDs," Proceedings of SPIE Conference on Light-Emitting Diodes: Research, Manufacturing, and Applications, vol. 3002, pp. 24–29, 1992.

[3.2] C. P. Kuo, R. M. Fletcher, T. D. Osentowski, M. C. Lardizabal, M. G. Craford, V. M. Robbins, "High performance ALGaInP visible light-emitting diodes," Applied Physics Letters, vol. 57, no. 27, pp. 2937–2939, 1990.

[3.3] K. Takaoka, G. Hatakoshi, "InGaAlP-based red VCSEL & RCLED," IEICE Technical Report, vol. LQE200-128, pp. 51–56, 2001.

[3.4] D. C. O'Brien, G. E. Faulkner, K. Jim, E. B. Zyambo, D. J. Edwards, et al., "High speed integrated optical wireless transceivers for in-building optical LANs," Proceedings of SPIE Conference on Wptical Wireless Communication III, vol. 4214, Boston, USA, pp. 104–114, 2001.

[3.5] D. M. Jolburn, R. J. Mears, R. J. Samsudin, "A CMOS 155Mb/s optical wireless transmitter for indoor networks," Proceedings of SPIE Conference on Optical Wireless Communications III, vol. 4214, Boston, USA, pp. 124–132, 2001.

[3.6] A. Ishizuka, K. Nakajima, H. Koyano, "Simple Packaging Technologies for Optical Transceiver Module Adaptable to Large Core-Diameter Fiber Link," IEICE Transactions on Electronics, vol. J84–C, no. 9, pp. 822–830, 2001.

Chapter 4

Proposal of Indoor Visible Light Wireless Communication Systems utilizing White LED Lighting Equipment and Their Performance Evaluation for Lighting Design

Future electric lights will be comprised of white LEDs. White LEDs with a high power output are expected to serve in the next generation of lamps. In this chapter, an indoor visible light wireless communication system utilizing white LED lighting is proposed. In the proposed system, these devices are used not only for illuminating rooms but also for a wireless optical communication system. This system is suitable for private networks such as consumer communication networks. However, it remains necessary to investigate the properties of white LEDs when they are used as optical transmitters. Based on numerical analyses and computer simulations, it was confirmed that the proposed system could be used for indoor optical transmission.

4.1 Proposal of New LED Lighting Equipments with Function of Wireless Data Transmission

In 21st century, high data rate transmission will pervasively play an important role in our life. To achieve high data rate transmission the radio frequency has been mainly considered in offices and at our homes. However the radio frequency spectrum is so congested that there is a limit to make it.

On the other hand, white LED has lower power consumption, lower voltage, longer lifetime, smaller size, faster response, and cooler operation, compared with conventional lighting devices. The white LED will eventually replace incandescent or fluorescent lights in offices and homes [4.1–4.3].

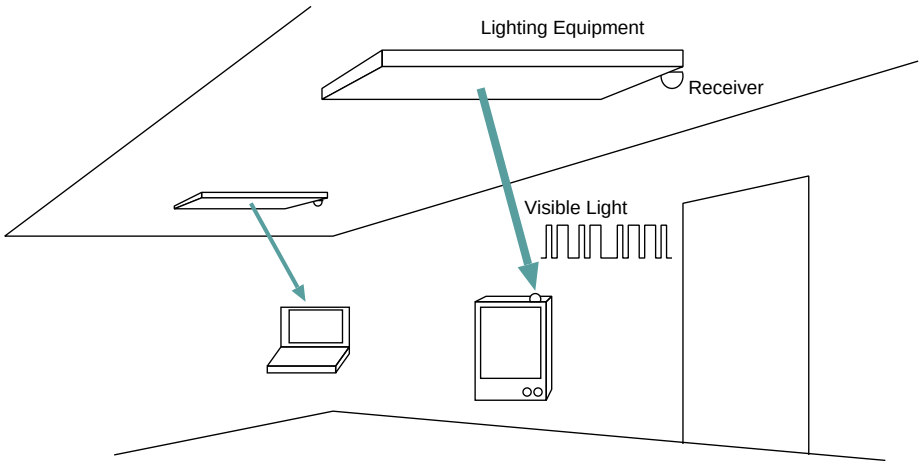

Figure 4.1: A proposed system image.

We propose a visible light wireless data transmission system utilizing LED lighting [4.4–4.10]. In this system, lighting equipment has the capacity for wireless optical communication. The proposed system has the following advantages:

- Compared with infrared wireless communication, visible LED light has higher power.
- Lighting equipment with white LEDs is easy to install and aesthetically pleasing.

In order to realize this system, study of optical properties as lighting equipment and an optical transmitter is required. Thus, based on a lighting engineering, some numerical analyses for the proposed system are performed, and are reported herein. Through numerical analyses and computer simulations, we will find that the proposed system is viable candidate for indoor wireless data transmission systems.

4.1.1 Visible Light Wireless Data Transmission Lighting Equipment

This chapter proposes and studies an indoor visible light data transmission system that utilizes white LED lighting as shown in Fig. 4.1. White LED lighting equipment does not only illuminate a room but also modulate electric signals into visible lightwave signals, and these signals are emitted into the air. The blinking rate of modulated lightwave is sufficiently rapid that human eyes cannot detect it. Therefore, the role of lighting is not spoiled by wireless optical communication. Moreover, since this transmitter is lighting equipment, the color of light from the lighting equipment should be white. By employing a multi-chip white LED, there is a possibility of communication by the light of primary color [4.10]. In this paper, we will focus our attention on one-chip white color LED. And we will discuss the relation between energy of lighting and communication performance.

Table 4.1: Design parameters of LED lighting equipments.

	General Lighting	Downlight
Semiangle at Half Power of LED [deg.]	80	20
Luminous Intensity at each LED [cd]	23.81	207.11
Optical Output Power at each LED [W]	0.452	0.452
Number of LEDs	10×10	3×3
Interval between LEDs [cm]	4	4

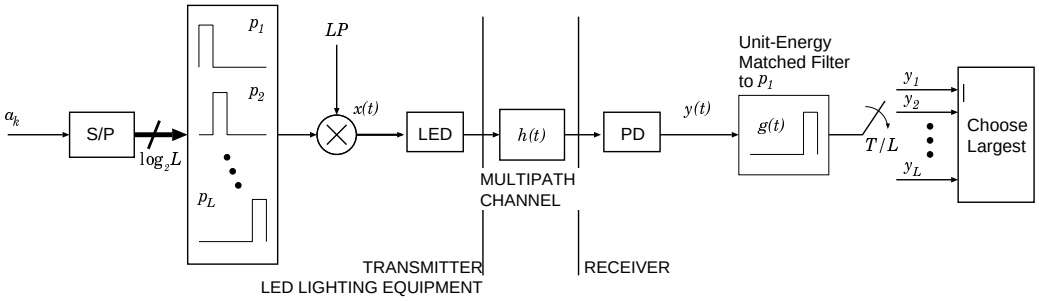

Figure 4.2: L-PPM system.

Here, we should notice that the visible light wireless communication system utilizing lighting equipment is not bidirectional communication scheme. As the method of solving the uplink problem, we can consider radio wave, infrared, and visible light for medium [4.11]. Especially, the uplink using visible light has characteristic. The light from the lighting equipment is reflected by a corner cube reflector to the lighting source. The reflected light is modulated by an optical shutter at the receiver. Therefore the large power from the lighting equipment is used for uplink data transmission [4.11]. This uplink problem remains as a matter to be discussed further. In this study, we will limit the discussion to the downlink data transmission in visible light wireless communication using lighting equipment.

Proposal LED Lighting Equipments

First, we design two proposal lighting equipments. They are general lighting and downlight. Table 4.1 reports the design parameters. The general lighting has 100 LEDs, and semiangle at half power of each LED is 80 deg.. And the downlight has 9 LEDs, and semiangle at half power of each LED is 20 deg.. These parameters are calculated by measurements of white LED on the market in chapter 3.

Pulse Position Modulation

As the Fig. 4.2 shows, in these system, IM/DD is applied as a method of optical pulse modulation for the proposed system. The a_k input bits are grouped in blocks of length

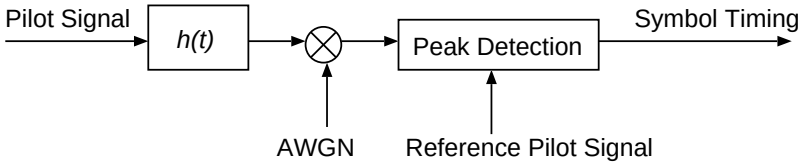

Figure 4.3: Symbol timing controller.

$\log_2 L$, at a symbol rate of $1/T = R_b/\log_2 L$, and from each block one of L possible signals is chosen to be transmitted. In L-PPM, the symbol interval is divided into L time slots (this indicates that a symbol can represent $\log_2 L$ bits), and the optical signal is "on" during the l-th slot. In short, the position of the "on" pulse slot indicates the information. In L-PPM, the power efficiency increases in proportion to the number of slots (L) in each L-PPM symbol at the cost of wide bandwidth. The increase of PPM bandwidth, however, is not very important in a wireless optical channel, since it already has wide bandwidth available. The transmitted pulses are described as follows:

$$x(t) = LP \sum_k p_{l[k]}(t - kT), \tag{4.1}$$

where $\{p_l\}$ is a family of pulse shapes given by:

$$p_l(t) = \begin{cases} 1 & \text{for } t \in [(l-1)T/L, lT/L) \\ 0 & \text{elsewhere} \end{cases}, \quad \text{for } l \in \{1, 2, \ldots, L\}. \tag{4.2}$$

These PPM pulses are transmitted and suffer from intersymbol interference (ISI). Since average power of transmitted signal is constant all of the time, a flicker is not generated over kbit/s. Transmitted optical pulses from LED lighting equipment is received at a user terminal, which is composed of photodiode and can convert optical pulses into electric signals. The received pulses are passed through a matched filter $g(t)$ which has unit energy and is matched to the first-position pulse shape $p_1(t)$:

$$g(t) = \sqrt{\frac{L}{T}} p_1(-t). \tag{4.3}$$

The L different receiver branches are able to share this single filter by sampling its output at a rate of L/T, yielding the same L sufficient statistics y_1 through y_L. The receiver compares y_1 through y_L and decides on the l-th symbol when y_l is the largest. In this dissertation, we use 2-PPM scheme for visible light wireless communication.

Symbol Timing

When the receiver demodulates the distorted signal by wireless channel, a symbol timing is important to achieve high BER performance. Figure 4.3 shows the construction of symbol

timing controller. The optimum symbol timing is searched by correlation between the received pilot signal and reference pilot signal. The system searches the high correlation with oversampling rate of 8. After the setting of the symbol timing, data is demodulated.

4.1.2 Radiation Pattern and Illuminance Distribution of LED Lighting Equipments

Figures 4.4(a) and 4.4(b) show the radiation pattern of each lighting equipment. The semiangle at half power of the general lighting and the downlight are 81.57 deg. and 20.18 deg., respectively. We can know that light distribution of plural LED is different from the radiation pattern of each LED.

When an LED has Lambertian radiation, a horizontal illuminance E from lighting equipment, which consists of plural same LEDs, is given by

$$E = \sum_{i}^{LED} \frac{I(0)\cos^{m}\phi_i}{d_i^2}\cos(\psi_i), \tag{4.4}$$

where $I(0)$ is luminous intensity on optical axis at an LED, m is the order of Lambertian emission at an LED, ϕ is the angle of irradiance, ψ is the angle of incidence, and d is the distance between an LED and a detector's surface. From this equation, illuminance distribution of the general lighting and the downlight are shown in Fig. 4.5(a) and 4.5(b), respectively. Here, Fig. 4.5 shows the relation between H and horizontal distance. as shown in Fig. 4.6. We can know that the illuminance of general lighting at H=3.0 m is about 280 lx. And the illuminance of downlight at H=3.0 m is about 220 lx. We can also see that the downlight has strong attenuation, compared with general lighting. At 2 m from the center of the lighting equipment, we feel dim light.

4.1.3 Received Optical Power for Data Transmission

In an optical link, the received power P_r on directed path from lighting equipment, which consists of plural LEDs, is given as:

$$P_r = \sum_{i}^{LED} P_{ti}H_i(0). \tag{4.5}$$

where P_t is optical output power. The channel DC gain on directed path $H(0)$ is given as described in section 2.2.

Figure 4.7 to 4.9 present the received optical power of each proposed lighting equipment. Here, we define a tracking as a maintaining of an optical axis to center of the nearest lighting. To put it briefly, the angle of incidence becomes 0 deg.. We have an assumption that the tracking is performed by user. When the light is blocked by some people, the user is discernible by the visual senses. And the user will move to viewable space, as if you take picture in a crowd. From these figures, when vertical distance between lighting equipment and receiver increases H, the ratio of power attenuation becomes small. And we can also see the system with tracking has high received power especially at the general

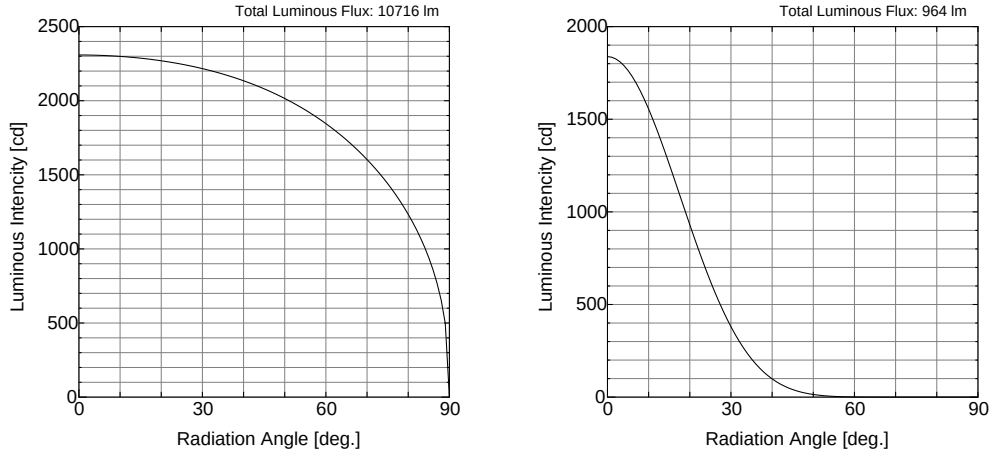

(a) General Lighting. (b) Downlight.

Figure 4.4: Radiation pattern.

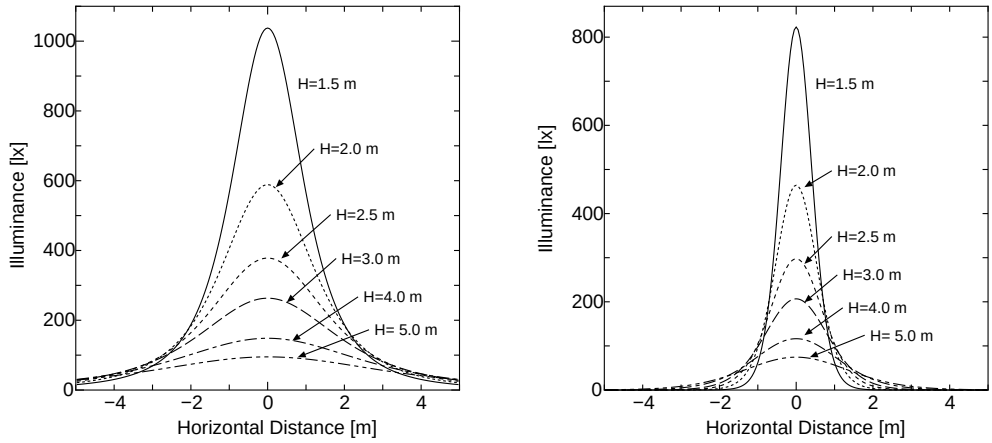

(a) General Lighting. (b) Downlight.

Figure 4.5: Illuminance distribution at each height between the light equipment and the receiver.

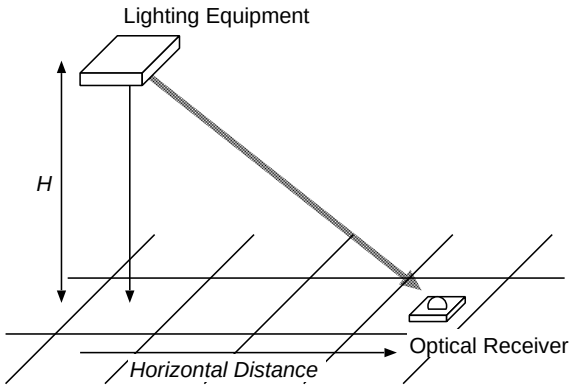

Figure 4.6: Calculation of illuminance.

Table 4.2: SNR calculation parameters.

Detector Physical Area of a PD	1 [cm^2]
Gain of an Optical Filter	1.0
O/E Conversion Efficiency	0.54 [A/W]
Open-Loop Voltage Gain	10
Fixed Capacitance	112 [pF/cm^2]
FET Channel Noise Factor	1.5
FET Transconductance	30 [mS]
Absolute Temperature	298 [K]
Background Light Current	5100 [μA]

lighting. This is because that the large surface area of lighting equipment gives large angle dependence at receiver. Figure 4.10 shows the relation between received optical power and electrical SNR at each data rate. The electrical SNR is given as described in section 2.2 and 2.3. And the parameters of SNR calculation are listed in Table 4.2. $T_s(\psi)$=1, $g(\psi)$=1, A=1 cm^2, T_k=298 K, G=10, g_m=30 mS, Γ=1.5, η=112 pF, I_2=0.562, I_3=0.0868, and I_{bg}=5100 μA. The background current is a measured value of direst sun light [4.12]. From this figure, with increasing data rate, the required received power increases. At 100 Mbit/s, the required received optical power is about 22 dBm. Therefore, from these figures, we can see that the communication area changes significantly by data rate. And, whether the system has tracking or not, we can obtain high received optical power for communication easily.

4.1.4 Propagation Delay by Wide Surface Area of Lighting Equipment

A useful measure of the severity ISI induced by a multipath channel $h(t)$ is the channel root mean square (RMS) delay spread τ_{RMS}. The RMS delay spread of a channel is a remarkably accurate predictor of ISI induced SNR penalties, independent of the particular

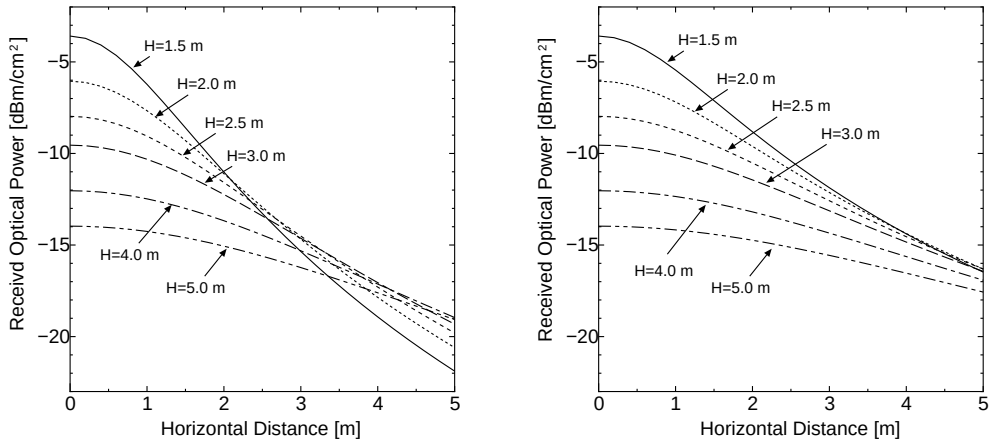

(a) Non tracking. (b) Tracking.

Figure 4.7: Received optical power of the general lighting.

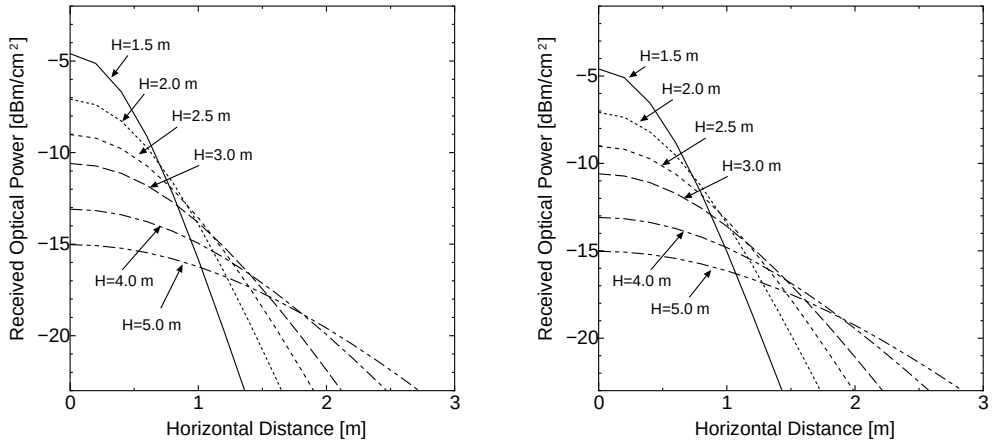

(a) Non tracking. (b) Tracking.

Figure 4.8: Received optical power of the downlight.

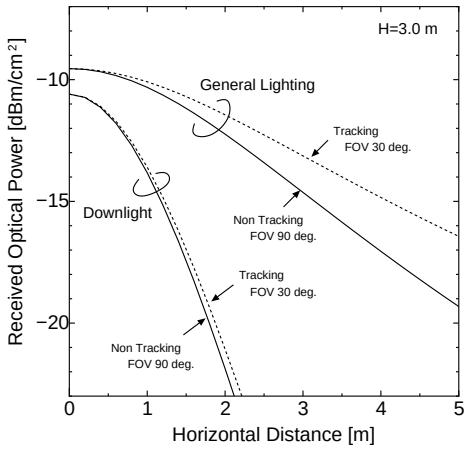

Figure 4.9: Received optical power.

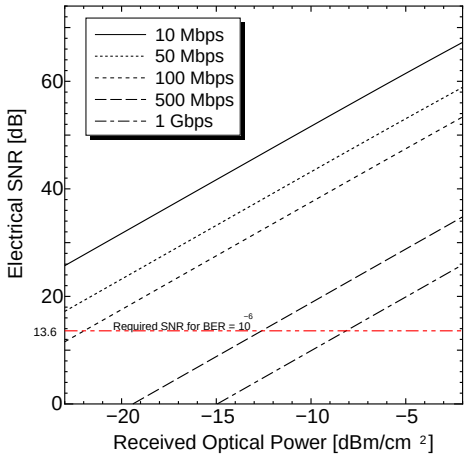

Figure 4.10: Received optical power vs. electrical SNR.

time dependence of that channel 's impulse response [4.13]. The RMS delay spread is computed from the impulse response using

$$\tau_{RMS} = \sqrt{\frac{\int_{-\infty}^{\infty}(t-\tau_0)^2 h^2(t)dt}{\int_{-\infty}^{\infty} h^2(t)dt}}, \tag{4.6}$$

where the mean delay time τ_0 is given by

$$\tau_0 = \frac{\int_{-\infty}^{\infty} t \cdot h^2(t)dt}{\int_{-\infty}^{\infty} h^2(t)dt}. \tag{4.7}$$

The impulse response $h(t)$ and RMS delay spread τ_{RMS} can be considered to be deterministic quantities, in the sense that as long as the positions of the transmitter, receiver and intervening reflectors are fixed, $h(t)$ and τ_{RMS} are fixed. This stands in contrast to the case of time varying radio channels, where the RMS delay spread is interpreted as a statistical expectation of a random process [4.14]. Figure 4.11 and 4.12 present RMS delay spread and mean delay time, respectively. The general lighting is consisted of 10×10 LEDs, and the interval between LEDs is 4 cm. And the downlight is consisted of 3×3 LEDs. From these figures, we can see that the RMS delay spread and the mean delay time increase with horizontal distance from lighting equipment. The downlight with small surface area has small delay, compared with the general lighting. Whether the system has the tracking or not, the performance is almost the same. In infrared wireless communication, large surface area like 40 cm $\times$ 40 cm is not possible, commercially. However in visible light wireless communication, there is a possibility that the lighting equipment has a larger surface area. Therefore, it suggests that the ISI can be main problem.

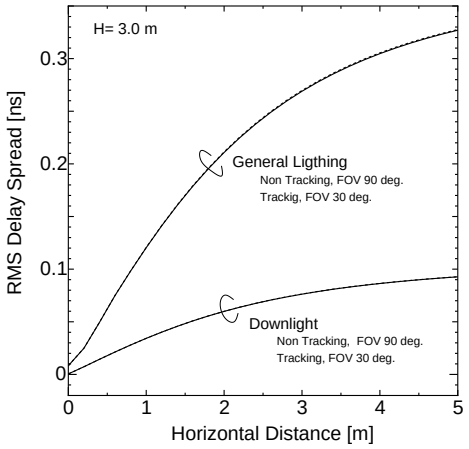

Figure 4.11: RMS delay spread at H=3.0 m.

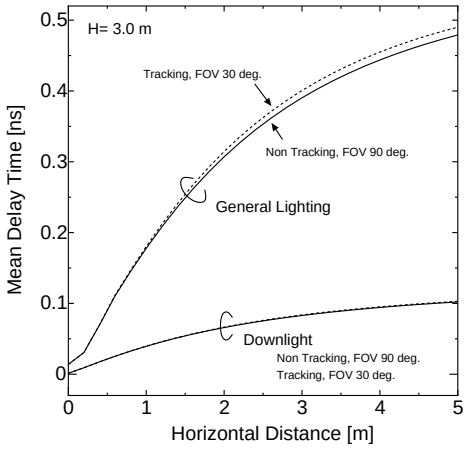

Figure 4.12: Mean delay time at H=3.0 m.

4.1.5 BER Performance of Proposal Systems

Figure 4.13 and 4.14 present the BER performance at each data rate. From these figures, by increasing data rate, the communication area becomes small. When required BER is 10^{-6}, the communication area of general lighting without tracking at 10 Mbit/s is about 12 m in radius. And the system with tracking is about 19 m in radius. At the general lighting, the communication area of the system with tracking is large. This is because that the received power is large by angle dependence at receiver. At the downlight, the communication area of without tracking at 10 Mbit/s is about 2.7 m in radius. And the system with tracking is about 2.9 m in radius.

Next, we show the relation between illuminance and BER performance at H=3.0 m in Fig. 4.15 and 4.16. From Fig. 4.15, when the receiver has no tracking and data rate is 100 Mbit/s, an illuminance of 15 lx and over achieves the required BER. And the illuminance of 200 lx and over can achieve the data transmission at 500 Mbit/s. From these figures, we can see that the downlight system achieves the high BER performance with lower illuminance, compared with the general lighting.

4.2 Influence of Multiple Lighting Equipments that Transmit Different Information

Next, we will discuss an influence of multiple lighting equipments. Here, we define that two lighting equipments transmit different information. The receiver is located directly below the lighting equipment A as shown in Fig. 4.17. Therefore the lighting equipment B is interference source to the receiver. And we also define that the receiver does not have the tracking system.

Figure 4.18 presents the relation between BER and the distance between lighting equip-

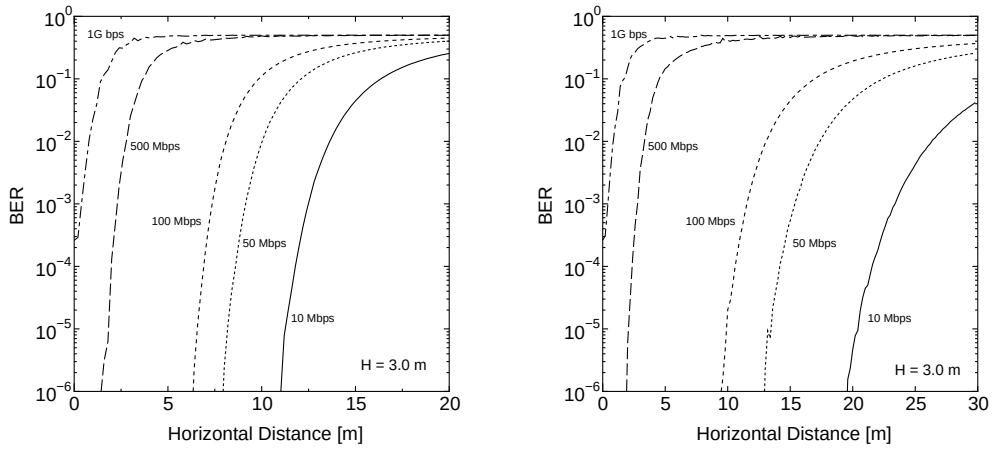

(a) Non tracking. (b) Tracking.

Figure 4.13: BER performance of the general lighting.

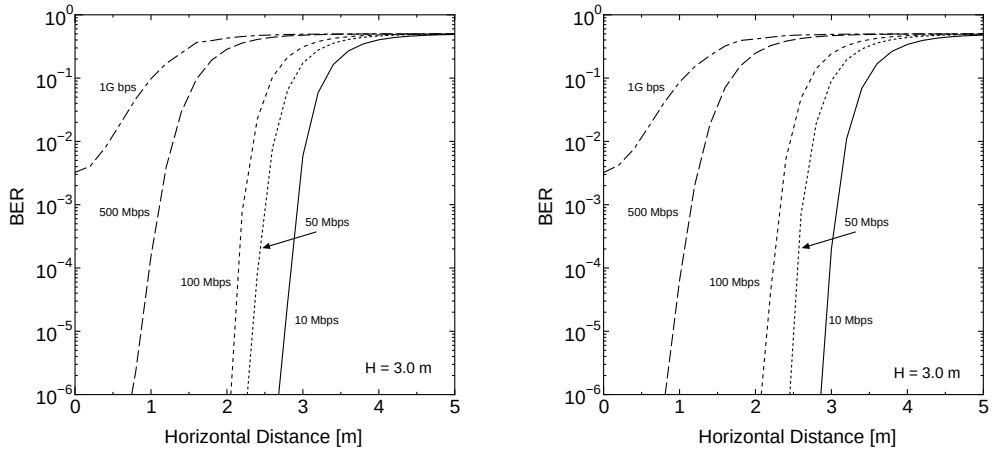

(a) Non tracking. (b) Tracking.

Figure 4.14: BER performance of the downlight.

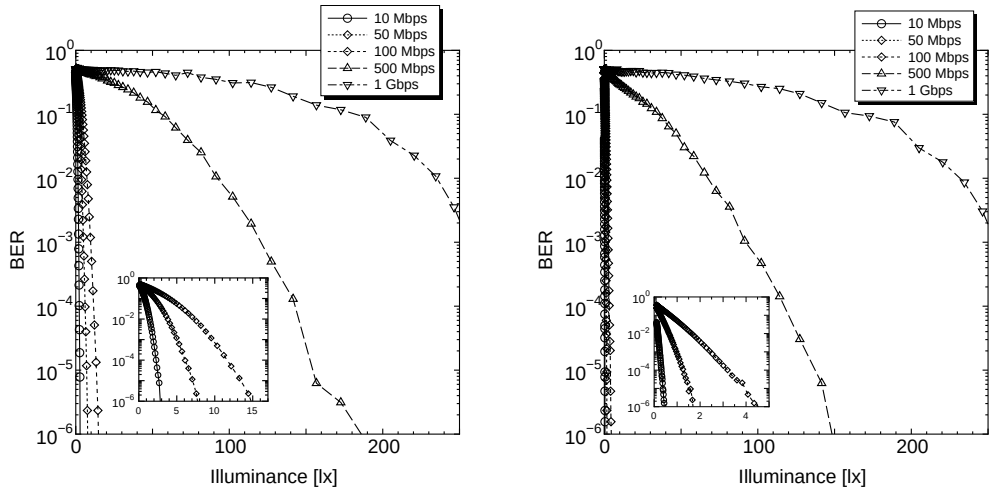

(a) Non tracking. (b) Tracking.

Figure 4.15: Illuminance and BER performance of the general lighting at H=3.0 m.

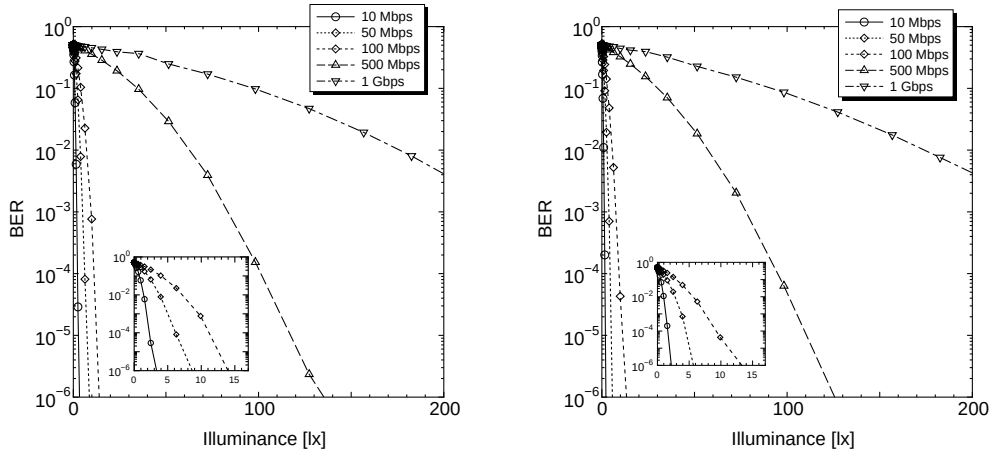

(a) Non tracking. (b) Tracking.

Figure 4.16: Illuminance and BER performance of the downlight at H=3.0 m.

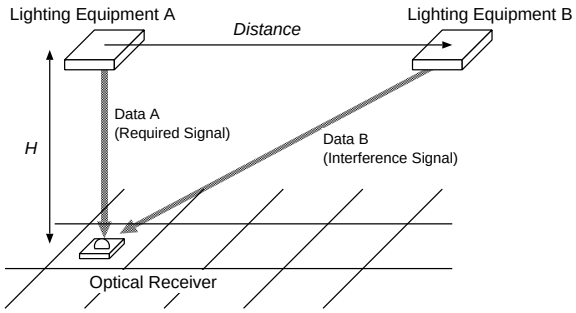

Figure 4.17: Influence of multiple lighting equipments.

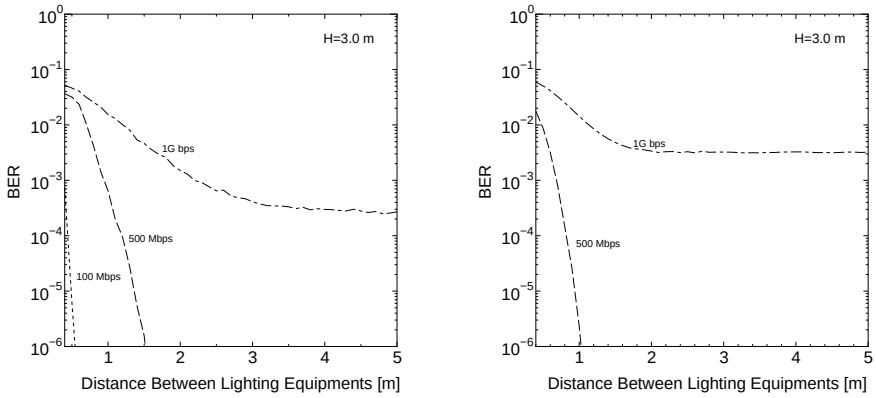

(a) General lighting. (b) Downlight.

Figure 4.18: BER performance by plural lighting equipments at H=3.0 m. (Non tracking, FOV 90 deg.)

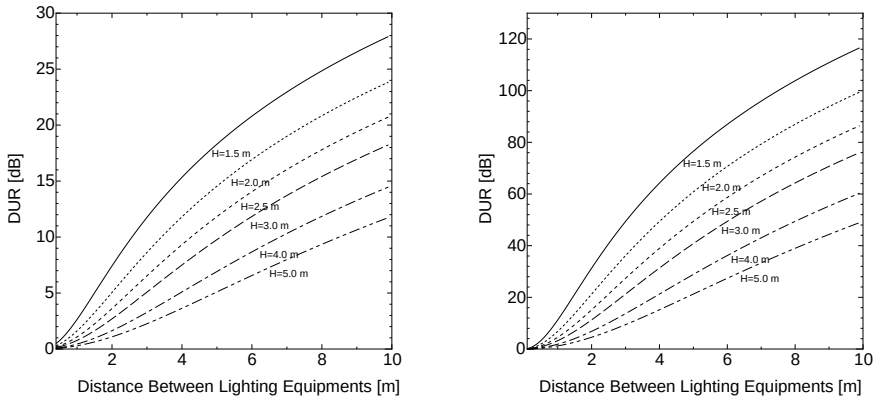

(a) General lighting. (b) Downlight.

Figure 4.19: DUR and distance between lighting equipments. (Non tracking, FOV 90 deg.)

ments. At the general lighting with 500 Mbit/s data transmission, when the lighting equipment B, which is interference source, is installed over 1 m apart, the high BER performance is achieved. At the downlight, the distance between lighting equipment is 1 m at similar condition. In the case under 100 Mbit/s, by a bit of the distance, the high BER performance is achieved. This is because that the sufficient SNR overcomes the ISI as shown in Fig. 5.6 and 4.10. Figure 4.19 shows the relation between desired and undesired ratio (DUR) and the distance. From this result, by calculated DUR by measurement, we can know a communication quality of the lighting equipment. These results are useful to install the lighting equipment.

4.3 Summary

In this chapter, we have proposed a visible light wireless data transmission system utilizing LED lighting equipment. In this system, the lighting equipment has the capacity for wireless optical communication. Based on a lighting engineering, some numerical analyses for the proposed system have been performed. Firstly, the proposed lighting equipments as general lighting and downlight have been designed. The received optical power, RMS delay spread and BER performance have been shown at each lighting equipment. And the relation between illuminance and BER performance at each data rate has been elucidated. Secondly, the influence of multiple lighting equipments that transmit different information has benn discussed. By calculated DUR by measurement, communication quality of the lighting equipments is known and the results are useful to install the lighting equipment. Therefore, the availability of the proposed system to high data wireless transmission has been shown.

4.4 References

[4.1] C. P. Kuo, R. M. Fletcher, T. D. Osentowski, M. C. Lardizabal, M. G. Craford, "High performance AlGaInP visible light-emitting diodes," Applied Physics Letter, vol. 57, no. 27, pp. 2937–2939, 1990.

[4.2] S. Nakamura, "Present performance of InGaN-based blue / green / yellow LEDs," Proceedings of SPIE Conference on Light-Emitting Diodes: Research, Manufacturing, and Applications, vol. 3002, San Jose, CA, pp. 26–35, 1997.

[4.3] M. G. Craford, "LEDs challenge the incandescents," IEEE Circuit and Devices Magazine, vol. 8, no. 5, pp. 24–29, 1992.

[4.4] Y. Tanaka, S. Haruyama, M. Nakagawa, "Wireless Optical Transmissions with White Colored LED for Wireless Home Links," IEEE International Symposium on Personal, Indoor and Mobile Radio Communications, vol. 2, pp. 1325–1329, 2000.

[4.5] T. Komine, Y. Tanaka, S. Haruyama, M. Nakagawa, "Basic Study on Visible-Light Communication using Light Emitting Diode Illumination," International Symposium on Microwave and Optical Technology, pp. 45–48, 2001.

[4.6] Y. Tanaka, T. Komine, S. Haruyama, M. Nakagawa, "A Basic study of optical OFDM system for Indoor Visible Communication utilizing Plural White LEDs as Lighting," International Symposium on Microwave and Optical Technology, pp. 303–306, 2001.

[4.7] T. Komine, M. Nakagawa, "Fundamental Analysis for Visible-Light Communication System using LED Lights," IEEE Transactions on Consumer Electronics, vol. 50, issue 1, pp. 100–107, 2004.

[4.8] T. Komine, M. Nakagawa, "Performance Evaluation on Visible-Light Wireless Communication System using White LED Lightings," The Ninth IEEE Symposium on Computers and Communications, vol. 1, pp. 258-263, 2004.

[4.9] K. Fan, T. Komine, Y. Tanaka, M. Nakagawa, "The Effect of Reflection on Indoor Visible-Light Communication System utilizing White LEDs," The 5th International Symposium on Wireless Personal Multimedia Communications, pp. 611–615, 2002.

[4.10] Y. Tanaka, T. Komine, S. Haruyama, M. Nakagawa, "Indoor Visible Light Data Transmission System utilizing White LED Lights," IEICE Transactions on Communications, vol. E86–B, no. 8, pp. 2440–2454, 2003.

[4.11] T. Komine, S. Haruyama, M. Nakagawa, "Bi-directional Visible-Light Communication using Corner Cube Modulator," The 3rd IASTED International Conference on Wireless and Optical Communication, pp. 598–603, 2003.

[4.12] A. J. C. Moreira, R. T. Valadas, A. M. O. Duarte, "Optical Interference Produced by Artificial Light," Wireless Networks, vol. 3, no. 2, pp. 131–140, 1997.

[4.13] J. M. Kahn, J. R. Barry, "Wireless Infrared Communications," Proceedings of the IEEE, vol. 85, no. 2, pp. 265–298, 1997.

[4.14] J. D. Parsons, "The Mobile Radio Propagation Channel," Halsted Press, New York, 1992.

Chapter 5

Various New Proposals in Indoor Environment

In infrared wireless communication, multipath dispersion due to the reflection on walls in serious problem [5.1–5.12]. Particularly in a non-directed non-LOS link, this problem leads a serious ISI and degrades performance severely. A shadowing problem is another issue on indoor optical wireless channels. This is because the lightwave cannot penetrate opaque obstacles. This feature makes easy to secure transmission against casual eavesdropping, while the shadowing makes a stable transmission difficult in LOS links. Of course, non-LOS links allow the link to operate even when there exists the shadowing between the transmitter and receiver. Non-LOS links, however, suffer from multipath dispersion, because non-LOS links generally relay upon reflection of the light from the ceiling or some other diffusely reflecting surface. From the viewpoint of power efficiency, non-LOS links are inferior to LOS links also. In [5.13–5.16], some diversity techniques in non-LOS links are discussed so that multipath dispersion problem may be alleviated.

These problems are caused by power restriction based on eye-safety. In brief, to achieve high SNR, FOV is narrowed. As a consequence, shadowing problems are caused. On the other hand, to solve the shadowing problems, non-directed non-LOS link is proposed. However multipath dispersion problems lead an ISI. Therefore, in infrared wireless communication, an explosion of papers argue to solve the problems based on eye-safety.

In this dissertation, a visible light data transmission system utilizing white LED lighting is proposed in chapter 4. And we have shown that this visible light wireless communication system has large power, compared with infrared wireless communication system. On the other hand, generally, illuminating engineers install many lighting sources on the ceiling so that a dark area may not be generated. From the view of communication engineers, the transmission in LOS links without a shadowing can be achieved because many lighting sources, which are capable of an optical transmission, are distributed widely on the ceiling.

In this chapter, the diversity technique is proposed so that shadowing problem may be alleviated [5.17–5.23]. And, based on lighting engineering, some characteristics of the proposed system in particular visible light wireless environment are shown and discussed. Moreover, to overcome the ISI caused by optical path difference between plural lighting equipments, adaptive equalizer is proposed and discussed.

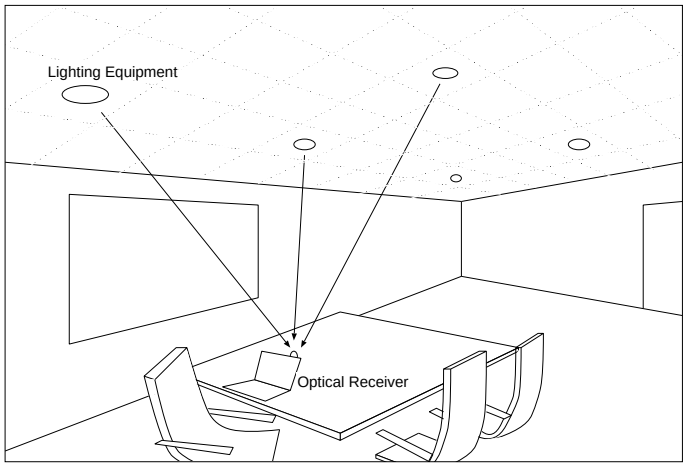

Figure 5.1: Proposed lighting equipment diversity system.

5.1 Basic Study on Communication Performance in Various Indoor Models

To alleviate the shadowing problem, we propose the lighting equipment diversity system. The system image is shown to Fig. 5.1. Generally, lighting equipments are distributed widely on the ceiling to function as lighting. From the view of communication, the transmission in LOS links without a shadowing can be achieved. In this section, as aforesaid, the proposed lighting equipment diversity system is evaluated in various particular visible light wireless environment and the characteristics are discussed.

5.1.1 Lighting Design in Indoor Environment Based on Lighting Engineering

We will discuss the communication performance at particular visible light wireless environments. Three typical models of visible light wireless environment is shown in Table 5.1. The model A assumes the small office with general lighting. The model B assumes the

Table 5.1: Three typical models of visible light wireless environment.

Model	Lighting Equipment	Room Size [m^3]	Number of Lighting Equipment
A	General Lighting	$5 \times 5 \times 3$	2×2
B	General Lighting	$10 \times 10 \times 3$	3×3
C	Downlight	$5 \times 5 \times 3$	4×4

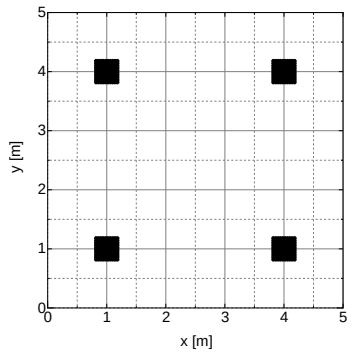

(a) Model A.

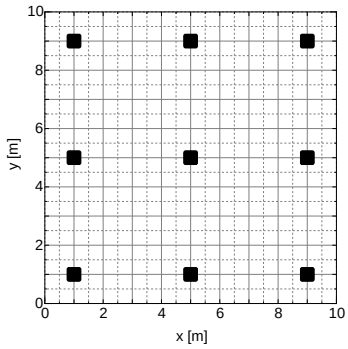

(b) Model B.

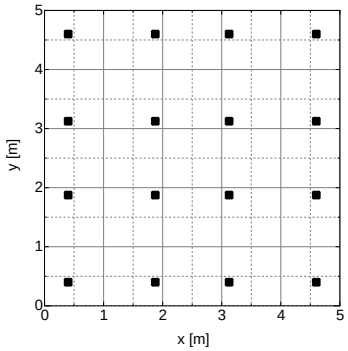

(c) Model C.

Figure 5.2: Position of Lighting Equipments.

large office with general lighting. The model C assumes the small office with downlight. We set a reflective index at ceiling, wall, and floor to 0.8, 0.5, and 0.2, respectively. The lighting equipments are installed on the ceiling. The position is shown in Fig. 5.2. We assume that the receiver is put on a desk. The height of the desk is 0.85 m. In these three model of visible light wireless environment, we show some basic characteristics.

5.1.2 Illuminance Distribution Based on Lighting Engineering

We now describe our algorithm for calculating a multiple-bounce horizontal illuminance. Although true reflections contain both specular and diffusive components [5.24, 5.25], we make the simplifying assumption that all reflectors are purely diffusive, ideal Lambertian. Experimental measurements have shown that many typical materials such as plaster walls, acoustic-tiled walls, carpets, and unvarnished wood are well-approximated as Lambertian reflectors [5.25–5.28]. The radiation intensity pattern emitted by a differential element of an ideal diffuse reflector is independent of the angle of the incident light [5.29].

Light from the source can reach the received point after any number of reflections.

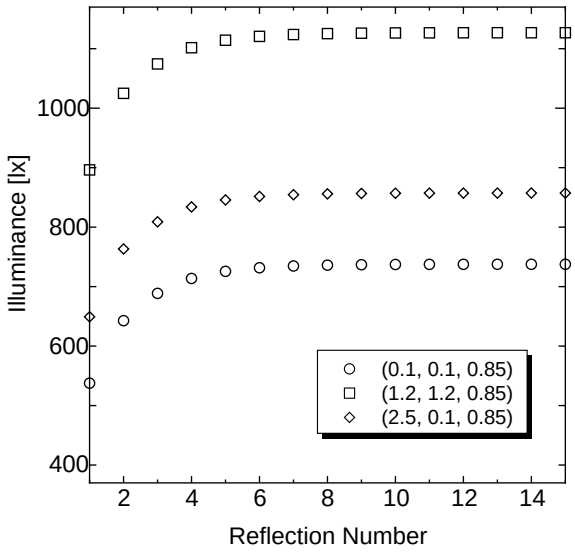

Figure 5.3: Number of reflection. (Model A)

Therefore, the horizontal illuminance can be written as an infinite sum:

$$E = \sum_{n=0}^{\infty} E_n, \tag{5.1}$$

where E_n is the horizontal illuminance of the light undergoing exactly n reflections. The LOS horizontal illuminance E_0 is given by

$$E_0 = \sum_{i}^{LED} \frac{I(0)\cos^m \phi_i}{{d_i}^2} \cos\psi_i, \tag{5.2}$$

while higher order terms ($n > 0$) can be calculated recursively:

$$E_n = \int_{wall} \frac{E_{n-1}}{\pi d^2} \rho \cos\phi \cos\psi dA_{wall}. \tag{5.3}$$

The integrations in Eq. (5.3) are performed with respect to the position on the surface of all reflectors. Here, $I(0)$ is luminous intensity on optical axis, d is the distance between transmitter and receiver, m is Lambertian factor, ϕ is irradiance angle, ψ is incidence angle, dA_{wall} is the differential area of the reflector surface at the position, and ρ is the reflectivity at the position. Intuitively, it says that the n-bounce horizontal illuminance from a single point-source can be found by first finding the distribution and timing of the power from the point-source onto the reflecting walls; then, using the walls as a distributed light source, computing the (n-1)-bounce horizontal illuminance.

Here, we discuss the reflection number. Figure 5.3 shows the relation between reflection number and total illuminance at each position on model A. Here, we assume that the

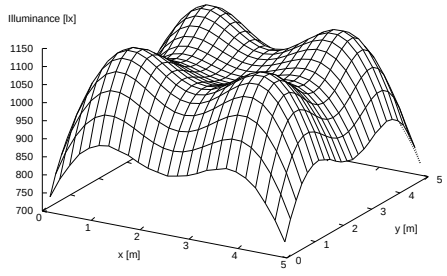

(a) Model A. (Max.: 1124.2 lx, Min.: 737.2 lx, Ave.: 1008.1 lx, Uniformity ratio: 0.73)

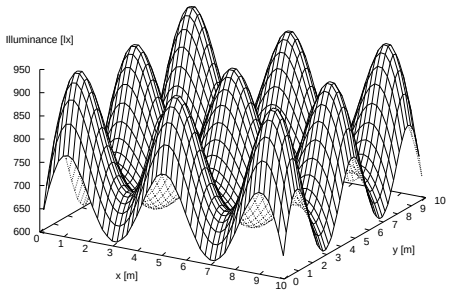

(b) Model B. (Max.: 937.8 lx, Min.: 607.7 lx, Ave.: 744.3 lx, Uniformity ratio: 0.82)

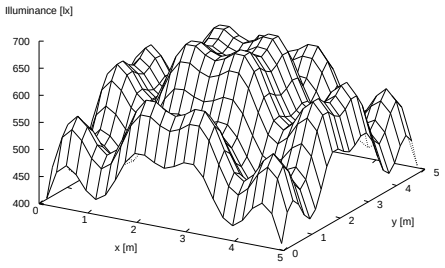

(c) Model C. (Max.: 671.3 lx, Min.: 408.4 lx, Ave.: 545.3 lx, Uniformity ratio: 0.75)

Figure 5.4: Illuminance distribution.

differential area of the reflector surface is 12.5×12.5 cm^2. From this result, at each position, we can see that illuminance becomes almost fixed value over 8th reflection.

The consideration for illuminance of lighting equipments is required. Generally, illuminance of lights is standardized by ISO (International Organization for Standardization). By this set of standards, illuminance between 300 and 1500 lx is required for office work [5.30]. And, generally, uniform illuminance on the desk is recommended. The uniformity ratio of illuminance is defined as the ratio of the minimum to the average illuminance. The uniformity ratio of over 0.7 is recommended by lighting engineering.

Figure 5.4(a) to 5.4(c) show the distribution of horizontal illuminance, based on numerical analysis at the optical receiver on the desk. Here, we have simulated the 10-bounce horizontal illuminance. From these figures, sufficient illuminance, 300 to 1500 lx by ISO, is obtained at all the places of the room. Therefore, this result shows that these setting of the lighting equipments are satisfy sufficient illuminance based on lighting engineering.

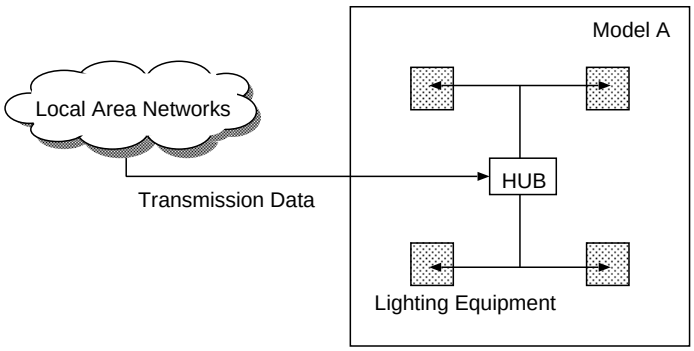

Figure 5.5: The lighting equipment diversity system.

5.1.3 Proposed Lighting Equipment Diversity System

To alleviate the shadowing problem, we propose the lighting equipment diversity system. Figure 5.5 shows the lighting equipment diversity system. A main hub connecting to the each lighting equipment is positioned at the center of the ceiling. The divided signal by function of hub is transmitted by each lighting equipment, synchronously.

5.1.4 Received Optical Power

The received optical power can be written as an infinite sum:

$$P_r = \sum_{n=0}^{\infty} P_{rn}. \tag{5.4}$$

The LOS received optical power P_{r0} is derived by the transmitted optical power P_t i, as follow,

$$P_{r0} = \sum_{i}^{LED} P_t H_i(0), \tag{5.5}$$

while higher order terms ($n > 0$) can be calculated recursively:

$$P_{rn} = \int_{wall} \frac{P_{rn-1}}{\pi d^2} \rho \cos\phi \cos\psi dA_{wall}. \tag{5.6}$$

The integrations in Eq. (5.6) are performed with respect to the position on the surface of all reflectors. Here, d is the distance between transmitter and receiver, ϕ is irradiance angle, ψ is incidence angle, dA_{wall} is the differential area of the reflector surface at the position, and ρ is the reflectivity at the position. The channel DC gain on directed path $H(0)$ is given as:

$$H(0) = \begin{cases} \frac{(m+1)A}{2\pi d^2} \cos^m \phi T_s(\psi) g(\psi) cos\psi, & 0 \le \psi \le \Psi_c \\ 0, & \psi > \Psi_c, \end{cases} \tag{5.7}$$

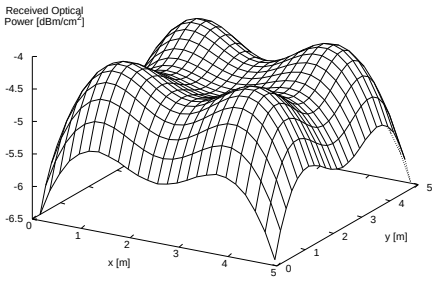

(a) Model A. (Non Tracking, FOV 90 deg., Max.: -4.23 dBm, Min.: -6.44 dBm, Ave.: -4.81 dBm)

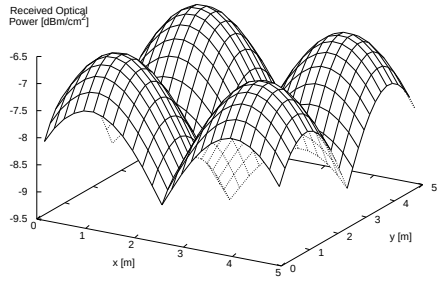

(b) Model A. (Tracking, FOV 30 deg., Max.: -6.60 dBm, Min.: -9.46 dBm, Ave.: -7.56 dBm)

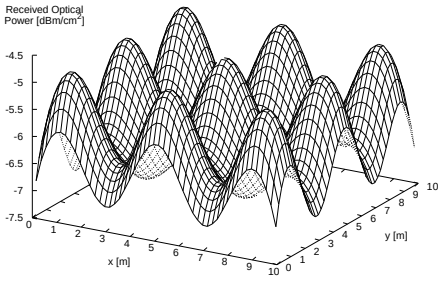

(c) Model B. (Non Tracking, FOV 90 deg., Max.: -4.87 dBm, Min.: -7.06 dBm, Ave.: -6.03 dBm)

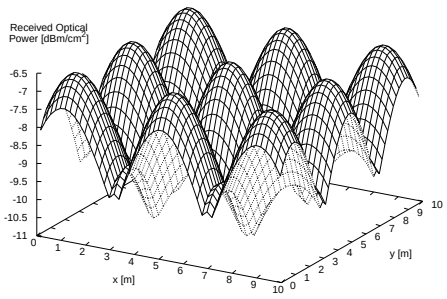

(d) Model B. (Tracking, FOV 30 deg., Max.: -6.60 dBm, Min.: -10.76 dBm, Ave.: -8.20 dBm)

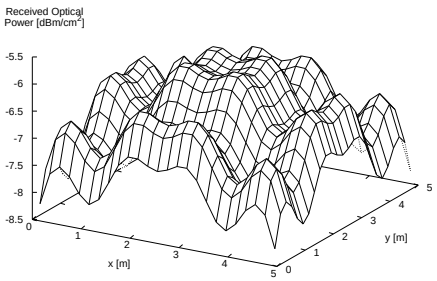

(e) Model C. (Non Tracking, FOV 90 deg., Max.: -5.90 dBm, Min.: -8.22 dBm, Ave.: -6.84 dBm)

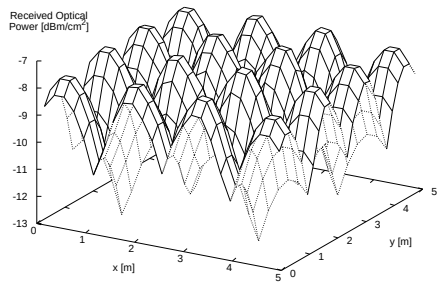

(f) Model C. (Tracking, FOV 30 deg., Max.: -7.29 dBm, Min.: -12.95 dBm, Ave.: -9.12 dBm)

Figure 5.6: Received optical power distribution.

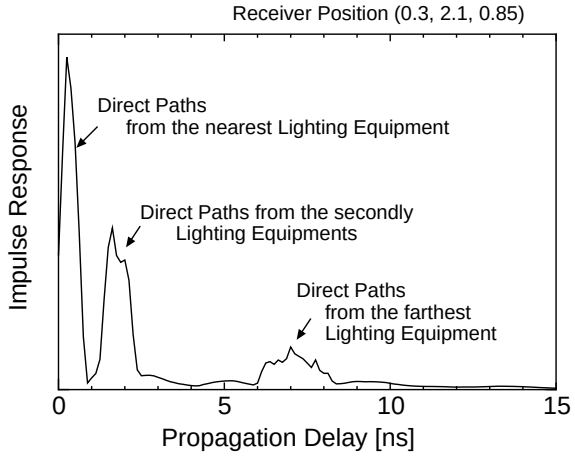

Figure 5.7: Impulse response at (0.3, 2.1, 0.85).

where m is Lambertian factor, A is the physical area of a detector in a photodiode, and Ψ_c is the concentrator FOV (semiangle). And the parameters of received optical power calculation are set as follows. $T_s(\psi)$=1, $g(\psi)$=1, A=1 cm^2.

Figure 5.6 shows the received optical power at each position of the receiver. In all cases, the received optical power at the corners of the room is small. Considering the actual situation, we seldom use a terminal in the corner of a room. Right under the lighting equipment, the received power is high. Here, we define a tracking as a maintaining of an optical axis to center of the nearest lighting equipment. We can see that the received power of the system with tracking is small, compared with non tracking system. Here, we assume that the gain by narrowing the range of FOV is not obtained. To put it briefly, the received power decreases by small FOV. However, the limited FOV reduces an ISI. And we can know that the received power is very high, compared with infrared wireless communication.

5.1.5 Propagation Delay by Plural Lighting Equipments

Figure 5.7 shows the impulse response at (0.3, 2.1, 0.85). Here, we define the impulse response as the sum of received signals from those lighting equipments and walls when an impulse is input to HUB in the ceiling as shown in Fig. 5.1. The first peak consists mainly of direct path from the nearest lighting equipment. And the next peak consists mainly of direct path from the secondly lighting equipments. After some delay, the lights from the farthest lighting equipment and reflected lights are received. In visible light wireless communication system, the lighting equipments are installed on a ceiling and it has large surface area. So, the receiver has particular impulse response differing from infrared wireless communication.

Figure 5.8 shows the distribution of RMS delay spread at each position of the receiver. From these figures, in all cases, the RMS delay spread is small at right under the each lighting equipment. Compared with the system with tracking system, non tracking system

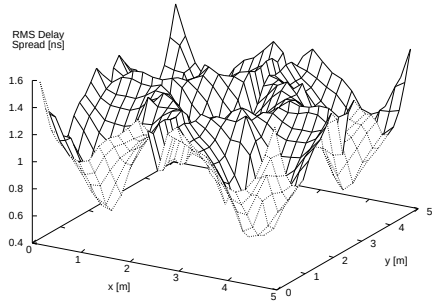

(a) Model A. (Non Tracking, FOV 90 deg., Max.: 1.58 ns, Min.: 0.55 ns, Ave.: 1.13 ns)

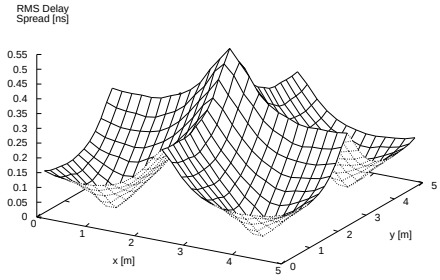

(b) Model A. (Tracking, FOV 30 deg., Max.: 0.51 ns, Min.: 0.02 ns, Ave.: 0.19 ns)

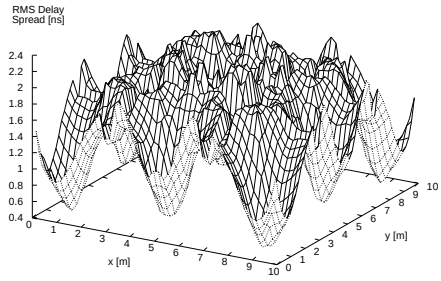

(c) Model B. (Non Tracking, FOV 90 deg., Max.: 2.30 ns, Min.: 0.47 ns, Ave.: 1.52 ns)

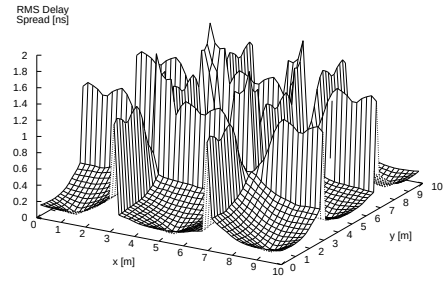

(d) Model B. (Tracking, FOV 30 deg., Max.: 1.88 ns, Min.: 0.00 ns, Ave.: 0.31 ns)

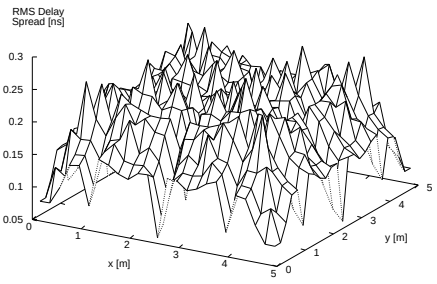

(e) Model C. (Non Tracking, FOV 90 deg., Max.: 0.28 ns, Min.: 0.06 ns, Ave.: 0.18 ns)

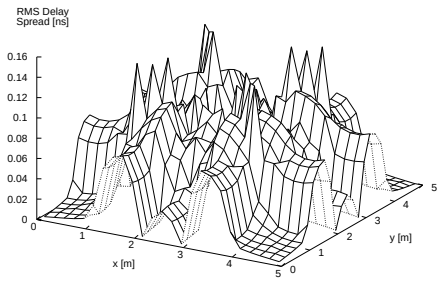

(f) Model C. (Tracking, FOV 30 deg., Max.: 0.15 ns, Min.: 0.00 ns, Ave.: 0.05 ns)

Figure 5.8: RMS delay spread.

Table 5.2: Simulation parameters.

Detector physical area of a PD	1 [cm^2]
Gain of an optical filter	1.0
Refractive index	1.0
O/E conversion efficiency	0.54 [A/W]
Open-loop voltage gain	10
Fixed capacitance	112 [pF/cm^2]
FET channel noise factor	1.5
FET transconductance	30 [mS]
Absolute temperature	298 [K]
Background light current	5100 [μA]

has low RMS delay spread. From Fig. 5.8(a) and 5.8(c), by increasing the number of lighting equipment, the RMS delay spread becomes large. From Fig. 5.8(e) and 5.8(f), the RMS delay spread is very small. This is because that the radiation power of narrowed pattern depends on the radiation angle, significantly. From these figures, we can know the RMS delay spread without tracking consists mainly of the delay between lighting equipments and the tracking system consists mainly of the delay by interior lighting equipment.

5.1.6 BER Performance

We show some numerical and simulation results. The electrical SNR is expressed as

$$SNR = \frac{(RP_r)^2}{\sigma_{shot}^2 + \sigma_{thermal}^2}, \tag{5.8}$$

where R is the detector responsivity. The shot noise variance is given by

$$\sigma_{shot} = 2qRP_rB + 2qI_{bg}I_2B, \tag{5.9}$$

where q is the electronic charge, B is equivalent noise bandwidth, I_{bg} is background current. I_2, noise bandwidth factor, is set to 0.562. The thermal noise variance is given by

$$\sigma_{thermal} = \frac{8\pi kT_k}{G}\eta AI_2B^2 + \frac{16\pi^2kT_k\Gamma}{g_m}\eta^2A^2I_3B^3, \tag{5.10}$$

The first term represents thermal noise from the feedback resistor; k is Boltzmann's constant, T_k is absolute temperature, and G is the open-loop voltage gain, η is the fixed capacitance per unit area, A is the detector area. In the second term, which describes thermal noise from the FET channel resistance, Γ is the FET channel noise factor, g_m is the FET transconductance, and $I_3 = 0.0868$. The parameters for simulation is shown in Table 5.2. The physical detection area of a PD is 1.0 cm^2. The gain at an optical filter is 1.0, and the refractive index of an optical concentrator is 1.0. The O/E (optical to electrical) conversion efficiency of a PD is 0.54 A/W, and a silicon PD whose peak sensitivity is in visible wavelength is assumed. The spectral response at a PD has wavelength selectivity, whereas we can design

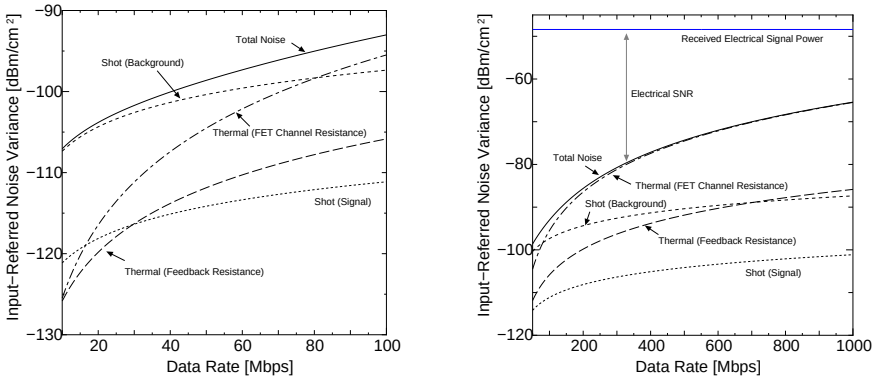

(a) Low data rate.

(b) High data rate.

Figure 5.9: Influence of each noise variance at corner of the room (Model A: (0.1, 0.1, 0.85)). Modulation scheme is 2-PPM.

the optical bandpass filter with multiple thin dielectric layers. Besides, white LEDs emit light at a wide wavelength. Consequently, we can use a desired wavelength at which the response at a PD is good. And we choose the following noise parameter values: T_K = 298 K, G = 10, gm = 30 mS, Γ = 1.5, η = 112 pF/cm^2, and I_{bg} = 5100 μA. The background current is a measured value from direct sun light.

Here, we discuss the influence of the each noise variance. Figure 5.9 shows the relation between input-referred noise variance and data rate. From this figure, when the data rate is under 80 Mbit/s, the total noise is influenced by the shot noise from background. When the data rate is over 80 Mbit/s, it is influenced by the thermal noise from FET channel resistance, greatly.

Figure 5.10 and 5.11 show the BER distribution at 500 Mbit/s and 800 Mbit/s, respectively. We can see that by high data rate, the communication area becomes small. And right under the lighting equipment, the high BER performance is achieved. Figure 5.12 show the relation between data rate and outage area rate. Here we define the outage area rate as the ratio of the area where BER is larger than required BER to the total service area. we set the required BER to 10^{-6}. We can see that the high data rate is caused the increase of the outage area rate. At model A an B, the system with tracking achieves low outage area rate. This is because that large radiation pattern causes ISI. At model C, the performance of non tracking system improves when the data rate is below 800 Mbit/s, and the performance of tracking system improves when the data rate is above 800 Mbit/s. This is because the interference between lighting equipments is small by narrowed radiation pattern.

Therefore, at high data rate, the tracking system is very effective. It means that ISI has a particularly great effect in communication performance at indoor visible light wireless environment.

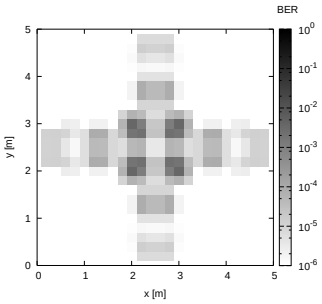

(a) Model A. (Non Tracking, FOV 90 deg.)

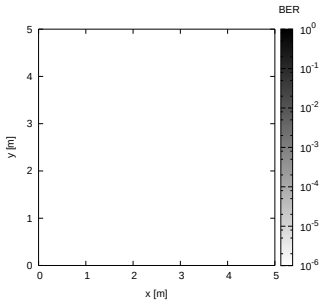

(b) Model A. (Tracking, FOV 30 deg.)

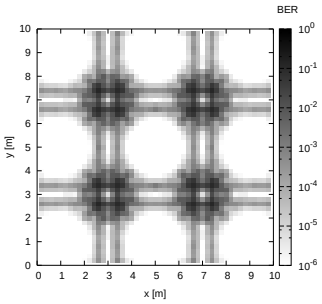

(c) Model B. (Non Tracking, FOV 90 deg.)

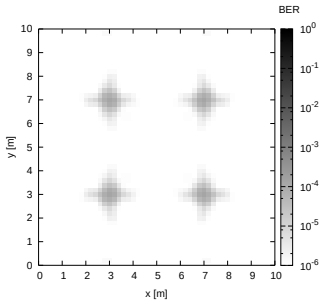

(d) Model B. (Tracking, FOV 30 deg.)

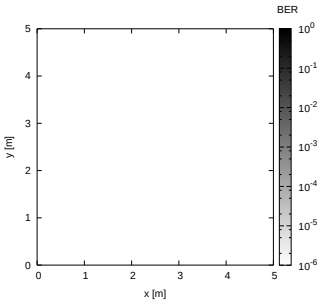

(e) Model C. (Non Tracking, FOV 90 deg.)

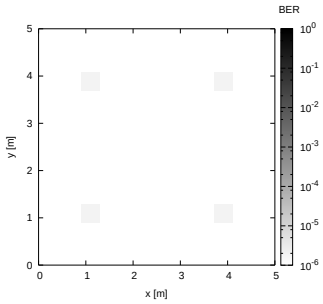

(f) Model C. (Tracking, FOV 30 deg.)

Figure 5.10: BER Distribution at 500 Mbit/s.

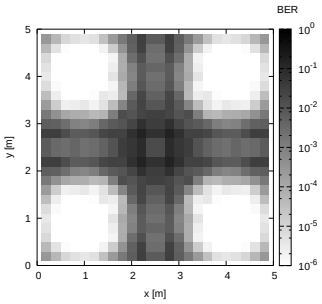

(a) Model A. (Non Tracking, FOV 90 deg.)

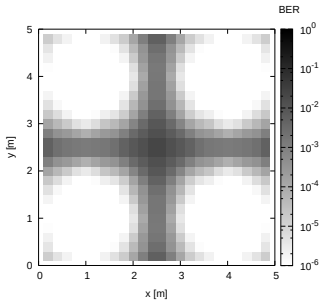

(b) Model A. (Tracking, FOV 30 deg.)

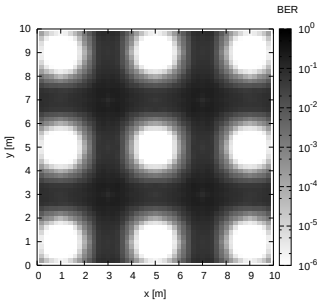

(c) Model B. (Non Tracking, FOV 90 deg.)

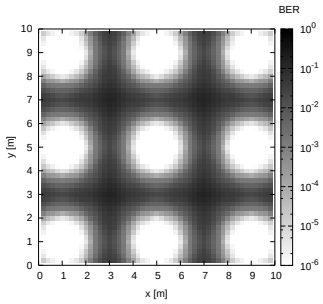

(d) Model B. (Tracking, FOV 30 deg.)

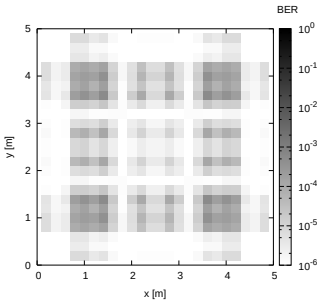

(e) Model C. (Non Tracking, FOV 90 deg.)

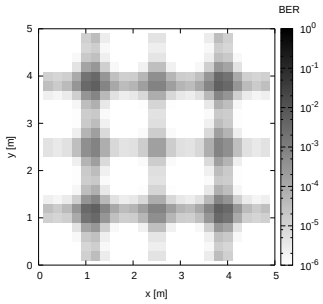

(f) Model C. (Tracking, FOV 30 deg.)

Figure 5.11: BER Distribution at 800 Mbit/s.

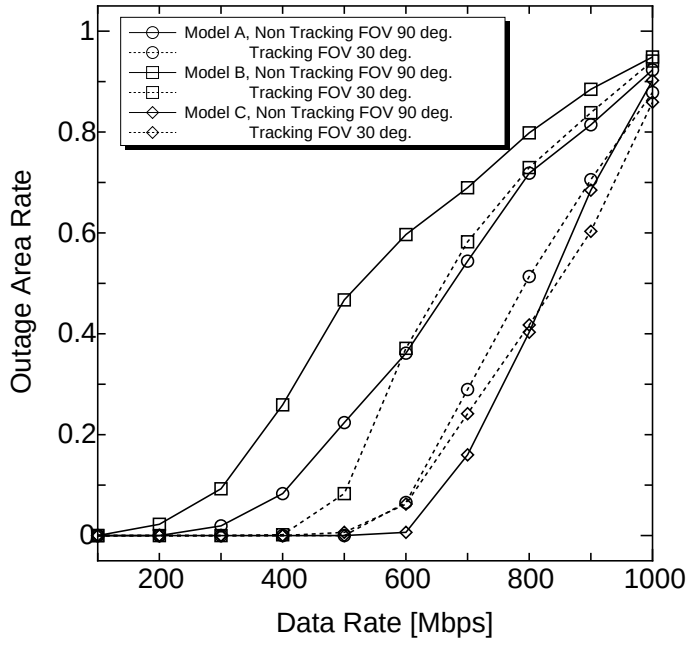

Figure 5.12: Outage Area Rate at each model.

5.2 Effective Lighting System to Shadowing and Its Performance Evaluation

In this section, we discuss about the effect of shadowing on visible-light wireless communication system using plural white LED lighting equipments including the specific impulse response [5.31, 5.32]. Generally, lightings are distributed within a room and the irradiance of light has a wide angle to function as lighting equipment, which helps minimize a shadowing effect. We consider the downlink transmission based on time-division multiple access (TDMA) and evaluate the effects of shadowing caused by pedestrians with theoretical analysis and computer simulation. We show that the visible-light communication system is robust against shadowing and has optimal number of the lighting equipment.

5.2.1 Influence of Intersymbol Interference by Lighting Equipment Diversity System

We discuss the influence of shadowing at the model A, which is shown in section 5.1.1. Here, we assume that the modulation scheme is OOK and 2-PPM. And we define the each lighting equipment as shown in Fig. 5.13.

Figure 5.14 shows the relation between outage area rate and bit rate at each number of the lighting equipment with function of communication on the service area. We define an outage area rate as the ratio of the area where BER is larger than 10^{-6} to the total service area. Here, we assume that all of the lighting equipments with the function of

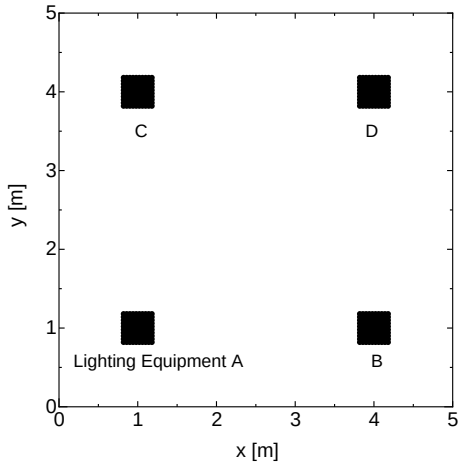

Figure 5.13: Position of the each lighting equipment.

communication device transmit same signals synchronously. From Fig. 5.14(a), we can see that the increase of the number of the lighting equipment causes the increase of the outage area ratio. From Fig. 5.14(b), the increase of the number of the lighting equipment does not result in the decrease of the outage area ratio. At high data rate like over 200 Mbit/s, we can also see that the performance is improved by the use of the 2 lighting equipment (AD) the most. In an infrared non-directed LOS link, the outage area performance is improved by the increase of base station [5.33]. However, in visible light wireless communication, the transmitter has large power and large emission characteristics to function as lighting. Thus high data rate transmission (200 Mbit/s or more) with OOK causes the increase of the outage area by ISI.

5.2.2 Effect of Shadowing

Traffic Consideration

Generally, a call blocking performance of the mobile wireless users in planar cellular arrays is formulated by Markov model [5.34]. In this paper, we assume that the network traffic depends on the Markov model (M/M/S(0)).

Call arrivals are assumed to be described by independent Poisson processes, one for each cell. We use λ, in units of calls per second per cell, for the call arrival rate. If τ is the mean call duration time (service time), then the call duration rate for one channel, measured when it is busy, is $\mu = \tau^{-1}$. The ratio $\chi = \lambda/\mu$ is the offered load, in Erlangs/cell.

The classical Erlang-B formula for the probability that a call in a cell is blocked when there are c channels in the cell, is

$$P[\text{Blocking}] = \frac{\chi^c/c!}{\sum_{j=0}^{c} \chi^j/j!}. \tag{5.11}$$

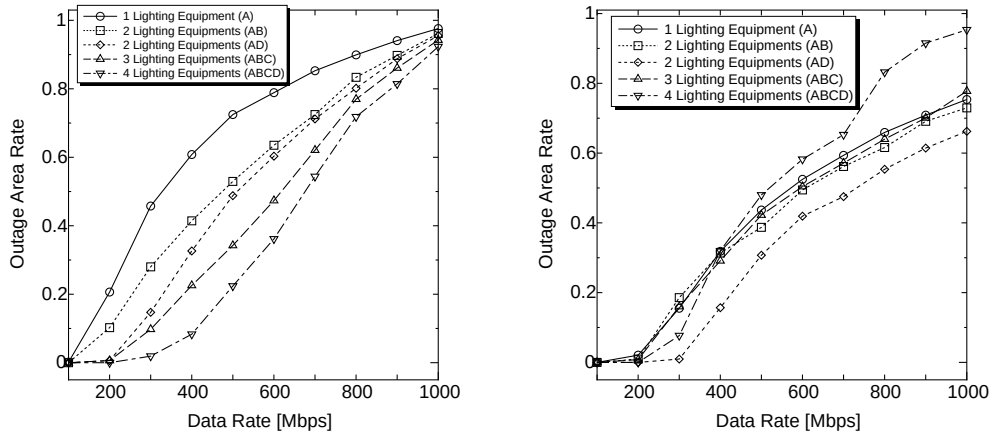

(a) 2-PPM. (b) OOK.

Figure 5.14: Outage area rate at each modulation scheme.

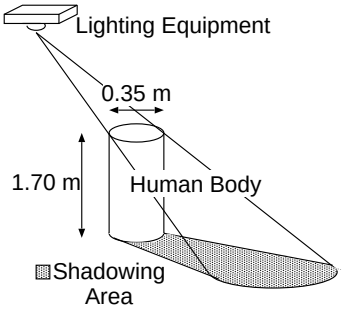

Figure 5.15: A model of the human body as pedestrian.

Outage Call Duration Rate

The parameters for simulation are shown in Table 5.3. We consider the downlink transmission based on TDMA. We assign a channel which is divided time slot in the same frequency band to each user. We model a human body by a column with a diameter of 0.35 m and a height of 1.70 m as shown in Fig. 5.15.

Here, we define an outage call duration rate as the ratio of the total duration when BER is larger than 10^{-6} to the total of call duration as shown in Fig. 5.16.

Figure 5.17 and 5.18 show the relation between outage call duration rate and mean density of pedestrians at each data rate. The offered load is set to 4 erl. From these figures, at 2-PPM, by increasing the lighting equipment, the performance of outage call duration rate is improved at each data rate. we can know that the performance at 2-PPM depends on the outage area rate performance at Fig. 5.14(a). At 500 Mbit/s, the multiple lighting

Table 5.3: Simulation conditions for influence of shadowing.

Access Method	TDMA (considered only downlink)
Number of channels	10
Mobile Terminals	Uniform Distribution
Traffic Model	Poisson Arrival
Call Duration	Exponential Distribution
Mean Call Duration Time	20.0 [s]
Generation of Pedestrian	Exponential Distribution
Motion of Pedestrians	
Velocity	Uniform Distribution 0 to 4 [km/h] (constant)
Orientation	Uniform Distribution 0 to 2 π [rad.] (constant)
Walking Time	5.0 [sec.] (constant)

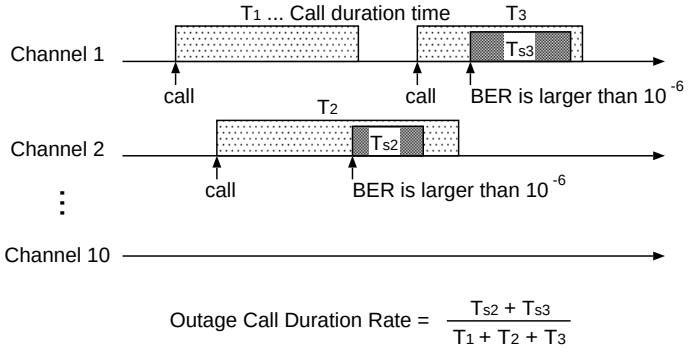

Figure 5.16: Outage call duration rate.

equipments with 2-PPM take almost the constant value. Therefore, by using the multiple lighting equipment, we can know the shadowing is avoided.

In Fig. 5.18, at OOK, we can see that the increase of the number of the lighting equipment does not depend on the improvement of the outage call duration rate. In this case, the performance is improved the most at the 2 lighting equipments. And the performance of 1 lighting equipment is overtaken the 4 lighting equipment. This is because, by increasing the mean density of pedestrians, the performance of the 1 lighting equipment is deteriorated and the performance of the 4 lighting equipments are approached toward the 2 lighting equipments in Figure 5.14(b) by blocking the optical path. Compared with these figures, the performance at 100 Mbit/s is better than the performance at 500 Mbit/s. This is because high data transmission causes the increase of the outage duration by ISI. Therefore, from these figures, we can know that there is an optimal number of the lighting equipment and it depends on data rate, mean density of pedestrians, room model, and so on.

Figure 5.19 and 5.20 show the outage call duration rate versus the offered load when

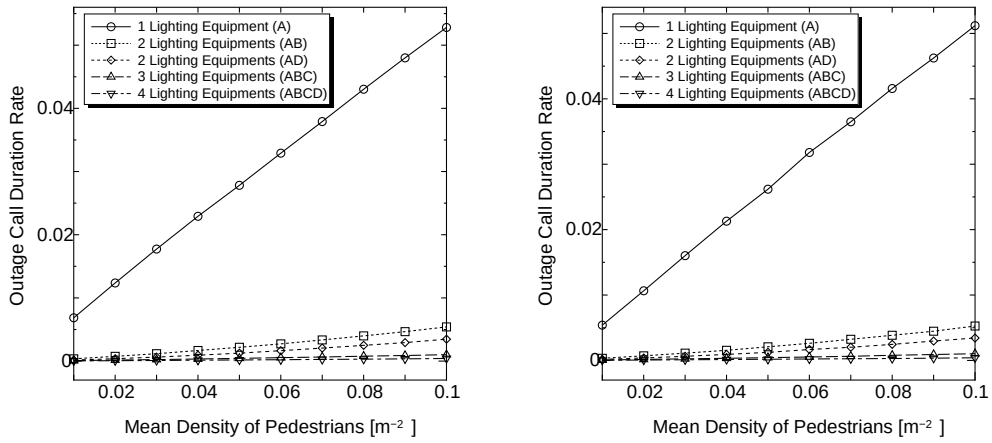

(a) 2-PPM. (b) OOK.

Figure 5.17: Outage call duration rate vs. mean density of pedestrians: bit rate is 100 Mbit/s, and the offered load is 4 erl.

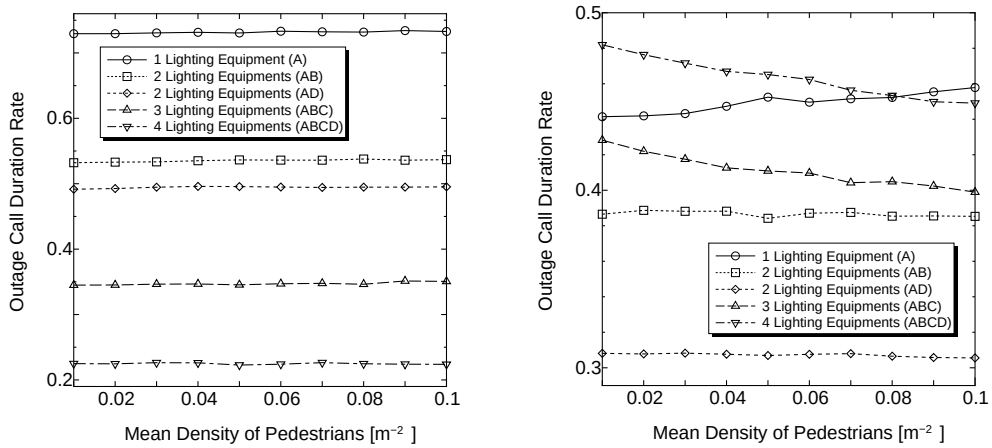

(a) 2-PPM. (b) OOK.

Figure 5.18: Outage call duration rate vs. mean density of pedestrians: bit rate is 500 Mbit/s, and the offered load is 4 erl.

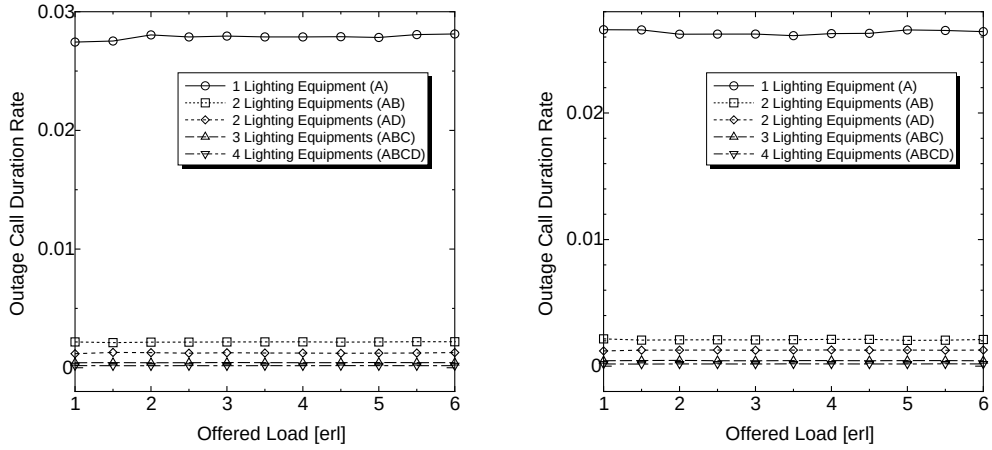

(a) 2-PPM. (b) OOK.

Figure 5.19: Outage call duration rate vs. offered load: bit rate is 100 Mbit/s, and the mean density of pedestrians is 0.05 m^{-2}.

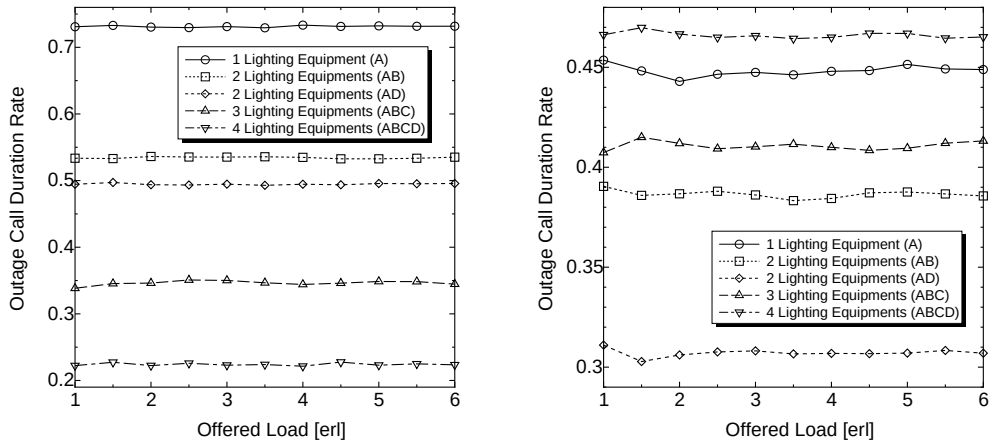

(a) 2-PPM. (b) OOK.

Figure 5.20: Outage call duration rate vs. offered load: bit rate is 500 Mbit/s, and the mean density of pedestrians is 0.05 m^{-2}.

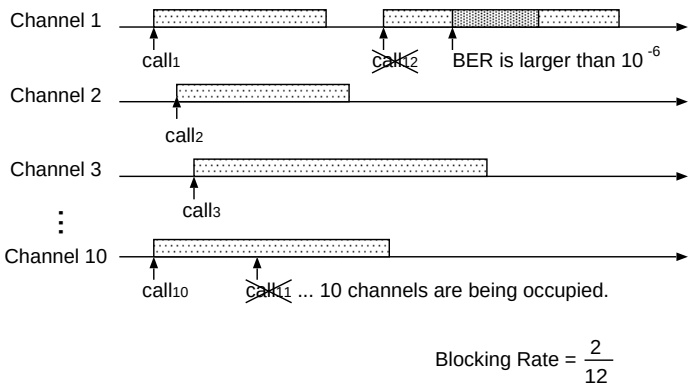

Figure 5.21: Blocking rate.

mean density of pedestrians is 0.05 m^{-2}.

We can see that the performance at 100 Mbit/s is better than the performance at 500 Mbit/s. We can also see that each of the system takes almost constant value of outage call duration rate for any value of the offered load. This is because as the offered load becomes larger, the duration becomes larger when the BER is larger than the required BER. Thus, the outage call duration rate, that is, the ratio takes almost the constant value. From Figure 5.20(b), we can see that the use of the 2 lighting equipments with the function of communication is very effective to improve the outage call duration rate performance.

Blocking Rate

Here, the blocking rate is defined as the ratio of the total duration when all 10 channels are being occupied or calls are blocked or BER is larger than 10^{-6} to the total of call duration as shown in Fig. 5.21. Figure 5.22 and 5.23 show the blocking rate versus the offered load at each data rate. Here the performance with Erlang-B formula corresponds to the performance when we assume that an error occurs only when all 10 channels have been already used. From Fig. 5.22, we can see that the blocking rate performance is improved by the use of the multiple lighting equipments at 100 Mbit/s. Compared Figure 5.22(b) with 5.23(b), the performance of blocking rate is deteriorated by the constraint of required BER. However, at 500 Mbit/s, we can see that the system with optimal number of the 3 lighting equipments can achieve better blocking rate performance. And the system with optimal number of the lighting equipments approximates the performance by Erlang-B formula.

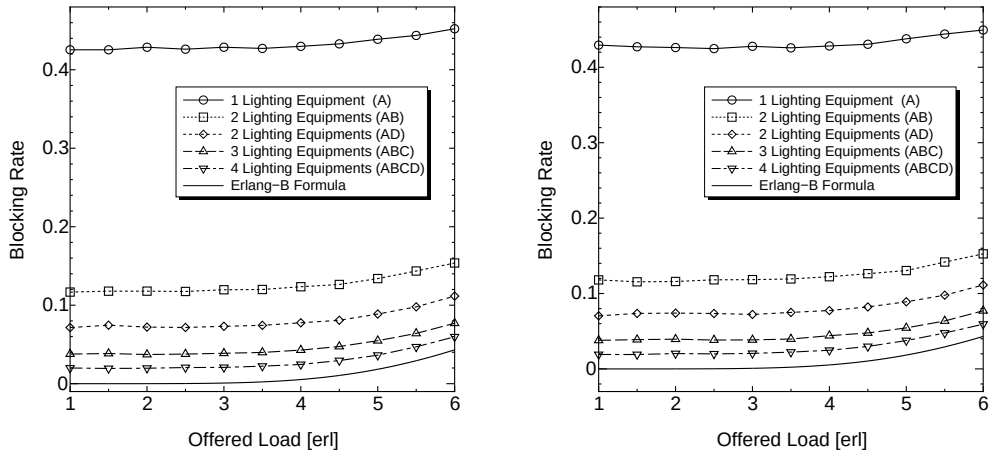

(a) 2-PPM. (b) OOK.

Figure 5.22: Outage call duration rate vs. offered load: bit rate is 100 Mbit/s, the mean density of pedestrian is 0.05 m^{-2}.

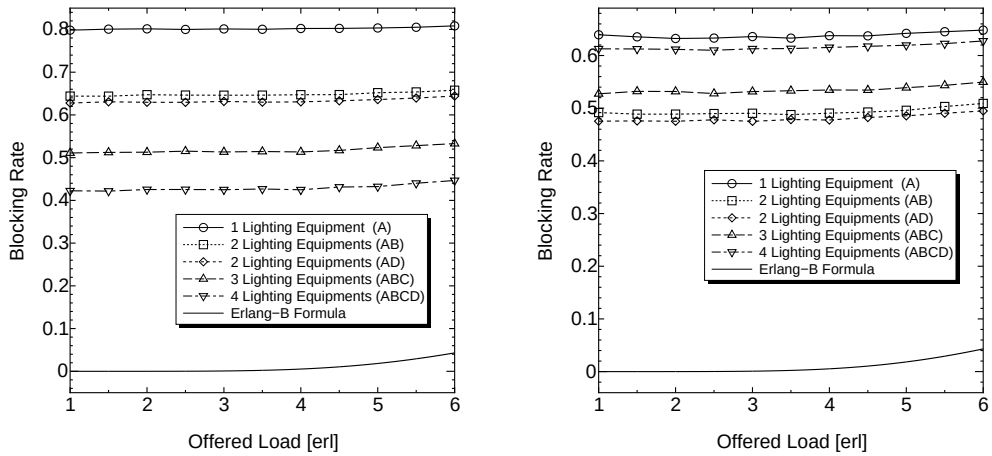

(a) 2-PPM. (b) OOK.

Figure 5.23: Outage call duration rate vs. offered load: bit rate is 500 Mbit/s, the mean density of pedestrian is 0.05 m^{-2}.

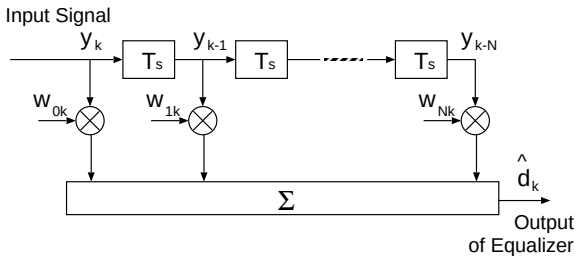

Figure 5.24: FIR equalizer.

5.3 Proposal of Adaptive Equalization for Visible Light Wireless Communication System that has Mobility

To mitigate the effects of the ISI, the zero forcing decision feedback equalizer (ZF-DFE) has been generally applied to the infrared wireless systems [5.35, 5.36]. However the performance of visible-light wireless systems with equalizer has not been clarified. Prior works of infrared wireless systems with equalizer assume that the impulse response is known to the receiver [5.37]. They also assume the impulse response is static during the communication. The assumptions are appropriate in infrared wireless communications. This is because a tracking is required by low transmission power for eye-safety. In other words, generally, the positions of the transmitted and receiver are fixed. However, in visible-light wireless systems, a tracking is not required be cause a transmitter emits large power. And the terminal is usually mobile.

In this section, we propose an adaptive equalization system and evaluate the performance of adaptive equalizer in visible-light wireless environment of model A in section 5.1.1. We assume the lighting equipment diversity system with OOK modulation. By transmitting the training sequences, we estimate the channel by least mean square (LMS) algorithm. And we show the effectual interval of training sequence for channel estimation.

5.3.1 System Description

FIR Equalizer

A linear equalizer can ber implemented as an FIR equalizer otherwise known as the transversal equalizer. In such an equalizer, the current and past values of the received signal are linearly weighted by the filter coefficient and summed to produce the output, as shown in Fig. 5.24. If the delays and the tap gains are analog, the continuous output of the equalizer is sampled at the symbol rate and the samples are applied to the decision device. The implementation is, however, usually carried out in the digital domain where the samples of the received signal are stored in a shift register. The output of this FIR

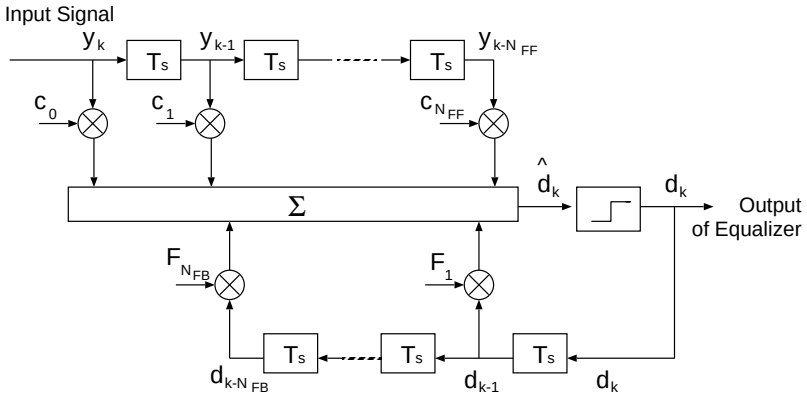

Figure 5.25: Decision feedback equalizer.

equalizer before decision making (threshold detection) is

$$\hat{d_k} = \sum_{n=0}^{N} (w_{nk}) y_{k-n}, \tag{5.12}$$

where w_{nk} represents the tap weights, $\hat{d_k}$ is the output at time index k, y_i is the input received signal at time $t_0 + iT$, t_0 is the equalizer starting time, and N is the number of taps. The minimum mean squared error $E[|e(n)|^2]$ that an FIR transversal equalizer can achieve is [5.38]

$$E[|e(n)|^2] = \frac{T}{2\pi} \int_{-\pi/T}^{\pi/T} \frac{N_0}{|F(e^{j\omega T})|^2 + N_0} d\omega \tag{5.13}$$

where $F(e^{j\omega T})$ is the frequency response of the channel, and N_0 is the noise spectral density.

Decision Feedback Equalization

The basic idea behind DFE is that once an information symbol has been detected and decided upon, the ISI that it induces on future symbols can be estimated and subtracted out before detection of subsequent symbols. The DFE can be realized in the direct transversal form. The form is shown in Fig. 5.25. It consists of a feedforward (FF) filter and a feedback (FB) filter. The FB filter is driven by decisions on the output of the detector, and its coefficients can be adjusted to cancel the ISI on the current symbol from past detected symbols. The equalizer has $N_{FF} + 1$ taps in the FF filter and N_{FB} taps in the FB filter, and its output can be expressed as [5.38]:

$$\hat{d_k} = \sum_{n=0}^{N_{FF}} c_n^* y_{k-n} + \sum_{i=1}^{N_{FB}} F_i^* d_{k-i}, \tag{5.14}$$

where c_n^* and y_n are tap gains and the inputs, respectively, to the FF filter, F_{ik}^* are tap gains for FB filter, and $d_i (i < k)$ is the previous decision made on the detected signal. That is,

once $\hat{d}_k$ is obtained using Eq. (5.14), d_k is decided from it. Then, d_k along with previous decisions $d_{k-1}, d_{k-2}, \cdots$ are FB into the equalizer, and $\hat{d}_{k+1}$ is obtained using Eq. (5.14).

Least Mean Squire Algorithm

Since an adaptive equalizer compensates for an unknown and time-varying channel, it requires a specific algorithm to update the equalizer coefficients and track the channel variations. A wide range of algorithms exist to adapt the filter coefficients. In this paper, we assume a LMS algorithm. A more robust equalizer is the LMS equalizer where the criterion used is the minimization of the mean square error (MSE) between the desired equalizer output and the actual equalizer output.

Here, we define the input signal to the equalizer as a vector $\boldsymbol{y}_k$ where

$$\boldsymbol{y}_k = \begin{bmatrix} y_k & y_{k-1} & y_{k-2} & \cdots & y_{k-N} \end{bmatrix}^T, \tag{5.15}$$

and a weight vector can be written as

$$\boldsymbol{w}_k = \begin{bmatrix} w_{0k} & w_{1k} & w_{2k} & \cdots & w_{Nk} \end{bmatrix}^T. \tag{5.16}$$

It follows that when the desired equalizer output is known, the error signal e_k is given by

$$e_k = d_k - \hat{d}_k. \tag{5.17}$$

To compute the mean square error $|e_k|^2$ at time instant k, Eq. (5.17) is squared to obtain

$$\xi = E[e_k^* e_k]. \tag{5.18}$$

The LMS algorithm seeks to minimize the mean square error given in Eq.. (5.18). The LMS algorithm is the simplest equalization algorithm and requires only 2N+1 operations per iteration. Letting the variable n denote the sequence of iterations, LMS is computed iteratively by

$$\hat{d}_k(n) = \boldsymbol{w}_N^T(n)\boldsymbol{y}_N(n), \tag{5.19}$$

$$e_k(n) = d_k(n) - \hat{d}_k(n), \tag{5.20}$$

$$\boldsymbol{w}_N(n+1) = \boldsymbol{w}_N(n) + \mu e_k^*(n)\boldsymbol{y}_N(n), \tag{5.21}$$

where the subscript N denotes the number of delay stages in the equalizer, μ is the step size which controls the convergence rate and stability of the algorithm, and a vector $\boldsymbol{y}_N$ is the input signal to the equalizer. Therefore, the LMS equalizer maximizes the signal to distortion ratio at its output within the constraints of the equalizer tap length. So, the convergence rate of the LMS algorithm is slow due to fact that there is only one parameter, the step parameter μ, that controls the adaptation rate.

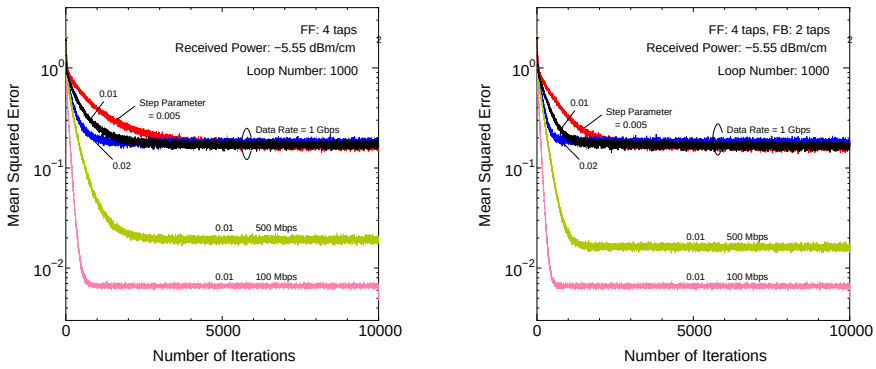

(a) FIR equalizer. FF:4

(b) DFE. FF:4, FB:2

Figure 5.26: Mean square error. Received optical power is -5.55 dBm/cm^2, loop number is 1000.

5.3.2 Mean Square Error

Figure 5.26 shows the relation between the MSE by LMS algorithm and the length of training sequence at the receiver position of (0.1, 2.1, 0.85). Figure 5.26(a) and 5.26(b) are FIR equalizer and DFE, respectively. The figure is drawn by the average of 1000 times. From this figure, we can see that the value of step parameter has no influence on the rate of convergence, but does determine the tracking ability of the LMS equalizers. The larger the step parameter, the better the tracking ability of the equalizer. However, large step parameter causes the excess noise. And we can also see that high data rate is increased the MSE. This is because the received SNR is difficult at each data rate. From this results, we set the step parameter and the length of training sequence to 0.01 and 10000 bits, respectively.

5.3.3 BER Performance

Figure 5.27 to 5.30 show the distribution of BER performance on the receiver position at every 0.20 m. We can see that the low BER area is increased by DFE, in particular high data rate. And the system with DFE mitigates the influence caused by ISI, effectively. We can also see that the performance on the center of the lighting equipments is deteriorated. That is because the power of first path and of the second path by ISI become approximately equal on the center of the equipments. Therefore, MSE becomes large.

Figure 5.31 shows the relation between data rate and outage area rate. We define an outage area rate as the ratio of the area where BER is larger than 10^{-6} to the total service area. We can see that the high data rate is caused the increase of the outage area rate. The system with FF: 4 taps and FB: 0 tap means FIR equalizer (linear equalizer). We can see that the system with DFE mitigates the influence caused by ISI, effectively. When data rate is over 200 Mbit/s, the FIR equalizer and DFE are effective. And, when data rate is over 700 Mbit/s, the DFE is very effective.

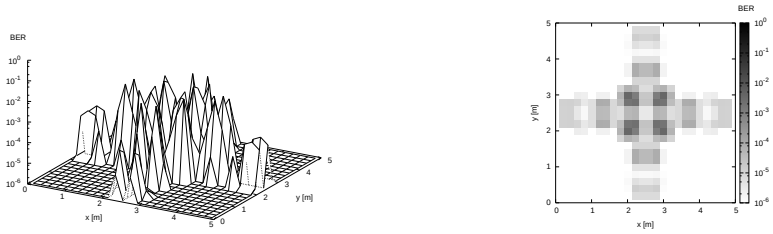

Figure 5.27: BER distribution without DFE. Data rate is 500 Mbit/s.

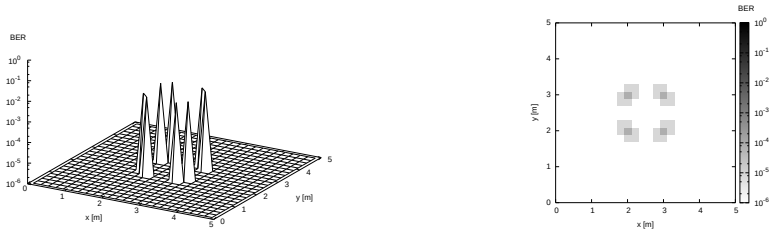

Figure 5.28: BER distribution with DFE. Data rate is 500 Mbit/s. FF tap is 4, FB tap is 2, step parameter is 0.01, training sequence is 10000 bits.

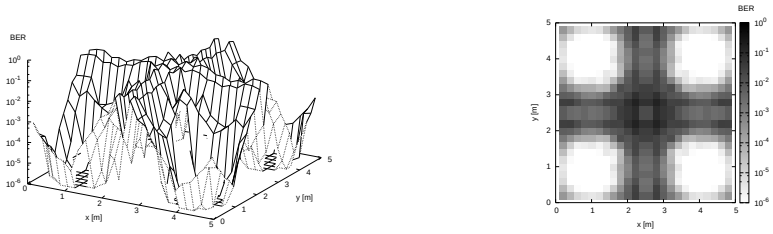

Figure 5.29: BER distribution without DFE. Data rate is 800 Mbit/s.

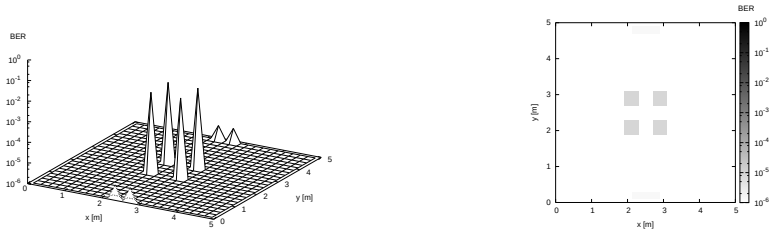

Figure 5.30: BER distribution with DFE. Data rate is 800 Mbit/s. FF tap is 4, FB tap is 2, step parameter is 0.01, training sequence is 10000 bits.

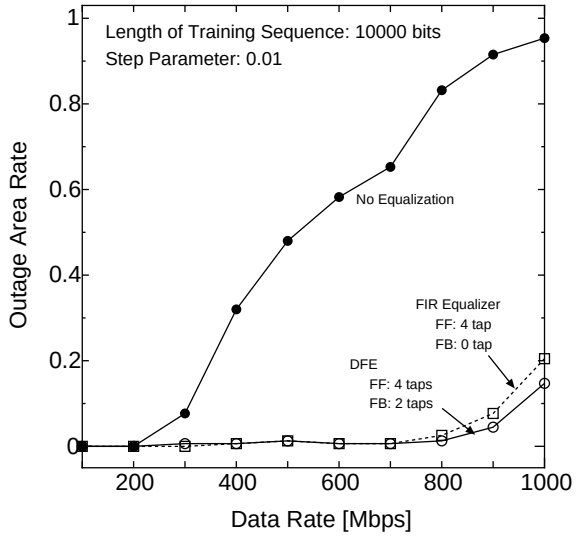

Figure 5.31: Outage area rate versus data rate. Step parameter is 0.01, length of training sequence is 10000 bits.

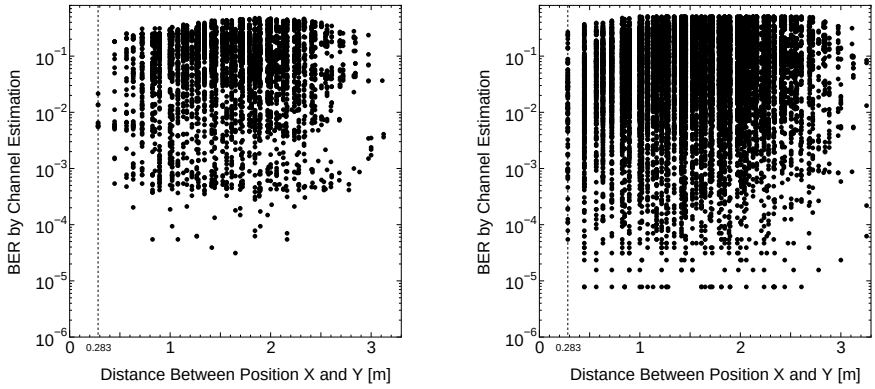

(a) Data rate is 500 Mbit/s. (b) Data rate is 800 Mbit/s.

Figure 5.32: Distance between position X and Y versus BER by channel estimation. FF tap is 4, FB tap is 2, Step parameter is 0.01, length of training sequence is 10000 bits.

5.3.4 Training Sequence Interval

Next, we discuss about the interval of training sequence. Figure 5.32 show the BER performance by channel estimation, when the weights by perfect estimation of the position X are used at position Y. The horizontal axis is the distance between position X and Y. At 500

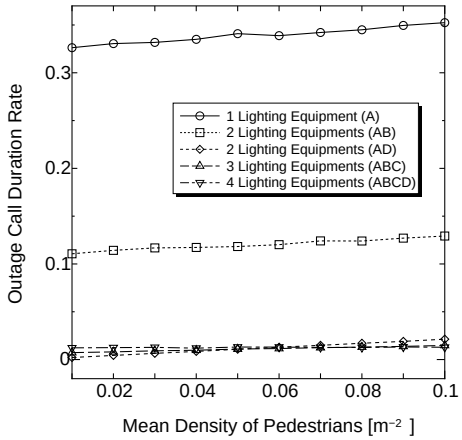

Figure 5.33: Outage call duration rate vs. mean density of pedestrians: bit rate is 500 Mbit/s, and the offered load is 4 erl.

Mbit/s and 800 Mbit/s, the error by channel estimation does not occur when the distance is below 0.283 m. So, the weights should be updated every 0.283 m. Therefore, when a mobile terminal moves at the speed of 3.6 km/h, the training sequence has to send at intervals of below 0.283 s.

5.3.5 Tolerance Properties to Shadowing

Figure 5.33 shows the relation between outage call duration rate and mean density of pedestrians at 500 Mbit/s. The offered load is set to 4 erl. From this figure, by using the multiple lighting equipment, we can know the shadowing is avoided. Compared with the system without equalization as shown in Fig. 5.18, we can also know that the probability, which the communication is broken up by the deterioration of communication quality, decreases greatly and the equalization system is very effective.

Figure 5.34 shows the blocking rate performance at 500 Mbit/s. From Fig. 5.34(a), by increasing the mean density of pedestrians, we can see that the blocking rate performance is deteriorated. From Fig. 5.34(b), compared with the OOK system without equalization as shown in Fig. 5.23(b), we can know that the blocking rate performance is achieved by equalization. At 500 Mbit/s, we can see that the system with optimal number of the 4 lighting equipments can achieve better blocking rate performance. And we can know that the equalization system is very effective for shadowing problem.

5.4 Summary

The proposed lighting equipments has large power, compared with infrared wireless communication system, for function of lighting equipment. On the other hand, generally, illuminating engineers install many lighting sources on the ceiling so that a dark area may

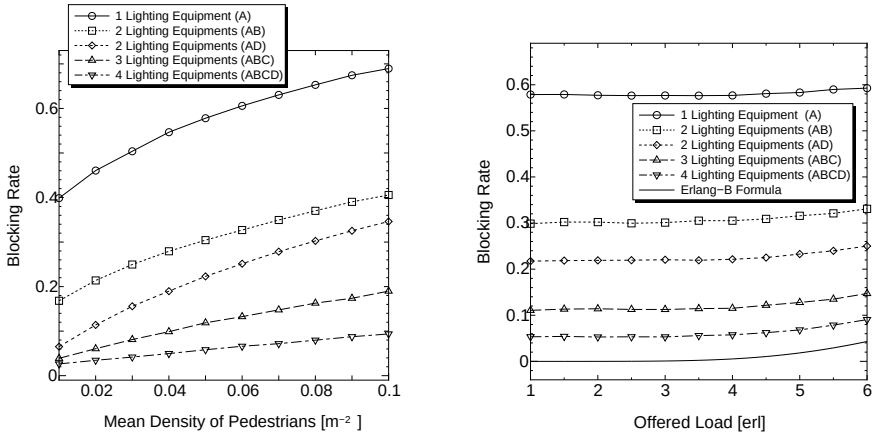

(a) Offered load is 4 erl.

(b) Mean density of pedestrian is 0.05 m^{-2}

Figure 5.34: Blocking rate performance at 500 Mbit/s.

not be generated. From the view of communication engineers, the transmission in LOS links without a shadowing can be achieved because many lighting sources, which are capable of an optical transmission, are distributed widely on the ceiling.

In this chapter, the diversity technique has been proposed so that shadowing problem is alleviated. And, based on lighting engineering, some characteristics of the proposed system in particular visible light wireless environment have been discussed. The system has specific delay profile by the plural lighting equipments which have large surface area. At some models, the numerical analyses of plural lighting equipments as illuminance, received optical power, and RMS delay spread during use as an optical transmitter have been performed and BER performance has been shown. And the influence of shadowing by the plural lighting equipments has been discuss. An optimal number of the lighting equipment for communication has been shown. And we showed that the system with optimal number of the lighting equipment was robust against shadowing and could accommodate more calls. Moreover, to overcome the ISI caused by optical path difference between plural lighting equipments, adaptive equalizer has been proposed. The performance of adaptive equalizer with LMS algorithm was evaluated. We showed that the effectual interval of training sequence for channel estimation alleviated the influence of shadowing. From these analyses, it was found that the idea of the proposed system was very promising for future high speed wireless access networks and ti could be one choice for an indoor optical wireless data transmission system.

5.5 References

[5.1] J. M. Kahn, W. J. Krause, J. B. Carruthers, "Experimental characterization of non-directed indoor infrared channels," IEEE Transactions on Communications, vol. 43, no. 2/3/4, pp. 1613–1623, 1995.

[5.2] J. R. Barry, J. M. Kahn, W. J. Krause, E. A. Lee, D. G. Messerschmitt, "Simulation of multipath impulse response for indoor wireless optical channels," IEEE Journal on Selected Areas in Communications, vol. 11, no. 3, pp. 367–379, 1993.

[5.3] J. B. Carruthers, J. M. Kahn, "Modeling of nondirected wireless infrared channels," IEEE Transactions on Communications, vol. 45, no. 10, pp. 1260–1268, 1997.

[5.4] C. R. A. T. Lomba, R. T. Valadas, A. M. de Oliveira Duarte, "Propagation losses and impulse response of the indoor optical channel : A simulation package," Proceedings of International Zurich Seminar on Digital Communications, pp. 285–297, 1994.

[5.5] R. Pérez-Jiménez, V. M. Melián, M. J. Betancor, "Analysis of multipath impulse response of diffuse and quasi-diffuse optical links for ir-wlan," Proceedings of IEEE Conference on Computer Communications, pp. 924–930, 1995.

[5.6] R. Vento, J. Rabadán, R. Pérez-Jiménez, A. Santamaría, F. J. López-Hernández, "Experimental characterization of a direct sequence spread spectrum system for in-house wireless infrared communications," IEEE Transactions on Consumer Electronics, vol. 45, no. 4, pp. 1038–1045, 1999.

[5.7] K. Samaras, D. C. O'Brien, D. J. Edwards, "Numerical calculation of channel capacity for wireless infrared multipath channels," Electronics Letters, vol. 34, no. 15, pp. 1462–1464, 1998.

[5.8] M. Abtahi, H. Hashemi, "Simulation of indoor propagation channel at infrared frequencies in furnished office environments," Proceedings of International Symposium on Personal, Indoor and Mobile Radio Communications, pp. 306–310, 1995.

[5.9] M. R. Pakravan, "Estimation of indoor infrared channel parameters using neural networks," Proceedings of International Symposium on Personal, Indoor and Mobile Radio Communications, pp. 311–315, 1995.

[5.10] M. R. Pakravan, M. Kavehrad, "Distribution of infrared light power for indoor broadband wireless communications," Proceedings of International Symposium on Personal, Indoor and Mobile Radio Communications pp. 316–320, 1995.

[5.11] Y. Higashihara, K. Tsukamoto, N. Morinaga, "A consideration on signal transmission characteristics in indoor wireless networks via optical diffuse channel," ITEJ Technical Report, vol. 16, no. 36, pp. 13–18, 1992.

[5.12] A. Sato, M. Asano, H. Uehara, I. Sasase, "The influence of multipath distortion on the transmitted pulse in diffuse indoor infrared channels," Proceedings of IEEE Pacific Rim Conference on Communications, pp. 636–639, 1997.

[5.13] J. M. Kahn, R. You, P. Djahani, A. G. Weisbin, B. K. Teik, A. Tang, "Imaging diversity receivers for high-speed infrared wireless communication," IEEE Communications Magazine, vol. 36, no. 12, pp. 88–94, 1998.

[5.14] A. Sato, T. Otsuki, I. Sasase, "A study of shadowing on non-directed LOS indoor wireless system with site diversity," IEICE Transactions on Communications, vol. J83-B, no. 12, pp. 1692–1701, 2000.

[5.15] J. B. Carruthers, J. M. Kahn, "Angle diversity for nondirected wireless infrared communication," IEEE Transactions on Communications, vol. 48, no. 6, pp. 960–969, 2000.

[5.16] M. Funabiki, S. Miyamoto, K. Hirohashi, N. Morinaga, "Zone construction for PPM/CDMA-based non-directed line-of-sight indoor infrared wireless communication system," Proceedings of International Symposium on Personal, Indoor and Mobile Radio Communications, vol. 2, pp. 726–730, 1999.

[5.17] Y. Tanaka, S. Haruyama, M. Nakagawa, "Wireless Optical Transmissions with White Colored LED for Wireless Home Links," IEEE International Symposium on Personal, Indoor and Mobile Radio Communications, vol. 2, pp. 1325–1329, 2000.

[5.18] T. Komine, Y. Tanaka, S. Haruyama, M. Nakagawa, "Basic Study on Visible-Light Communication using Light Emitting Diode Illumination," International Symposium on Microwave and Optical Technology, pp. 45–48, 2001.

[5.19] Y. Tanaka, T. Komine, S. Haruyama, M. Nakagawa, "A Basic study of optical OFDM system for Indoor Visible Communication utilizing Plural White LEDs as Lighting," International Symposium on Microwave and Optical Technology, pp. 303–306, 2001.

[5.20] T. Komine, M. Nakagawa, "Fundamental Analysis for Visible-Light Communication System using LED Lights," IEEE Transactions on Consumer Electronics, vol. 50, issue 1, pp. 100–107, 2004.

[5.21] T. Komine, M. Nakagawa, "Performance Evaluation on Visible-Light Wireless Communication System using White LED Lightings," The Ninth IEEE Symposium on Computers and Communications, vol. 1, pp. 258-263, 2004.

[5.22] K. Fan, T. Komine, Y. Tanaka, M. Nakagawa, "The Effect of Reflection on Indoor Visible-Light Communication System utilizing White LEDs," The 5th International Symposium on Wireless Personal Multimedia Communications, pp. 611–615, 2002.

[5.23] Y. Tanaka, T. Komine, S. Haruyama, M. Nakagawa, "Indoor Visible Light Data Transmission System utilizing White LED Lights," IEICE Transactions on Communications, vol. E86–B, no. 8, pp. 2440–2454, 2003.

[5.24] A. S. Glassner, "An Introduction to Ray Tracing," Academic Press, San Diego, 1989.

[5.25] A. Satoh, E. Ogawa, "Fundamental Characteristics of In-House Infrared Propagation and Environmental Noise," IEEE Antennas and Propagation Society International Symposium, pp. 205–208, 1986.

[5.26] F. R. Gfeller, U. Bapst, "Wireless in-house data communication via diffuse infrared radiation," Proceedings of the IEEE, vol. 67, no. 11, pp. 1474–1486, 1979.

[5.27] J. M. Kahn, W. J. Krause, J. B. Carruthers, "Experimental Characterization of Non-Directed Indoor Infrared Channels," IEEE Transactions on Communications, vol. 43, pp. 1613–1623, 1995.

[5.28] D. Hash, J. Hillery, J. White, "IR RoomNet: Model and Measurement," IBM Communication ITL Conference, 1986.

[5.29] J. R. Barry, "Wireless Infrared Communications," Kluwer Academic Press, Boston, MA, 1994.

[5.30] R.S. Berns, "Billmeyer and Saltzman's Principles of Color Technology," John Wiley & Sons Inc., 2000.

[5.31] T. Komine, S. Haruyama, M. Nakagawa, "A Study of Shadowing on Indoor Visible-Light Wireless Communication utilizing Plural White LED Lightings," Kluwer Wireless Personal Communications, vol. 34, num. 1–2, pp. 211–225, 2005.

[5.32] T. Komine, M. Nakagawa, "A Study of Shadowing on Indoor Visible-Light Wireless Communication utilizing Plural White LED Lightings," The 1st International Symposium on Wireless Communication Systems, pp. 36–40, 2004.

[5.33] A. Sato, T. Otsuki,I. Sasase, "A study of shadowing on non-directed LOS indoor wireless system with site diversity," IEICE Transactions on Communications, vol. J83-B, no. 12, pp. 1692–1701, 2000.

[5.34] G. J. Foschini, B. Gopinath, Z. Miljanic, "Channel Cost of Mobility," IEEE Transactions on Vehicular Technology, vol. 42, no. 4 pp. 414–424, 1993.

[5.35] M. D. Audeh, J. M. Kahn, J. R. Barry, "Decision-Feedback Equalization of Pulse-Position Modulation on Measured Nondirected Indoor Infrared channels," IEEE Transactions on Communications, vol. 47, no. 4, pp. 500–503, 1999.

[5.36] D. C. M. Lee, J. M. Kahn, "Coding and Equalization for PPM on Wireless Infrared Channels," IEEE Transanctions on Communications, vol. 47, no. 2, pp. 255–260, 1999.

[5.37] J. R. Barry, J. M. Kahn, W. J. Krause, E. A. Lee, D. G. Messerschmitt, "Simulation of Multipath Impulse Response for Indoor Wireless Optical Channels," IEEE Journal on Selected Areas in Communications, vol. 11, no. 3, pp. 367–379, 1993.

[5.38] T. S. Rappaport, "Wireless Communications: Principles and Practice, 2nd Edition," Prentice Hall PTR, 2002.

Chapter 6

Integrated System of Visible Light Wireless Communication and Power Line Communication for Improvement of Convenience and User-Friendliness

In indoor visible light wireless communication, since lighting equipment is usually distributed over the ceiling, it is difficult to install new communication cables between other fixed network and the lighting equipment. This wiring problem is especially serious for existing offices and houses.

On the other hands, power line communications make it possible to use ubiquitous electricity power lines for the medium of communications. In a house, already installed power lines and outlets behave as data networks and ports. Since many data equipments and electric appliances are already connected to outlets, there is no necessity to introduce tangled cables for data communications. In fact, the standardization activities of high speed (several Mbit/s) PLC systems have recently started in many countries [6.1], and variety of high speed PLC systems are being to be purchased off-the-shelf. In PLC, each terminal connected to the power line can communicate. Nowadays, to overcome the intrinsic characteristics of power line such as intense noise and multipath effect, the technique of orthogonal frequency division multiplexing (OFDM), which is able to obtain high digital communication speed and to accommodate the evil communication environments, is generally considered as one of the most suitable modulation techniques [6.3].

In this chapter, we propose to make use of the existing power line for visible light wireless communication [6.4]. We can assume that the power line has already installed in the poison of lighting equipment on the ceiling, because lighting equipment always need power supply. Here, we use the power line for communication between the lighting equipment and other fixed networks. Therefore, it remedies the wiring problem in indoor visible light wireless communication. Moreover it is possible to emit the lights according to signal waveform transmitted through power line, with no need of demodulation. It

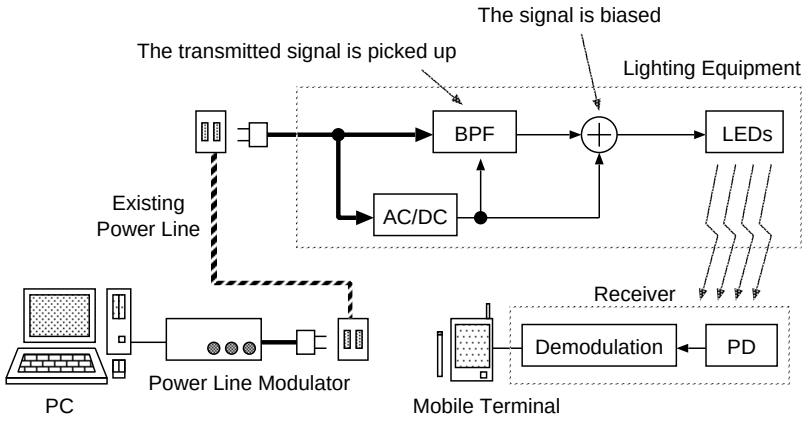

Figure 6.1: Proposed system model.

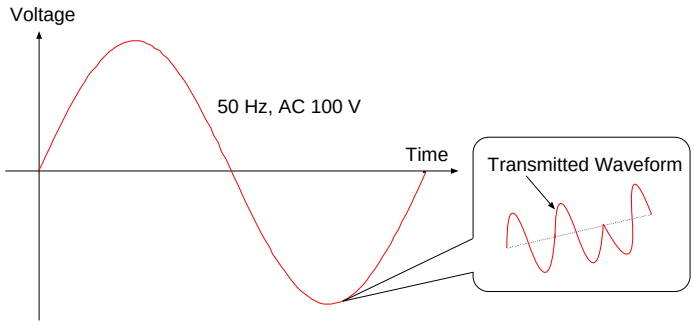

Figure 6.2: Waveform on power line.

means that, this system can also be considered as a very simple integration between power line communication and wireless communication. Thus, there is no necessity to lay a new communication cable in a ceiling. And, by screwing the electric bulb into a socket, the data transmission becomes possible. Therefore, the system has convenience and user-friendliness.

6.1 System Description

The proposed system is shown in Fig. 6.1. The main features of the proposed system are easy wiring and easy installing. We assume that power-line modulator has been plugged into and power line network has already been built. The waveform of signals in power line is shown in Fig. 6.2. Like optical intensity modulation, the transmitted signals are added to cyclic waveform of the alternating current (AC). The power supply is obtained from the existing power line in the ceiling. In the lighting equipment, the power line is

divided as shown in Fig. 6.1. The first one is supplied to the band pass filter (BPF) and the bias circuit, after being rectified by direct current as the drive power supply of each circuit. The other one takes off the waveform of AC 100 V (50 or 60 Hz in Japan) by letting BPF pass. That is, only the waveform of the transmitted signal is taken out, which is the AC waveform. Since LED passes only a direct current, the signal is biased. The power of each LED in the LED lighting is varied according to the waveform of this signal. (The frequency to transmit information is short enough to be humanly imperceptible, so that it does not affect function of lighting.) The light from the lighting equipment is received at the mobile terminal. The signal is demodulated according to the receive level of light. By doing so, this system can be realized with very easy composition.

6.2 Narrowband Power Line Noise

According to the Japanese regulations, unlicensed PLC should use frequency in the range of 10 k to 450 kHz. In this paper, PLC in these low-frequency ranges is named as narrowband PLC. Noise in PLC is mainly caused by all electric appliances that are connected to power line. In PLC, the statistical behavior of this man-made noise is quite different from that of stationary additive white Gaussian noise, which is commonly used for communication systems.

According to previous experiments and measurements, the dominant components of the noise in narrowband PLC can be categorized into three classes: stationary continuous noise, cyclic stationary continuous noise, and cyclic impulsive noise synchronous to mains.

- Stationary continuous noise: This noise is time invariant. Its power is almost constant over time in terms of minutes to hours.
- Cyclic stationary continuous noise: This noise changes its level continuously and cyclically synchronous to the mains frequency. Many electric appliances often emit this non-stationary but non-impulsive noise.
- Cyclic impulsive noise, asynchronous to mains: Impulses of this noise often has repetition rate much higher than the mains frequency, between 50 to 200 kHz. Switching power supplies often causes these impulses.

The noise in narrowband PLC represented by sum of these three components is assumed to be cyclo-stationary additive Gaussian noise whose mean is zero. The time-frequency dependent variance of noise waveform is represented as [6.3, 6.5]

$$\sigma^2(t, f) = \sigma^2(t)a(f) \tag{6.1}$$

where

$$\sigma^2(t) = \sum_{i=1}^{3} A_i |\sin(2\pi/T_{AC}t + \theta_i)|^{n_i} \tag{6.2}$$

and

$$a(f) = \frac{e^{-af}}{\int_{f_0}^{f_0+W} e^{-af} df}. \tag{6.3}$$

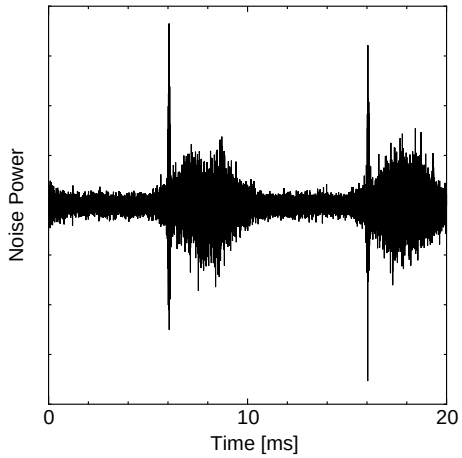

Figure 6.3: Snap-shot of generated noise waveforms.

Table 6.1: Noise parameters on power line.

A_1	A_2	θ_2	n_2	A_3	θ_3	n_3	a
0.13	2.6	128	9.3	16	161	9600	8.8×10^{-6}

In the above equations, T_{AC} is a cycle duration of the mains alternating current, typically 1/50 or 1/60 seconds. In Eq. (6.1), the function $\sigma^2(t)$ denotes the instantaneous power of the noise, and $a(f)$ represents the noise power spectral density normalized by the total noise power in the frequency range f_0 to $f_0 + W$. The instantaneous power of the noise Eq. (6.2) can be represented by a set of parameters, (A_1, A_2, A_3) for amplitude, (θ_1, θ_2, θ_3) for phase, and (n_1, n_2, n_3) for impulsiveness or power concentration in time domain. Figure 6.3 shows the computer-generated waveform with parameters given in Table 6.1, which are extracted from the measured noise waveforms.

6.3 Performance Evaluation

In power line communication, to overcome the intrinsic characteristics of power line such as intense noise and multipath effect, the technique of OFDM is generally considered. Here, we evaluate the performance of the integrated system on narrowband OFDM power line.

Figure 6.4 shows a block diagram of the integrated OFDM system where QPSK is used as a modulation scheme of the subcarrier. In the power line modulator, the input signals are modulated by OFDM. And the signals are added to cyclic waveform of the AC. The signals are transmitted to the lighting equipment through the power line. In the lighting equipment, the OFDM signals are picked up by BPF. Since LED passes only a direct current, the OFDM signals are biased. The power of each LED in the LED lighting

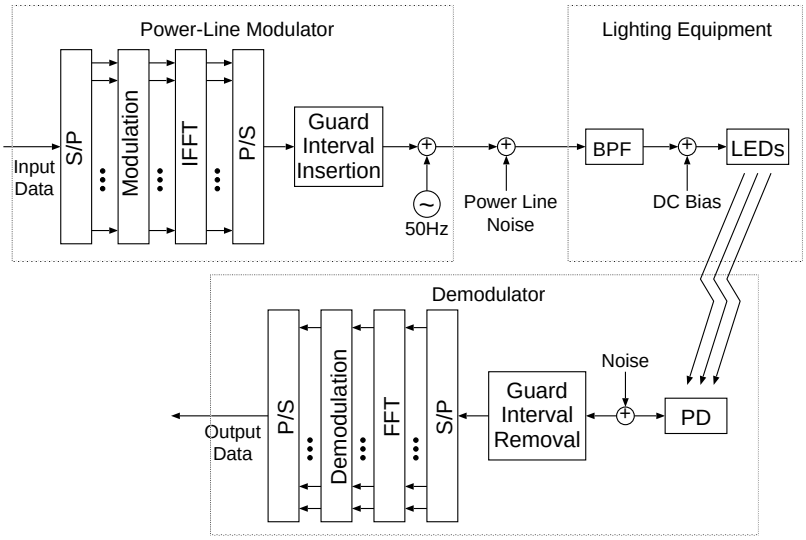

Figure 6.4: Integrated OFDM-QPSK System.

Table 6.2: Simulation parameter for the integrated system.

Cyclic-duration of AC [s]	1/50
Lowest frequency [kHz]	10
Highest bandwidth [kHz]	450
Number of Carrier	32

is varied according to the waveform of the OFDM signal. And received OFDM signal is demodulated by the mobile terminal.

Now, we will show the results on narrowband OFDM system based on computer simulation. We divide frequency band of 10 k - 450 kHz into 32 carriers. Cyclic-duration of AC is 50 Hz as shown in Table 6.2.

6.3.1 Flicker

The proposed lighting equipment emits the light according to the OFDM signal including noise on power line. So, we should discuss a flicker of the lighting equipment. Flicker is evaluated according to the extent of the fluctuation (flicker) of brightness perceived by the human eye. The limit value of flicker caused by electrical equipment is stipulated by IEC1000-3-3 (an international standard pertaining to the limit values of voltage fluctuation and flicker for equipment that has a rated input current per phase of no more than 16 A). In the standard, a maximum relative voltage change shall not exceed 4%.

Figure 6.5 shows the relation between SNR_{pl} and the maximum relative voltage change. Here, we define SNR_{pl} as average SNR on narrowband power line shown in Fig. 6.4 and SNR_{vl} as SNR on visible light wireless. We can see that the high SNR_{pl} is caused the

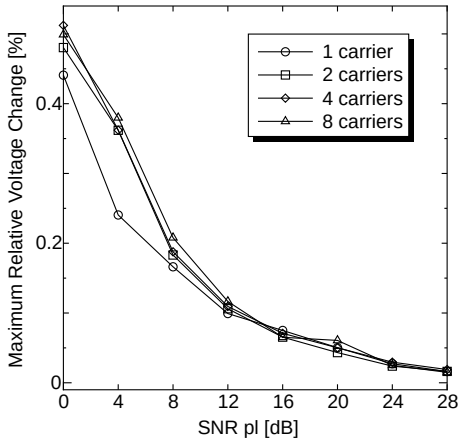

Figure 6.5: Maximum relative voltage change. Data rate is 27.3 kbit/s (1 carrier), 54.6 kbit/s (2 carriers), 109.2 kbit/s (4 carriers) and 218.4 kbit/s (8 carriers).

decrease of the maximum relative voltage change. This is because flicker of the LED lighting depends on the noise on power line. And, although SNR_{pl} is 0 dB, the maximum relative voltage change does not exceed 4%. So, we can know that the signal include power line noise on the integrated OFDM system does not affect function of lighting.

6.3.2 BER Performance

Figure 6.6(a) to 6.6(d) show the relation between SNR_{pl} and BER of whole system at each SNR_{vl}. In these figures, we use some carriers in 32 carriers. In Fig. 6.6(b), we can see that the BER of the whole integrated OFDM system almost depends on the performance at power line when SNR_{vl} is over 34 dB. In Fig. 6.6(c), we can also see that the BER almost depends on the performance at power line when SNR_{vl} is over 40 dB. By using as lighting device, brightness of the LED lighting should not fluctuate based on the number of carrier. So, when the number of carrier increases, the energy per carrier becomes small. And, the required SNR_{vl} for depending on the performance at power line increases as shown in Fig. 6.7.

6.3.3 Communication Area

The lighting equipment is installed at a height of 3.0 m from a moble terminal. The calculation condition is shown in Fig. 6.8. The proposed lighting equipment is same construction of the general lighting in section 4.1.1. The proposed lighting equipment is filled with 100 (10×10) LEDs. The space between LEDs is 4 cm. The semi-angle at half-power and the center luminous intensity of an LED is 80 deg. and 23.81 cd, respectively. The transmitted optical power of an LED is 452 mW. And the FOV at a receiver is 90 deg., detector physical area of a PD is 1 cm^2, O/E conversion efficiency is 0.54, and background light current is 5100 μA. And the parameters for calculation of SNR_{pl} is shown in Table

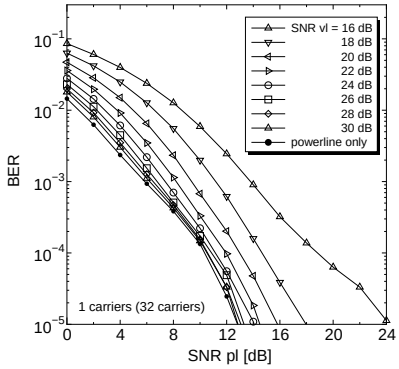

(a) 1 carrier. Data rate is 27.3 kbit/s.

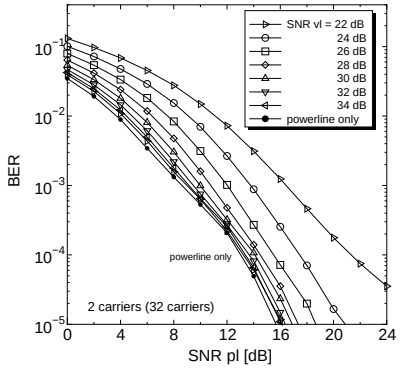

(b) 2 carriers. Data rate is 54.6 kbit/s.

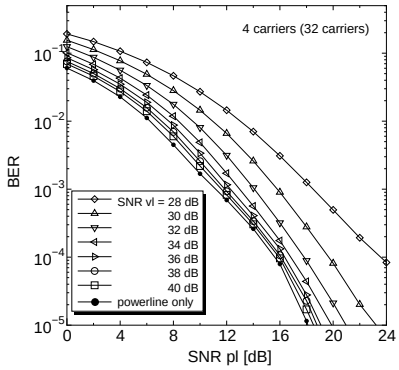

(c) 4 carriers. Data rate is 109.2 kbit/s.

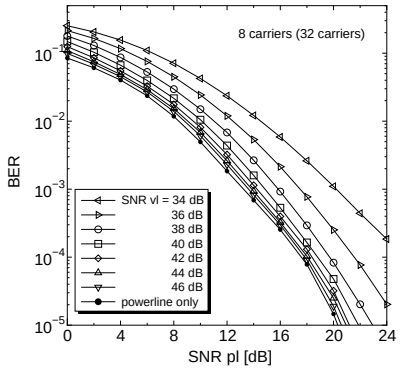

(d) 8 carriers. Data rate is 218.4 kbit/s.

Figure 6.6: The BER performance of the proposed integrated system.

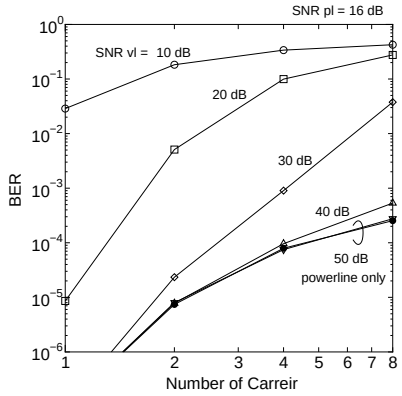

Figure 6.7: BER of whole system vs. number of carrier. SNR_{pl} is 16 dB. Data rate is 27.3 kbit/s (1 carrier), 54.6 kbit/s (2 carriers), 109.2 kbit/s (4 carriers) and 218.4 kbit/s (8 carriers).

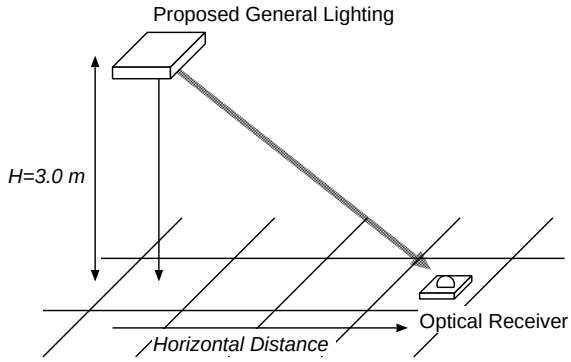

Figure 6.8: Numerical analysis condition.

Table 6.3: Parameters for SNR calculation.

FOV at a Receiver	90 [deg.]
Detector Physical Area of a PD	1 [cm^2]
Gain of an Optical Filter	1.0
Refractive Index	1.5
O/E Conversion Efficiency	0.54 [A/W]
Open-Loop Voltage Gain	10
Fixed Capacitance	112 [pF/cm^2]
FET Channel Noise Factor	1.5
FET Transconductance	30 [mS]
Absolute Temperature	298 [K]
Background Light Current	5100 [μA]

6.3. Figure 6.9 shows the relation between SNR_{vl} and the distance from the center of the lighting equipment on the desk. We define a tracking as the maintaining of the receiver's optical axis to the center of the LED lighting. When the number of carrier is 4 and the distance is 16 m, the SNR_{vl} is about 40 dB with tracking. From Fig. 6.6(c), we can see that the integrated OFDM system depends on the power line greatly if SNR_{vl} obtains more than 40 dB. Therefore, we can know that the integrated OFDM system depends on the power line performance when the receiver exists in the radius of 16 m from the center of the LED lighting on the desk. The area is enough for communication indoor wireless networks.

6.4 Summary

In this chapter, along with the popularization of OFDM system at power line communication, we evaluate the performance of the integrated system on narrowband OFDM power line. As a result, we can know that the signal of integrated OFDM system does not affect function of lighting. When the number of carrier increases, the required SNR_{vl} becomes large. However, the integrated OFDM system gets enough communication area due to

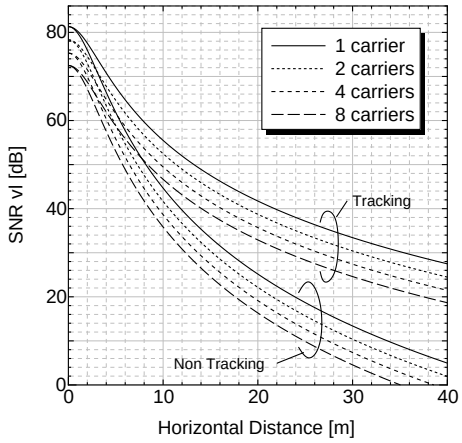

Figure 6.9: Horizontal distance vs. SNR_{vl}. Data rate is 27.3 kbit/s (1 carrier), 54.6 kbit/s (2 carriers), 109.2 kbit/s (4 carriers) and 218.4 kbit/s (8 carriers).

high energy for lighting function. And the system depends on the performance at narrowband power line. Therefore, it is possible to apply the integrated system to narrowband OFDM power line communication. Consequently, the visible light wireless system will expect as indoor communication system of next generation. Further research on these would make LED lighting communication feasible.

6.5 References

[6.1] "`http://www.homeplug.org/`"

[6.2] F. J. Canete, L. Diez, J. A. Cortes, J. T. Entrambasaguas, "Broadband modelling of indoor power-line channels," IEEE Transactions on Consumer Electronics, vol. 48, issue 1, pp. 175–183, 2002.

[6.3] M. Katayama, "Introduction to Robust, Reliable, and High-Speed Power-line Communication Systems," IEICE Transactions on Fundamentals, vol. E84–A, no. 12, pp. 2958-2965, 2001.

[6.4] T. Komine, M. Nakagawa, "Integrated System of White LED Visible-Light communication and Power-Line Communication," IEEE Transactions on Consumer Electronics, vol. 49, no. 1, pp. 71-79, 2003.

[6.5] H. Niwa, O. OONO, M. Katayama, T. Yamazato, A. Ogawa, N. Isaka, "A Spread-Spectrum System with Dual Processing Gains Designed for Cyclic Noise in Power Line Communications," IEICE Transactions on Fundamentals, vol. E80–A, no. 12, pp. 2526-2533, 1997.

Chapter 7

Conclusion

As portable computers and communication terminals become more powerful and are more widely deployed, the demand for high speed wireless networks is increasing. An infrared wireless transmission technique represents an attractive choice for many indoor applications. Its advantages include the availability of a wide bandwidth that is unregulated worldwide and that can be reused in a very dense fashion, immunity to eavesdropping, the ability to achieve very high bit rates, low signal-processing complexity, and potentially very low cost. However, there remains some problems which should be solved in this field.

On the other hands, visible LED has many advantages, such as low power consumption, high tolerance to humidity, and small heat generation. The LED is used in full color displays, traffic signals, and many other means of illumination. Now, white LED is considered as a strong candidate for the future lighting technology. Compared with conventional lighting methods, white LED has lower power consumption, lower voltage, longer lifetime, smaller size, and cooler operation. The Ministry of Economy, Trade and Industry of Japan estimates, if the LED replaces half of all incandescent and fluorescent lamps currently in use, Japan could save equivalent output of six mid-size power plants, and reduce the production of greenhouse gases. A national program underway in Japan has already suggested that white LED deserves to be considered as a general lighting technology of the 21st century owing to electric power energy consumption.

We have proposed an optical wireless communication system that employs white LED for indoor wireless networks in chapter 4. In this system, the LED is not only used as a lighting device, but also used as a communication device. It is a kind of optical wireless communication that uses the "visible" white ray for communication purposes. Based on lighting engineering, their communication performance is evaluated. In chapter 5, various new schemes in indoor visible light environment have been proposed and discussed. In this chapter, diversity technique has been proposed so that shadowing problem may be alleviated and the availability of the system has been shown. Moreover, to overcome the intersymbol interference caused by optical path difference between lighting equipments, adaptive equalizer has been proposed. In chapter 6, integrated system of visible light wireless communication and power line communication for improvement of convenience and user friendliness has been proposed.

In this dissertation, some newer transmission schemes which can apply the advan-

tages of a visible light wireless communication has been proposed, solving conventional problems at optical wireless communication. Moreover, about each proposed system, numerical analysis and the computer simulations were performed and the validity of the system was discussed.

Following sections are the conclusion from each chapters, with detailed conclusion from each new proposal.

This dissertation has focused on the following issues, in particular.

7.1 Conclusion From Chapter 4

In chapter 4, we have proposed a visible light wireless data transmission system utilizing LED lighting equipment. In this system, the lighting equipment has the capacity for wireless optical communication. Based on a lighting engineering, some numerical analyses for the proposed system have been performed. Firstly, the proposed lighting equipments as general lighting and downlight have been designed. The received optical power, RMS delay spread and BER performance have been shown at each lighting equipment. And the relation between illuminance and BER performance at each data rate has been elucidated. Secondly, the influence of multiple lighting equipments that transmit different information has benn discussed. By calculated DUR by measurement, communication quality of the lighting equipments is known and the results are useful to install the lighting equipment. As a result, the availability of the proposed system to high data wireless transmission has been shown.

7.2 Conclusion From Chapter 5

In infrared wireless communication, multipath dispersion due to the reflection on walls in serious problem. Particularly in a non-directed non-LOS link, this problem leads a serious ISI and degrades performance severely. A shadowing problem is another issue on indoor optical wireless channels. This is because the lightwave cannot penetrate opaque obstacles. This feature makes easy to secure transmission against casual eavesdropping, while the shadowing makes a stable transmission difficult in LOS links. Of course, non-LOS links allow the link to operate even when there exists the shadowing between the transmitter and receiver. Non-LOS links, however, suffer from multipath dispersion, because non-LOS links generally relay upon reflection of the light from the ceiling or some other diffusely reflecting surface. From the viewpoint of power efficiency, non-LOS links are inferior to LOS links also.

The proposed lighting equipments has large power, compared with infrared wireless communication system, for function of lighting equipment. On the other hand, generally, illuminating engineers install many lighting sources on the ceiling so that a dark area may not be generated. From the view of communication engineers, the transmission in LOS links without a shadowing can be achieved because many lighting sources, which are capable of an optical transmission, are distributed widely on the ceiling.

In this chapter, the diversity technique has been proposed so that shadowing problem is alleviated. And, based on lighting engineering, some characteristics of the proposed

system in particular visible light wireless environment have been discussed. The system has specific delay profile by the plural lighting equipments which have large surface area. At some models, the numerical analyses of plural lighting equipments as illuminance, received optical power, and RMS delay spread during use as an optical transmitter have been performed and BER performance has been shown. And the influence of shadowing by the plural lighting equipments has been discuss. An optimal number of the lighting equipment for communication has been shown. And we showed that the system with optimal number of the lighting equipment was robust against shadowing and could accommodate more calls. Moreover, to overcome the ISI caused by optical path difference between plural lighting equipments, adaptive equalizer has been proposed. The performance of adaptive equalizer with LMS algorithm was evaluated. We showed that the effectual interval of training sequence for channel estimation alleviated the influence of shadowing. From these analyses, it was found that the idea of the proposed system was very promising for future high speed wireless access networks and it could be one choice for an indoor optical wireless data transmission system.

7.3 Conclusion From Chapter 6

In indoor visible light wireless communication, since lighting equipment is usually distributed over the ceiling, it is difficult to install new communication cables between other fixed network and the lighting equipment. This wiring problem is especially serious for existing offices and houses. In this chapter, we have proposed to make use of the existing power line for visible light wireless communication. Here, we used the power line for communication between the lighting equipment and other fixed networks. Moreover it was possible to emit the lights according to signal waveform transmitted through power line, with no need of demodulation. It was also proposed, the socket of the existing electric bulb could be used in the proposed system. Therefore, the system has convenience and user-friendliness. we have evaluated the performance of the integrated system on narrowband OFDM power line. As a result, we could know that the signal of integrated OFDM system does not affect function of lighting. When the number of carrier increases, the required SNR_{vl} becomes large. However, the integrated OFDM system gets enough communication area due to high energy for lighting function. And we could know that the system depended on the performance at narrowband power-line. Therefore, it is possible to apply the integrated system to narrowband OFDM power-line communication. Consequently, the visible-light wireless system will expect as indoor communication system of next generation. Further research on these would make LED lighting communication feasible.

7.4 Future Indoor Visible Light Wireless Communications

Integration of radio and optical technology, integration of wired and wireless communication technology will progress increasingly in future. In a future high-speed all digital

network, an optical wireless communication technique will be more important than now. An optical wireless communication is attractive in many indoor applications, such as short-range high speed data transmission, telemetry, video broadcasting, fixed wireless access networks, and so on.

At home, The digital data from an external network are stored in a home server. This home server has an power line modulation unit. The required data are modulated at a home server and are guided into power line to each room. At a room, required signals are picked up at lighting equipment and are emitted into the air. Therefore, in home network, lighting equipment at each room are simple because a modulation is not needed at lighting equipment. And the system has convenience and user friendliness. At office, each floor is connected by high speed LANs. And the data are guided into cable to each room. The signals are remodulated to optical at the lighting equipment and are emitted into the air. The high speed transmission which is over 100 Mbit/s is required on the each room and the system should have continuous connection. As method of approach, visible light wireless communication which has potential of high speed transmission will be used.

Therefore, all electrical appliances in our home and office will be wireless-linked each other in future. These wireless systems exist throughout our home and office, ranging from short-distance point-and-shoot systems to cellular systems that cover whole rooms. These devices automatically select the link which offers the best performance at that time. As we roam through our home taking our portable communicator with us, it remains linked to the network by seamlessly switching between different rooms. All rooms are interconnected within our home and linked to the high-speed external network. Thus, visible light wireless communication systems will be more important in near future.

Anyway, author believes that a visible light wireless communication system is one of the solutions for future high speed communication networks and many studies about this will make our future life enjoyable.

Acknowledgments

I am greatly indebted to many people for their support, encouragement and assistance throughout this work. First and foremost, I would like to express my deepest gratitude to Professor Masao Nakagawa for his invaluable advice and continuous encouragement, since I joined his laboratory. His unfailing support made me possible to accomplish this work.

I would also like to thank my thesis committee members, Professor Shinichiro Haruyama, Professor Iwao Sasase, Professor Yasuhiro Koike, and Professor Yoshinori Matsumoto of Keio University for their helpful discussion and careful reviewing this dissertation.

I am pleased to acknowledge many individuals who helped me constantly in my research and student life in Nakagawa Laboratory: in particular, Dr. Yuichi Tanaka, Assistant Professor Takeo Fujii, Dr. Kyesan Lee, Dr. Sigit Puspito Wigati Jarot, Mr. Takemi Arita, Dr. Takehiko Yamaguchi, and many others for their discussions and help.

I am also very grateful to my colleagues and friends who have shared enjoyable time at Keio University: Mr. Masashige Shirakabe, Mr. Kenji Okada, Mr. Hisanori Tanada, Mr. Yasunori Sakai, Mr. Shinya Terashi, Mr. Cho Chihong, Mr. Kim Young Woon, and many others. I would also like to thank the members of the optical wireless communication research group in Nakagawa Laboratory: Mr. Shinya Masumura, Ms. Masako Akanegawa, Mr. Motoyoshi Maehara, Mr. Shuhei Horikawa, Mr. Kanei Fan, Mr. Yasuo Sugawara, Mr. Shogo Kitano, Mrs. Norharyati Binti Harum, Mr. Yousuke Ito, Mr. Satoshi Miyauchi, Mr. Akihiro Shimura, Mr. Yuzo Nishide, Miss. Haswani Che Wook, Miss. Asami Furuya, Mr. Masanori Ishida, Mr. Hidemitsu Sugiyama, Mr. Shogo Abe, Mr. Tetsushi Matsuzawa, Mr. Akihiro Mitsunaga, Mr. Tsubasa Saito, Mr. Dai Yamagaka, Mr. Masakazu Yamaguchi, Mr. Hideaki Kotake, Miss. Shoko Nishida for their valuable discussions and comments through the study of visible light wireless communication systems. Besides, I am especially grateful to Mr. Osamu Takyu and Mr. Jun Hwan Lee for their helpful suggestions, valuable discussions and encouragement.

Last, but no means last, I wish to express my heartfelt thanks to my parents who have supported and encouraged me all the time from my hometown Mishima.

List of Papers

Transaction Papers

[1] T. Komine, M. Nakagawa, "Integrated System of White LED Visible-Light Communication and Power-Line Communication," IEEE Transactions on Consumer Electronics, vol. 49, no. 1, pp. 71–79, February 2003.

[2] Y. Tanaka, T. Komine, S. Haruyama, M. Nakagawa, "Indoor Visible Light Data Transmission System utilizing White LED Lights," IEICE Transactions on Communications, vol. E86–B, no. 8, pp. 2440–2454, August 2003.

[3] T. Komine, M. Nakagawa, "Fundamental Analysis for Visible-Light Communication System using LED Lights," IEEE Transactions on Consumer Electronics, vol. 50, issue 1, pp. 100–107, February 2004.

[4] T. Komine, S. Haruyama, M. Nakagawa, "A Study of Shadowing on Indoor Visible-Light Wireless Communication utilizing Plural White LED Lightings," Kluwer Wireless Personal Communications, vol. 34, num. 1–2, pp. 211–225, July 2005.

International Conferences

[1] T. Komine, Y. Tanaka, S. Haruyama, M. Nakagawa, "Basic Study on Visible-Light Communication using Light Emitting Diode Illumination," 8th International Symposium on Microwave and Optical Technology (ISMOT 2001), pp. 45–48, June 2001.

[2] Y. Tanaka, T. Komine, S. Haruyama, M. Nakagawa, "A Basic study of optical OFDM system for Indoor Visible Communication utilizing Plural White LEDs as Lighting," 8th International Symposium on Microwave and Optical Technology (ISMOT 2001), pp. 303–306, June 2001.

[3] Y. Tanaka, T. Komine, S. Haruyama, M. Nakagawa, "Indoor Visible Communication utilizing Plural White LEDs as Lighting," The 12th Annual IEEE International Symposium on Personal, Indoor and Mobile Radio Communications (PIMRC 2001), pp. F81–F85, September 2001.

[4] T. Komine, M. Nakagawa, "Integrated System of White LED Visible-Light Communication and Power-Line Communication," The 13th Annual IEEE International Symposium on Personal, Indoor and Mobile Radio Communications (PIMRC 2002), pp. 1762–1766, September 2002.

[5] K. Fan, T. Komine, Y. Tanaka, M. Nakagawa, "The Effect of Reflection on Indoor Visible-Light Communication System utilizing White LEDs," The 5th International Symposium on Wireless Personal Multimedia Communications (WPMC 2002), pp. 611–615, October 2002.

[6] T. Komine, S. Haruyama, M. Nakagawa, "Bi-directional Visible-Light Communication using Corner Cube Modulator," The 3rd IASTED International Conference on Wireless and Optical Communications (WOC 2003), pp. 598–603, July 2003.

[7] T. Komine, M. Nakagawa, "Performance Evaluation on Visible-Light Wireless Communication System using White LED Lightings," The Ninth IEEE Symposium on Computers and Communications (ISCC 2004), vol. 1, pp. 258-263, June 2004.

[8] T. Komine, M. Nakagawa, "A Study of Shadowing on Indoor Visible-Light Wireless Communication utilizing Plural White LED Lightings," The 1st International Symposium on Wireless Communication Systems 2004 (ISWCS 2004), pp. 36–40, September 2004.

[9] S. Miyauchi, T. Komine, Y. Ushiro, S. Yoshimura, S. Haruyama, M. Nakagawa, "Parallel Wireless Optical Communication Using High Speed CMOS Image Sensor," The 2004 International Symposium on Information Theory and its Applications (ISITA 2004), pp. 72–77, October 2004.

[10] J. H. Lee, T. Komine, S. Haruyama, M. Nakagawa, "LED Panel Lighting Communication with Delay Feedback Control for High Data Rate Downlink Transmission," The 9th World Multi-Conference on Systemics, Cybernetics and Informatics (WMSCI 2005), vol. 2, pp. 13–16, July 2005.

[11] M. Ishida, S. Miyauchi, T. Komine, S. Haruyama, M. Nakagawa, "An Architecture for High-Speed Parallel Wireless Visible Light Communications using 2D Image Sensor and LED Transmitter," First International Wireless Summit (IWS 2005), pp. 1523–1527, September 2005.

[12] T. Komine, S. Haruyama, M. Nakagawa, "Adaptive Equalization for Indoor Visible-Light Wireless Communication Systems," The 11th Asia-Pacific Conference on Communications (APCC 2005), pp. 294–298, October 2005.

[13] Haswani Che Wook, T. Komine, S. Haruyama, M. Nakagawa, "Visible Light Communication with LED-based Traffic Lights Using 2-Dimensional Image Sensor," IEEE Consumer Communications and Networking Conference (CCNC 2006), January 2006.

[14] S. Miyauchi, T. Komine, M. Ishida, S. Haruyama, M. Nakagawa, "An Analysis of LED-Allocation Algorithm for High-Speed Parallel Wireless Optical Communication System," The IEEE Radio and Wireless Symposium (RWS 2006), January 2006.

[15] T. Komine, S. Haruyama, M. Nakagawa, "Performance Evaluation of Narrowband OFDM on Integrated System of Power-Line Communication and Visible-Light Wireless Communication," International Symposium on Wireless Pervasive Computing 2006 (ISWPC 2006), January 2006.

Technical Reports and Other Presentations

[1] T. Komine, Y. Tanaka, S. Haruyama, M. Nakagawa, "Basic Study on Visible-Light Communication using White LED light," IEICE Technical Report, OCS2001–71, October 2001.

[2] Y. Tanaka, T. Komine, S. Haruyama, M. Nakagawa, "A Consideration of Inter-symbol Interference on Indoor Visible Light Communication System utilizing Multiple White LED Lights," IEICE Technical Report, OCS2001–70, October 2001.

[3] K. Fan, T. Komine, Y. Tanaka, M. Nakagawa, "The Effect of Reflection on Indoor Visible-Light Communication System using LED," IEICE Technical Report, IT2001–90, ISEC2001–128, SST2001–206, ITS2001–144, March 2002.

[4] Y. Tanaka, T. Komine, S. Haruyama, M. Nakagawa, "A Consideration on Modulation Schemes for Indoor Visible Light Communiaction System utilizing White LED Lights," IEICE Technical Report, IT2001–89,ISEC2001–127,SST2001–205, ITS 2001–143, March 2002.

[5] T. Komine, Y. Tanaka, M. Nakagawa, "Integrated System of White LED Visible-Light Communication and Electrical Power-Line Communication," IEICE Technical Report, IT2001–91, ISEC2001–129, SST2001–207, ITS2001–145, March 2002.

[6] T. Komine, S. Haruyama, M. Nakagawa, "Bidirectional Visible-Light Communication using Corner Cube Modulator," IEICE Technical Report, DSP2002–145, SAT2002–95, RCS2002–214, January 2003.

[7] K. Fan, T. Komine, S. Haruyama, M. Nakagawa, "The Application of The Visible-lighting Communication System in International Space Station," IEICE Technical Report, WBS2003–40, SAT2003–32, June 2003.

[8] T. Komine, S. Haruyama, M. Nakagawa, "A Consideration of Interference and Reflection on Visible-Light Communication System using White LED Lights," IEICE Technical Report, WBS2003–37, SAT2003–29, June 2003.

[9] S. Horikawa,T. Komine, S. Haruyama, M. Nakagawa, "Pervasive Visible Light Positioning System using White LED Lighting," IEICE Technical Report, CAS2003–142, DSP2003–244, CS2004–194, March 2004.

[10] S. Miyauchi, T. Komine, T. Ushiro, S. Yoshimura, S. Haruyama, M. Nakagawa, "Parallel Optical wireless Communication using High Speed CMOS Image Sensor," IEICE Technical Report, CS2004–18, OCS2004–28, PN2004–23, May 2004.

[11] Y. Nishide, T. Komine, S. Haruyama, M. Nakagawa, "The Methods to Simulate the Maximum Transmission Speed of White LED Visible-Light Communication," IEICE Technical Report, RCS2004–124, August 2004.

[12] M. Ishida, S. Miyauchi, T. Komine, S. Haruyama, M. Nakagawa, "A High Speed Design for Parallel Wireless Visible Light Communication using 2D Transceiver," IEICE Technical Report, OCS2005–20, May 2005.